# Mesoscale Modeling of Sediment Transport and Morphologic Changes at Tidal Inlets: Years 1 & 2

*Prepared by:*

P.A. Work, Y. Zhang, and E.J. Hayter
Civil Engineering Department
Clemson University

*and*

T.W. Kana
Department of Geological Sciences
University of South Carolina

*Sponsored by:*


JANUARY 1996

# Mesoscale Modeling of Sediment Transport and Morphologic Changes at Tidal Inlets: Years 1 & 2

by

P.A. Work, Y. Zhang, and E.J. Hayter
Civil Engineering Department
Clemson University

and

T.W. Kana
Department of Geological Sciences
University of South Carolina

Sponsored by:

South Carolina Sea Grant Consortium

January 1996

Table of Contents

List of Tables

List of Figures

# Mesoscale Modeling of Sediment Transport and Morphologic Changes at Tidal Inlets: Years 1 & 2

## I. INTRODUCTION

### 1.A Overview

This report outlines Years 1 and 2 progress on a four year project to develop a mesoscale model of sediment transport and morphologic changes at tidal inlets (SC Sea Grant R/CP–10 to the University of South Carolina and Clemson University). The primary objective of the project is to develop a numerical (computer) model which simulates long–term (year–to–decadal) tide– and wave–induced shoreline and bathymetric changes around tidal inlets typical of the South Carolina coast and similar mesotidal, mixed wave energy settings. Such a model would bridge a gap between qualitative or empirical large–scale morphological models (e.g., Hayes 1979; Wright and Short 1983) and quantitative small–scale numerical models, and would operate at time scales considered to be of most concern to regulatory agencies (i.e., 10 to 30 years). If successful, the proposed mesoscale model will be able to predict the timing, magnitude, and direction of shoreline response to inlet and ebb tidal delta changes, and will serve as a useful tool in shore protection planning and design. Figure 1.1 outlines the overall study plan including the work elements for Years 1 and 2.

In the last ten years considerable progress has been made in the development of numerical simulation models of (1) shoreline change around coastal structures (e.g., Hanson and Kraus 1986; Kraus 1988), (2) erosion after storms (e.g., Larson and Kraus 1989b; Nairn 1990), or (3) beach profile adjustment following nourishment (e.g., Larson and Kraus 1989a; Halcrow and Partners 1991), and (4) hydrodynamic and sediment transport processes around tidal inlets (e.g., Veeramachaneni and Hayter 1988; Vemulakonda *et al.* 1988). These models tend to be driven by a set of wind, wave, and tide parameters operating at short time scales measured in hours, days, or weeks. Common time steps for such models are 5 to 30 minutes. Output generally emphasizes movement of a particular reference contour (e.g., the mean sea level or low water line), changes in the ebb tidal delta, or the development of a post–storm bar and subsequent onshore migration and reattachment at the beach (e.g., Nairn 1990). While these models provide practical tools for simulating small–scale or short–term events, they have not been designed to simulate longer term, or regional, shoreline trends.

The present study was initiated in September 1993 and began with assembly of literature and data on shoreline change modeling. The investigators have met several times and initiated correspondence with researchers from other institutions. Table 1.1 summarizes meetings and

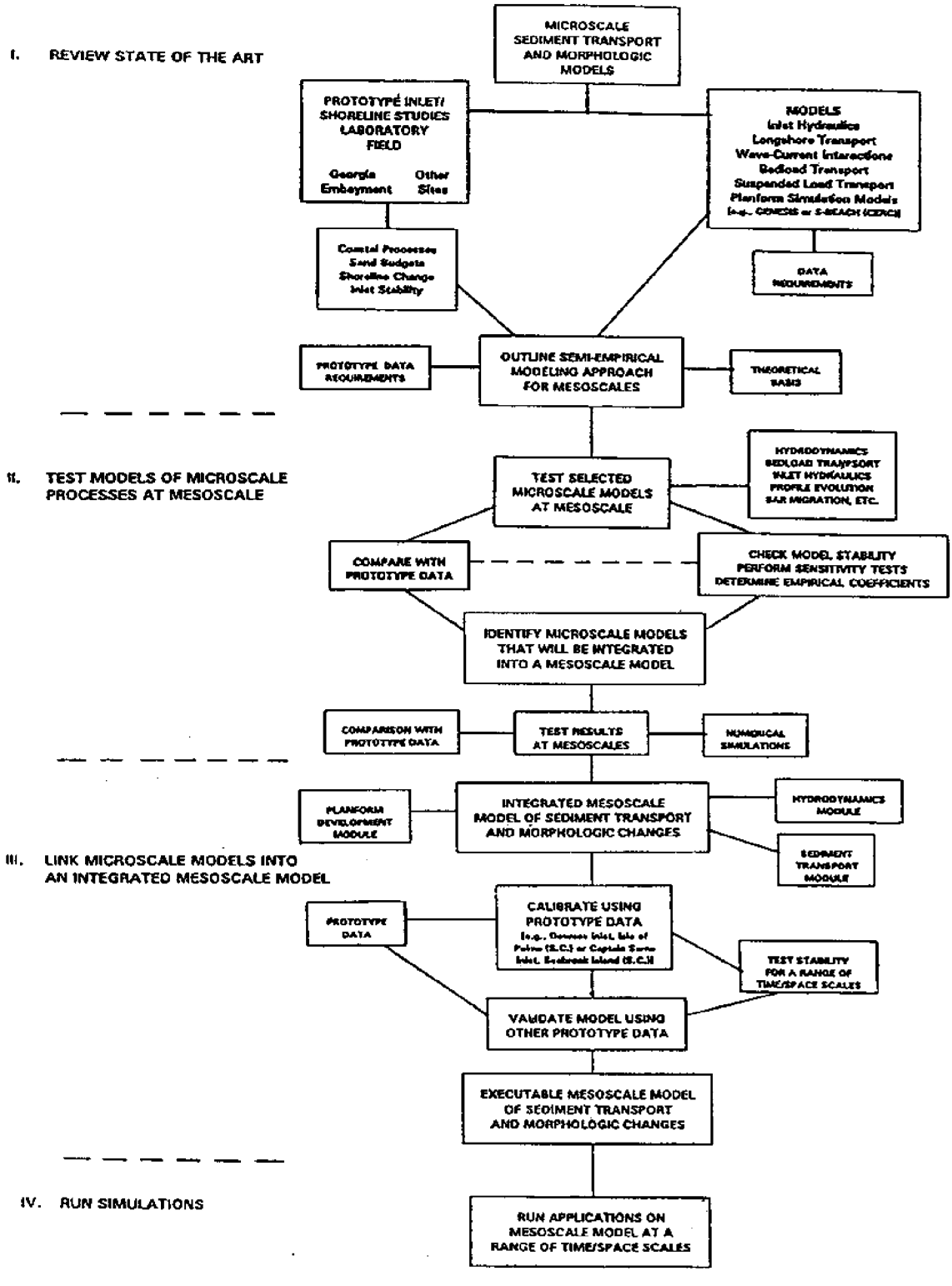


Fig. 1.1 Outline of overall study plan

professional interactions to date relevant to the present project. The specific objectives and methodology for the first two years of the study are presented in the next two sections.

### 1.B Year 1 Objective and Procedures

The objective of Year 1 was to *outline a semi–empirical modeling approach* that can combine and link existing models of inlet processes and responses (i.e., shoreline planforms, inlet hydrodynamics, and coastal sediment transport models) and be adapted for longer term simulations at mesoscales (i.e., 1–20 years).

The investigators followed a two–pronged approach to accomplish this objective:

1) Extension of microscale models toward mesoscale, and

2) Development of more detailed empirical (morphological) models from macroscale toward mesoscale.

The focus of the first part was on review of the literature and existing microscale computer simulation models with an eye toward assessing the feasibility of scaling up to mesoscale by way of increased time steps and coarser grid sizes to reduce computation time. The review of microscale models also attempted to distinguish algorithms that are well established and tested from those that have a weaker theoretical basis. The idea here was that the final model will be constrained, and accuracy controlled, by the weaker algorithms.

The second part of the Year 1 approach considered existing macroscale (geologic) models and attempted to refine them with details of shoreline change and profile adjustment operating at mesoscales. A primary focus was on the process of shoal bypassing at tidal inlets and a more detailed description of how this process controls sediment budgets along many inlet dominated shorelines.

### 1.C Year 2 Objective and Procedures

The objectives of Year 2 was to *test the feasibility of selected microscale models* to simulate longer term processes at realistic time and space scales, and to develop a hybrid model. The latter consists of a mesoscale model that is coupled to a microscale hydrodynamic and sediment transport model.

The first objective was accomplished by applying the selected models to Murrell's Inlet and to a hypothetical ocean–tidal inlet–bay system over a range of time–steps and spatial scales to determine the limits of the models' applicability. A hydrodynamic and sediment transport model (CWSTM–H) developed by Veeramachaneni and Hayter (1988) was applied to the hypothetical tidal inlet system, and two wave transformation models were applied to Murrell's Inlet.

The second objective was accomplished by coupling the CWSTM–H model to the first version of the mesoscale model. The CWSTM–H model was used to generate the required input data for the mesoscale model.

### 1.D Report Contents

The remaining sections of this report describe the following: Section II – a review of existing models relevant to the study; Section III – listing of data requirements and availability for application to a mesoscale model; Section IV – recommended mesoscale modeling approach integrating hydrodynamic and sediment transport algorithms and plan for software development and testing; and Section V – objectives and proposed methodology for Years 3 and 4.

Table 1.1 Summary of meetings and relevant contacts during Years 1 and 2.

| | |
|---|---|
| September 1993 | • Initiate project |
| 23 September | • Meeting at Clemson (TWK,EJH,PAW) |
| 16–18 November | • Large–Scale Coastal Change Conference, St. Petersburg, FL (TWK)<br>Meetings with researchers from Delft Hydraulics Laboratory (Netherlands), Danish Hydraulics Laboratory, Wallingford Research Station (UK), CERC, and others. |
| 13–14 December | • Investigators' meeting at Folly Beach (TWK,EJH,PAW) |
| 19 January 1994 | • Investigators' meeting at USC/Columbia (TWK,EJH) |
| 22 March | • Investigators' meeting at USC/Columbia (TWK,EJH,PAW) |
| 26 March | • Field trip to North Inlet (TWK, students) |
| 8 April | • Florida Dept of Environmental Protection Ebb Tidal Shoal Dredging Workshop, Tallahassee, FL (EJH) |
| 17 April | • Field trip to Isle of Palms – Coastal Society Meeting (TWK,SCSG) |
| 17 April | • Field trip to Isle of Palms – Coastal Society Meeting (TWK,SCSG) |
| 9 June | • Investigators' meeting at Folly Beach |
| June–August | • Literature review (TWK, student) |
| 6–8 September | • CERC Inlet Modeling Workshop (EJH) |
| 17–18 October | • Investigators' meeting at College of Charleston (TWK,EJH,PAW) |
| 24–28 October | • 24$^{th}$ Intl. Coastal Engineering Conference (Kobe, Japan)<br>Meetings with foreign investigators (TWK) |
| 17–20 November | • Southeast Coastal Ocean Research Conference, Sea Brook Island, SC (EJH,PAW) |
| 22 December | • Investigators' meeting at Clemson University (TWK,EJH,PAW) |
| 9 January 1995 | • Investigators' meeting at Clemson University (TWK,EJH,PAW) |
| 7 February | • Investigators' meeting, Columbia (TWK,PAW) |
| 1–9 September | • Coastal Dynamics '95 conference, Gdansk, Poland (TWK,PAW) |
| 23 October | • Investigators' meeting, Columbia (TWK,EJH,PAW) |

# II. REVIEW OF EXISTING MODELS OF SHORELINE CHANGE AND TIDAL INLET PROCESSES

## 2.A Scales of Coastal Change

A spectrum of scales can be applied to studies of shoreline change. In fact, the position and morphology of the shoreline at any particular place owes its existence to a combination of factors ranging from global phenomena (such as sea–level position and tectonics) to local site–specific controls (such as sediment type, incident wave climate, and local weather patterns). During the past century, researchers have referred to scales and types of coastlines in geologic process terms, distinguishing "shorelines of submergence" from "shorelines of emergence" (Johnson 1919), or fluvial versus glacial versus biogenic shorelines. Following the development of plate tectonic theory, a more unified coastal classification was proposed whereby a shoreline's position, with respect to continental plates, as well as a shoreline's scale were also considered (Inman and Nordstrom 1971). The primary tectonic control under this classification was plate movement across the earth's surface. Where plates collided near the coast, mountains and troughs were more pronounced, giving rise to the term "collision" coast; that is, one having a narrow, steep profile. Coasts facing spreading centers in the ocean, where plate material is formed, became referred to as "trailing–edge" coasts, because their shorelines receded gradually from spreading centers, leaving a gently sloping, wide margin along the coastal profile. Inman and Nordstrom (1971) suggested that at least three orders of scale could be distinguished in coastlines.

| | |
|---|---|
| First order: | 1,000 kilometer (km) lengths, 100 km widths, and 10 km heights |
| Second order: | 100 km lengths, 10 km widths, and 1 km heights |
| Third order: | <10 km lengths, <1 km widths, and <100 meter (m) heights |

Applied to the U.S. East Coast, first–order features would be the inner shelf, barrier islands, and coastal plain from New York to Florida. Second–order features would be barrier island/lagoon systems such as Cape Hatteras/Pamlico Sound or estuaries such as the Delaware. Third–order features would be discrete barrier islands such as Pawleys or river deltas such as the Santee. Inman and Nordstrom (1971) suggested higher order features (berms, dunes, longshore bars, beach cusps, etc.) could be distinguished and classified similarly by a simple ordering of dimensions.

The Inman and Nordstrom (1971) classification scheme provided a useful framework for earlier descriptions of the coast (e.g., ria, glacial, biogenic, etc.) because it provided a context from which a particular shoreline was likely to evolve. Immediately the scheme implies

an order of magnitude for change as a function of geographic scale. First–order features along trailing–edge coasts are likely to exist anywhere within a 100–km swath from the continental shelf to the coastal plain during long geologic time. In contrast, higher order features such as discrete barrier islands exist over a narrower width at the sea's edge. This geographic hierarchy suggests a temporal hierarchy as well, with first–order features persisting longer than higher order features. A barrier/lagoon system, for example, may exist anywhere within the broad swath of a first–order, trailing–edge coast such as the U.S. East Coast. Therefore, a particular barrier island can only last as long as the first–order feature within which it lies. We know that both the first– and second–order features are subject to other processes besides plate tectonics which tend to cause much more rapid change.

The two factors that control shoreline position within the framework of plate tectonics are sediment supply and sea–level position. With widespread documentation of sea–level history since the Pleistocene epoch, it is clear that sea level cycles up and down with cycles of continental glaciation. A low stand is thought to have occurred less than 20,000 years before present (B.P.), placing East Coast shorelines about 100 m lower than today's coastline, out on the continental shelf. Since then, sea level has risen at a rate of 15–30 centimeters (cm) per century, or higher (Kraft 1971). Sea level continues to influence South Carolina shoreline change by its documented rise of $\sim$ 24 cm in the past century (Hicks *et al.* 1983) and continuing evidence of a secular rise (Barth and Titus 1984).

Within the context of global sea–level rise, the second factor controlling shoreline position, at millennial scales, is sediment supply. With no change in sediment input, sea–level rise causes "erosion" by simple inundation of the coast, with the sea transgressing gradually over the land. But if sediment supply changes at the coast, the effect will be an acceleration or deceleration of erosion. Numerous second–order features called river deltas prove that the shoreline can keep pace with rising sea level in almost any tectonic setting, provided sediment supply is adequate. It is also recognized that a sudden cutoff in sediment supply (from natural changes in the course of a river or man–made structures such as dams) can cause the shoreline to recede faster than expected.

The scales of shoreline classification discussed so far are, for the most part, excessively long in human terms, although short in geologic time. They can be broadly classed as "meta" (Augustinus 1993) and are outside the practical limits of the present project.

The next level of coastal classification relates to the primary driving forces. Price (1955), Hayes (1964), Davies (1973) and others have investigated the distribution of winds, waves, and tides along the coast and their influence on the movement of sediment. In simple terms, the energy of waves and tides is thought to be most important in controlling the present

morphologic evolution of the coast (Hayes 1976). Davies (1973) divided the world's shorelines by tide range using the terms micro, meso, and macro to distinguish tide ranges of 0–2 m, 2–4 m, and > 4 m, respectively. Hayes (1979) used this breakdown along with a qualitative estimate of incident wave energy to explain major morphological differences along depositional shorelines of varying tidal energy. Hayes (1979) described microtidal shorelines as being dominated by barrier islands, with tidal inlets widely spaced. Mesotidal depositional shorelines, in comparison, contain a mix of short barrier islands and numerous, closely spaced tidal inlets. In macrotidal settings, inlets and shoals dominate and sand bodies tend to orient perpendicular to the strand line as a result of the dominance of tidal energy over wave energy (Hayes 1979). The terms micro, meso, and macro provide a useful reference for distinguishing broad types of barrier–island shorelines. As Hayes (1979) and others have shown, microtidal shorelines with low wave energy may contain short barrier islands and numerous tidal inlets; similarly, mesotidal shorelines with high wave energy may be dominated by long, thin (microtidal) barrier islands.

South Carolina's coast is mesotidal with "moderate" wave energy. Its depositional shoreline is dominated by mesotidal barrier islands, although along the Grand Strand, slightly lower tide ranges and higher–than–average (for the state) wave energy reduce the number and size of tidal inlets (Brown 1977). As tide range increases toward the Georgia border, inlets become larger and more closely spaced. Figure 2.1 shows the distribution of barrier islands and inlets in South Carolina. Numbering around 40 over a distance of 200 miles (330 km), the average barrier island is about 5 miles (8.3 km) long. As Brown (1977) and others have shown, the inlets and their associated sand bodies generally increase in size toward the Georgia border (Fig. 2.2).

Barrier island length and inlet size in South Carolina defines a scale of shorelines that some have classified as "mega" (Larson and Kraus 1993) or "macro" (Kana and Hayter 1992). In relation to their general presence and persistence, almost all South Carolina inlets and barrier islands are positionally stable over century (i.e., macroscale) time frames. Therefore, a small–scale map of the coast (similar to Fig. 2.1) is likely to look the same one or two hundred years from now. At macroscales, South Carolina's coast will remain dominated by mesotidal barrier islands and numerous tidal inlets, and most of the inlets will remain linked to the past, as sites of ancestral river channels which dissect the coastal plain. At macroscales, inlets may shift slightly and shorelines move by hundreds of meters. But this scale of change remains small in relation to macroscale coastal features.

Completing the spectrum of coastal change are the familiar scales we observe daily, yearly, or over a generation – microscale and mesoscale. These have become a focus of interest

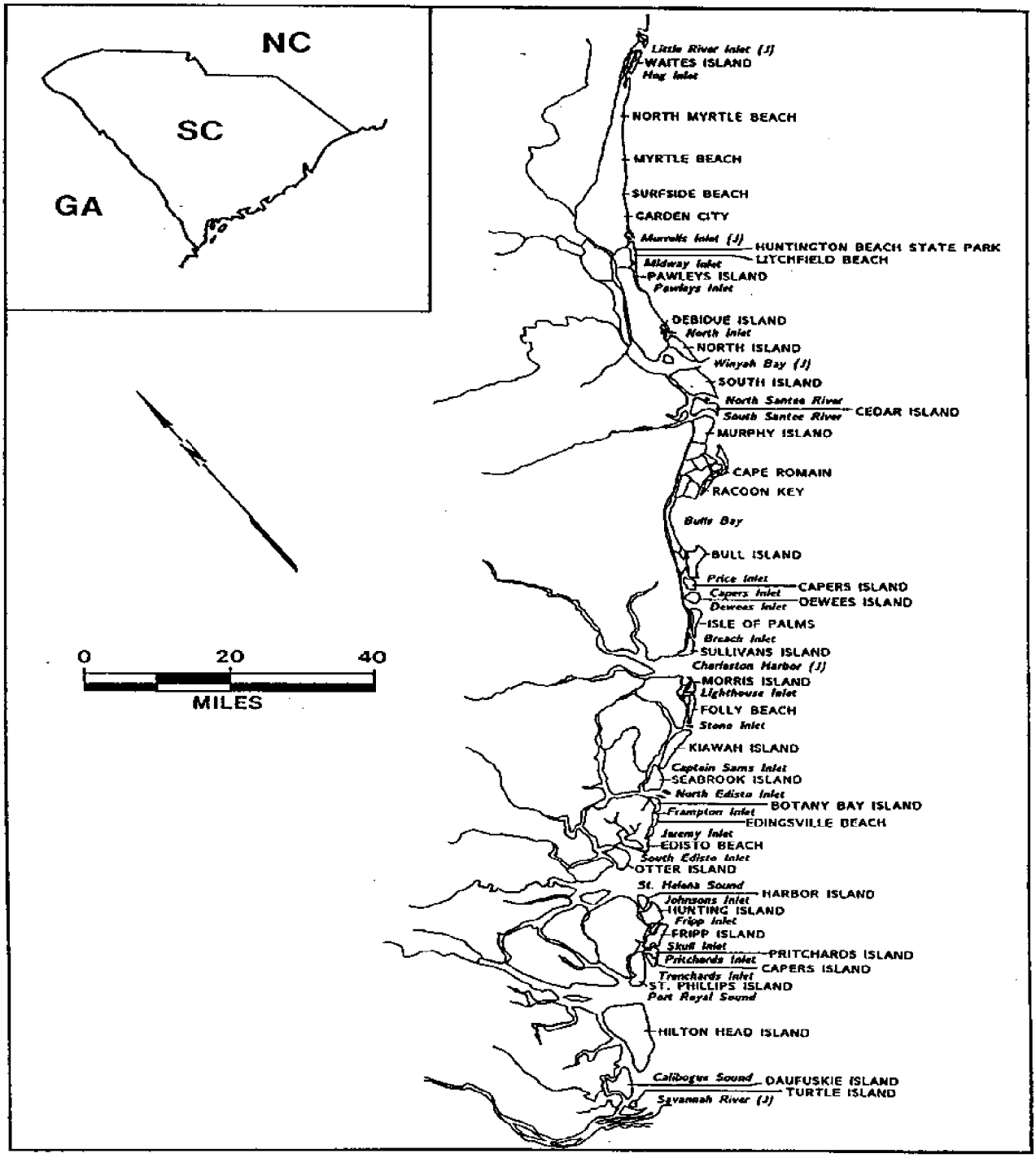


Figure 2.1 Beaches and inlets along the South Carolina coast. [From Kana 1989a]

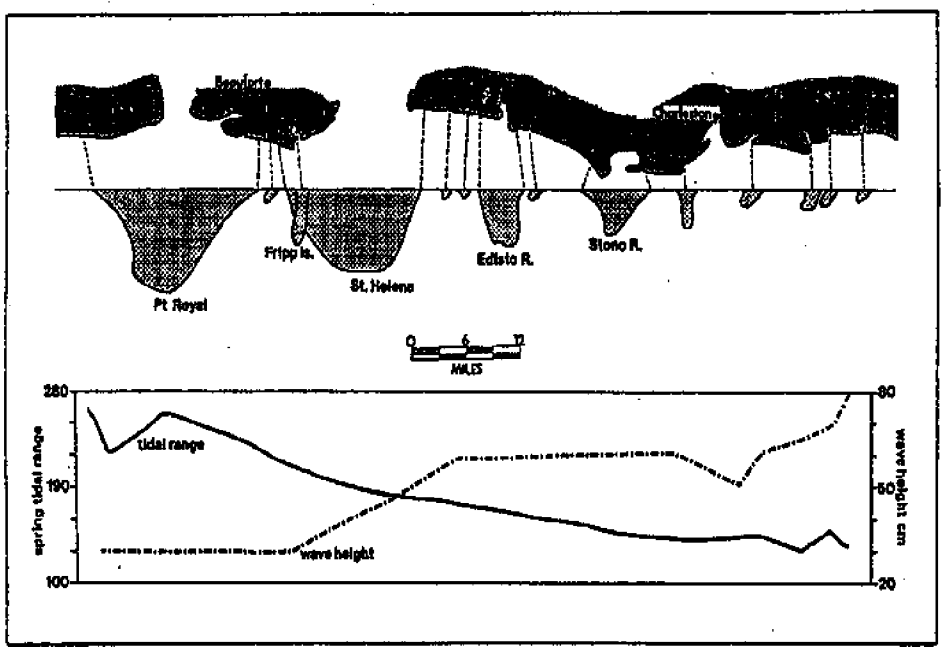


Figure 2.2 South Carolina inlets, tide range, wave height, and associated sand bodies. [From Brown 1977]

because they refer to the range of changes most likely to impact coastal development in the near future. Kana and Hayter (1992), Augustinus (1993) and others define mesoscale as time periods of a year to several decades and shoreline changes on the order of tens to hundreds of meters. Almost every erosion problem associated with coastal development today operates within this time and space frame. Along South Carolina's coast, shoreline change involving inlet migration (FitzGerald *et al.* 1978), shoal bypassing (Kana *et al.* 1985), dune ridge growth, washover formation, and inlet breaches occur at mesoscales.

Microscale coastal changes relate to much shorter period processes, including development of the beach profile, dune recession in storms, ridge and runnel evolution, movement of sedimentary bedforms, and longshore transport. Microscale changes occur in response to semi–diurnal movement of the tide, fortnightly variations in tide range, daily changes in wind and wave direction and magnitude, and in some cases, changes in river discharge at the coast.

The next sections describe in more detail the relationship of macro, meso, and microscale shoreline change and how the various scales must be considered in development of a mesoscale shoreline change model. Certain macroscale and mesoscale geomorphic (empirical) models are described and analyzed for their applicability to a mesoscale (predictive)

model. Numerous microscale models are then referenced and evaluated with respect to their suitability for scaling up to mesoscale.

## 2.B Macroscale Models

Several macroscale (conceptual) models have been proposed to explain and classify shorelines like South Carolina's. Hayes (1979), as previously mentioned, related barrier island morphology to tide range, assuming wave energy was approximately constant. Figs. 2.3–2.5 illustrate the general characteristics of micro, meso, and macrotidal coastal plain shorelines. Microtidal, medium–energy shorelines favor development of long, linear barrier islands with infrequent tidal inlets (Fig. 2.3). Washover features including washover fans into lagoons are common. Lagoons tend to be shallow and contain open, brackish water. At inlets, flood tidal deltas are large and are often coupled with washovers. Ebb–tidal deltas tend to be small or absent. The result along the ocean side is a relatively straight or broadly arcuate strandline with small–scale variations at the inlets.

Mesotidal barrier islands (Fig. 2.4) tend to be short and stubby, sometimes shaped like a drumstick (Hayes 1976) with a bulbous updrift end and recurved spit at the downdrift end. Tidal inlets are numerous with ebb–tidal deltas more prominent. Flood–tidal deltas are

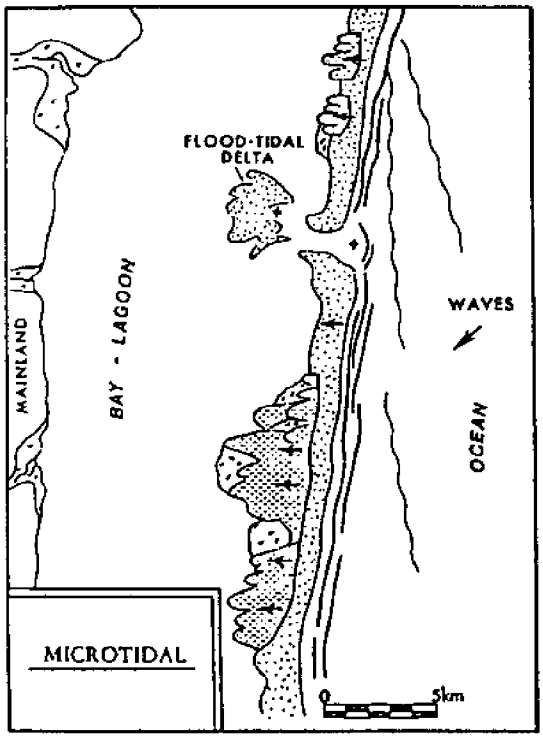


Figure 2.3 Hayes' (1979) morphologic model of a microtidal barrier island shoreline in a medium wave–energy setting. [From Hayes 1979]

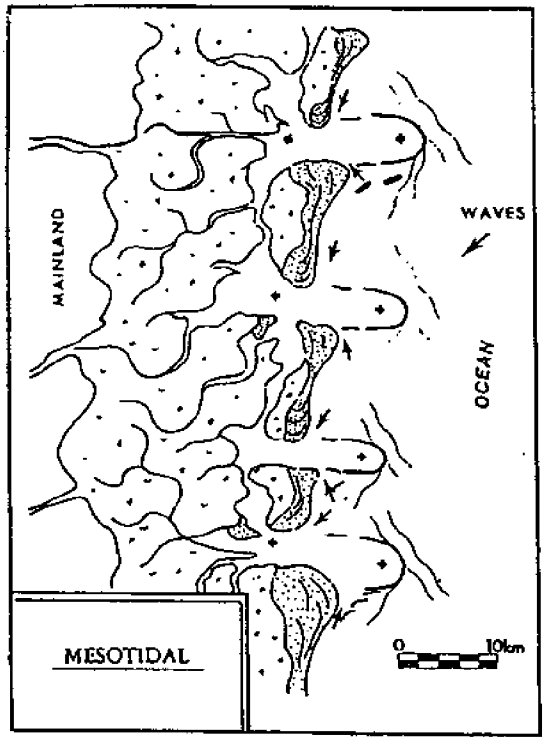


Figure 2.4 Typical mature mesotidal barrier island shoreline in a medium wave–energy setting with a marsh–filled lagoon and prominent ebb–tidal deltas. [From Hayes 1979]

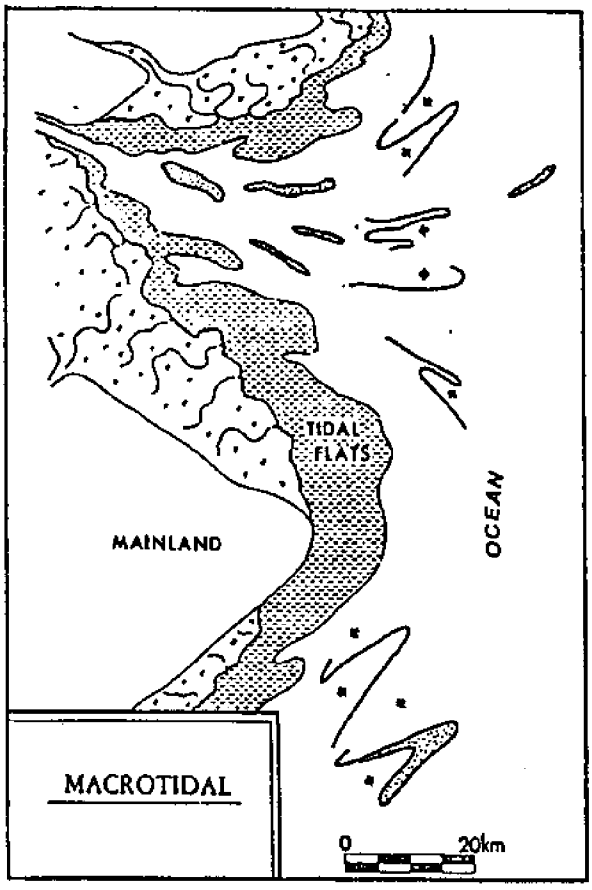


Figure 2.5 Hayes' (1979) model of a typical macrotidal shoreline in a medium wave–energy setting showing general absence of barrier islands. [From Hayes 1979]

generally smaller or absent, and lagoons are commonly filled with tidal marsh or exposed tidal flats at low tide. The strandline becomes more irregular along mesotidal coastal plain shorelines with offsets common between barrier islands. The downdrift offset between Dewees Island and the Isle of Palms is an example of the latter.

Macrotidal shorelines along the coastal plain (Fig. 2.5) tend to be dominated by open embayments and linear sand ridges oriented perpendicular to the strandline (parallel to tidal flows). In South Carolina, the closest approximation to this morphology occurs in St. Helena Sound south of Edisto Beach (Hayes 1976).

**Inlet Models**

Related to macroscale shoreline change models are empirical and geomorphic models of tidal inlets. Early studies related inlet formation, size, and persistence to a qualitative ratio

of tidal energy to longshore transport (Bruun and Gerritsen 1959). The size of inlets was shown to depend on the tidal prism available to maintain the channel (O'Brien 1969). O'Brien and other researchers (e.g., Jarrett 1976) developed empirical relationships between mean sea level cross–section at the inlet throat ($A_c$) and tidal prism ($T_p$) to compare the size of inlets. These regression relationships have the general form:

$$A_c = k\ T_p^x \tag{2.1}$$

where $k$ is an empirical constant varying from $7.75 \times 10^{-6}$ to $2.833 \times 10^{-4}$ and $x$ is a coefficient varying from 0.84 to 1.05. These ranges of values are derived independently for West Coast, Gulf Coast, and East Coast inlets (CERC 1984), using English or metric units for $T_p$ and $A_c$.

Another empirical model of tidal inlets relates to the size of ebb–tidal deltas. Walton and Adams (1976) proposed a relationship between delta volume ($\forall$) and tidal prism ($T_p$):

$$\forall = 13.8\ x\ 10^{-5}\ T_p^{1.23} \tag{2.2}$$

where the delta volume is in cubic yards, and $T_p$ is given in cubic feet. Walton and Adams (1976) found that U.S. ebb–tidal delta volumes range in size by over three orders of magnitude (Fig. 2.6).

The regional morphology of inlets, regardless of size, has been shown to fall into four characteristic planforms (Fig. 2.7) (Galvin 1971). Differences in morphology are qualitatively related to the ratio of longshore transport from one direction to the other. Inlets with a plentiful sediment supply and predominant transport direction may develop updrift or overlapping offsets, particularly if ebb–tidal deltas are small. Downdrift offsets (Fig. 2.7) develop where the updrift source of sand is small. Hayes *et al.* (1970) attributed downdrift offsets in natural inlets to the sheltering effect of large ebb–tidal deltas, as occurs at Dewees Inlet, whereby wave refraction reduces downdrift transport rates across the inlet or produces a transport reversal near the downdrift end of the inlet (Fig. 2.8).

Studies of tidal inlets have shown there are certain morphologic characteristics common to most. Hayes (1980) proposed a standard model for the morphology of ebb–tidal deltas and flood–tidal deltas (Figs. 2.9 and 2.10). Because they are rare in South Carolina, flood–tidal deltas are not discussed here. Hayes also proposed a geomorphic model for the updrift spit and channel margin complex which relates to the development of the ebb–tidal delta (Fig. 2.11). These models were developed from case studies which systematically identified net sediment transport directions from intertidal and subtidal bedforms (e.g., Hine (1975); Fig. 2.12) and, in

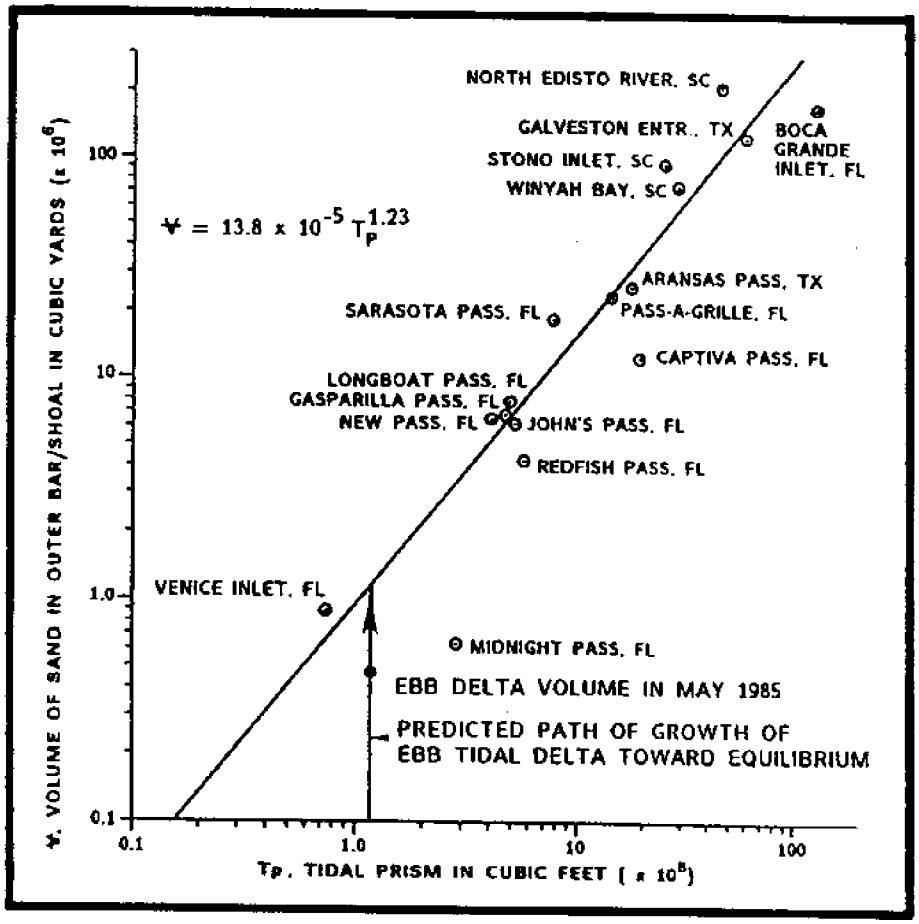


Figure 2.6 Regression surve of ebb–tidal delta volume versus tidal prism for mildly exposed coasts (after Walton and Adams 1976), including data from new Captain Sams Inlet. [From Kana and Mason 1988]

some cases, measured tidal discharge over a number of tidal cycles to confirm the net transport direction.

The morphology and patterns of sediment transport that these inlet models describe provide useful insight on the partitioning of sediment transport around inlets. As the diagram by Hine (1975) illustrates, the channels are dominated by tidally–driven currents. Shallow platform areas of the ebb–tidal delta are dominated by wave–driven currents. The principal direction of transport is further defined based on position within the ebb–tidal delta. In South Carolina and similar mesotidal settings, the main inlet channel contains ebb–oriented bedforms owing to the dominance of the ebb discharge from marsh–filled lagoons. Sediment supplied to the main ebb channel will be flushed seaward, fanning out and accumulating in seaward shoals as flow competency decreases. This produces a reverse gradient in bottom elevation along the channel in comparison to the usual gradient of foreshore profiles.

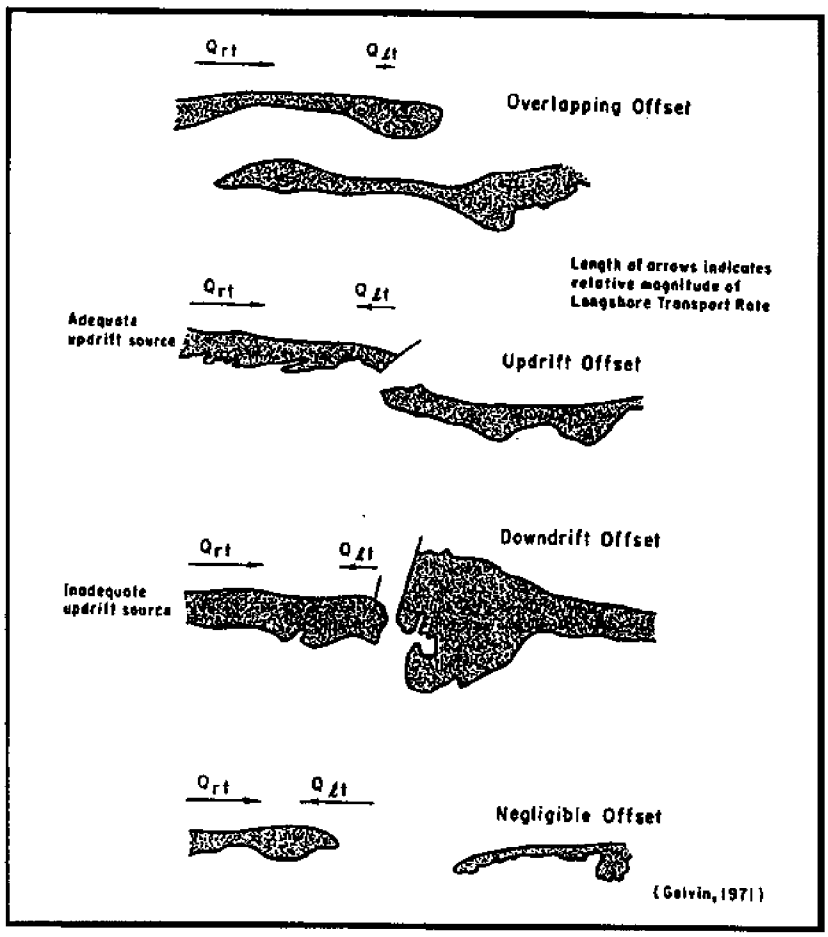


Figure 2.7 Four types of barrier–island offsets proposed by Galvin (1971). [From CERC 1984]

The terminus of the ebb–tidal delta occurs where ebb–tidal currents diminish to the sediment transport threshold. This distance offshore is also related to incident wave energy. As waves approach the shoreline, they refract and shoal before breaking in water depths approximating the wave height. Asymmetries in wave form before breaking and wave breaking produce landward–directed currents, driving sediment landward in opposition to the ebb flow. The result is a characteristic lobate development of the ebb–tidal delta with swash platforms forming to either side of the main ebb channel (Fig. 2.9) and the "terminal lobe" forming where ebb–tidal currents and incident wave–generated currents balance.

The sediment transport system in tidal inlets is completed by the combination of wave–generated longshore transport along the adjacent beaches which is usually directed toward the inlet because of sheltering effects inside the ebb–tidal delta. At the confluence of the barrier island and inlet, a secondary channel dominated by flood currents forms. Hayes (1980) refers to this as a marginal flood channel and explains its persistence based on time–velocity

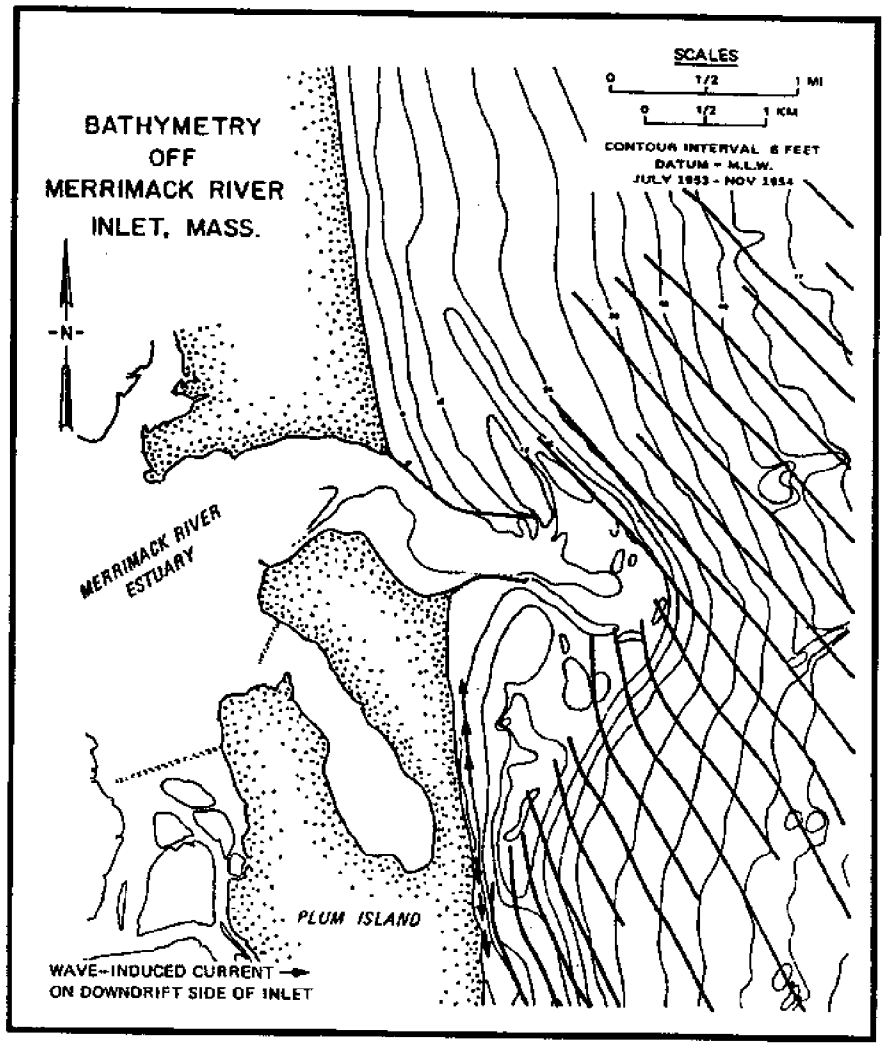


Figure 2.8 Wave refraction under northeast waves in vicinity of Merrimack Inlet, Massachusetts (after Hayes 1971). [From CERC 1984]

asymmetry of tidal currents in the channels (Fig. 2.13). Flow in marginal flood channels may be driven entirely by tidal hydraulics as demonstrated in wave basins where no waves are generated. However, if waves are present, oblique breaking toward the inlet in shallow water can enhance flood–directed flow. Therefore, the area around the marginal flood channel may be subject to some combination of tide–driven and wave–driven currents.

The foregoing sand circulation pattern around ebb–tidal deltas has been confirmed by FitzGerald *et al.* (1976) for Price Inlet, South Carolina (Fig. 2.14). This particular inlet is as close a match to the Hayes (1980) ebb–tidal delta model as any inlet in the United States.

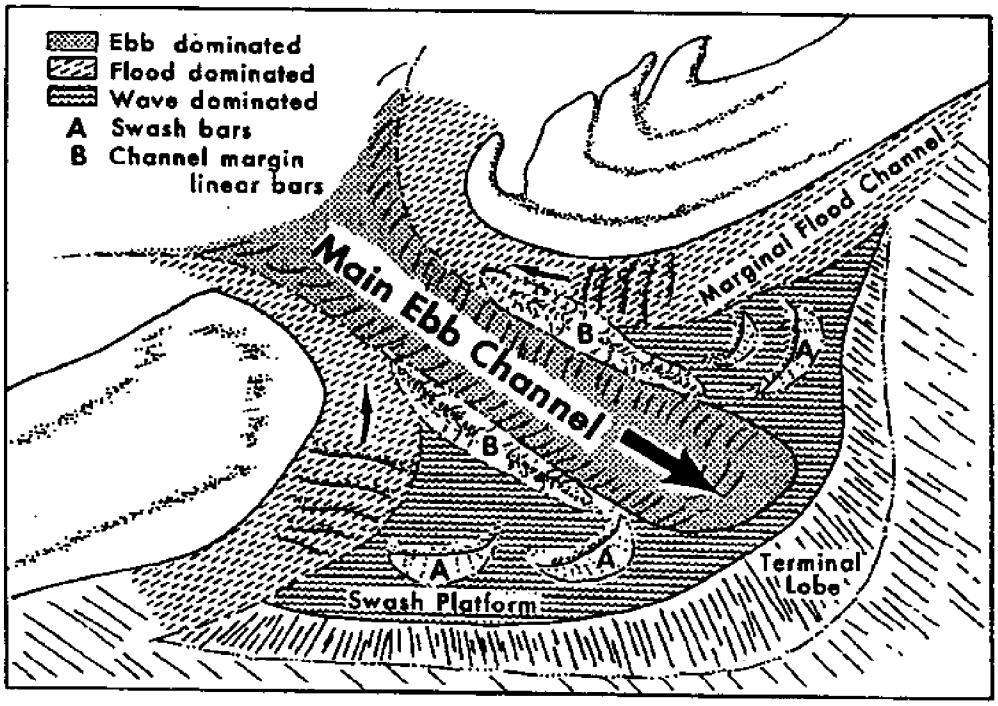


Figure 2.9 Typical ebb–tidal delta morphology (after Hayes 1979). Marginal flood channels separate the channel–margin linear bars from the adjacent beaches. [From FitzGerald *et al.* 1976]

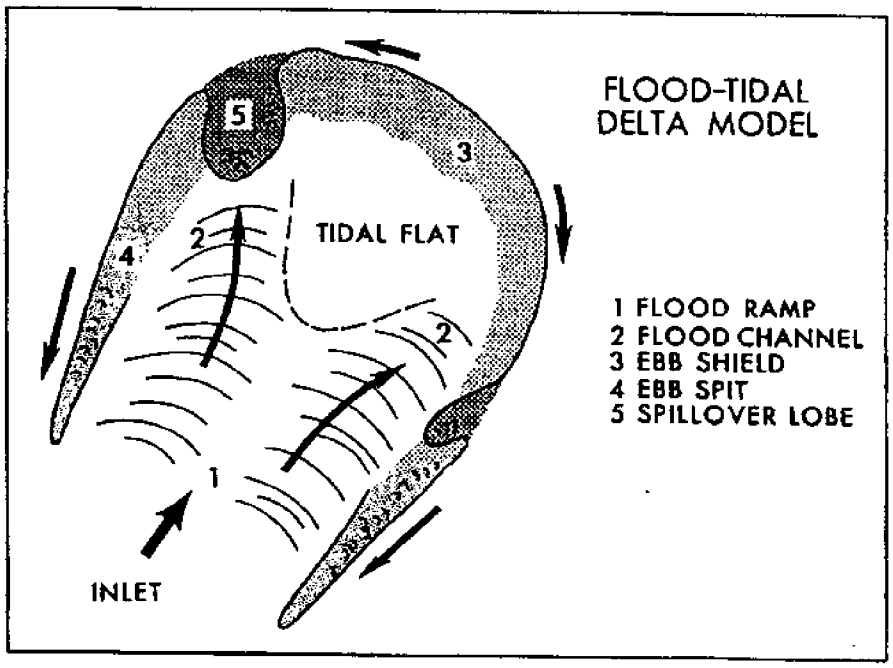


Figure 2.10 Hayes' (1979) model of morphology of flood–tidal deltas, showing the dominant direction of tidal currents. [From Hayes 1979]

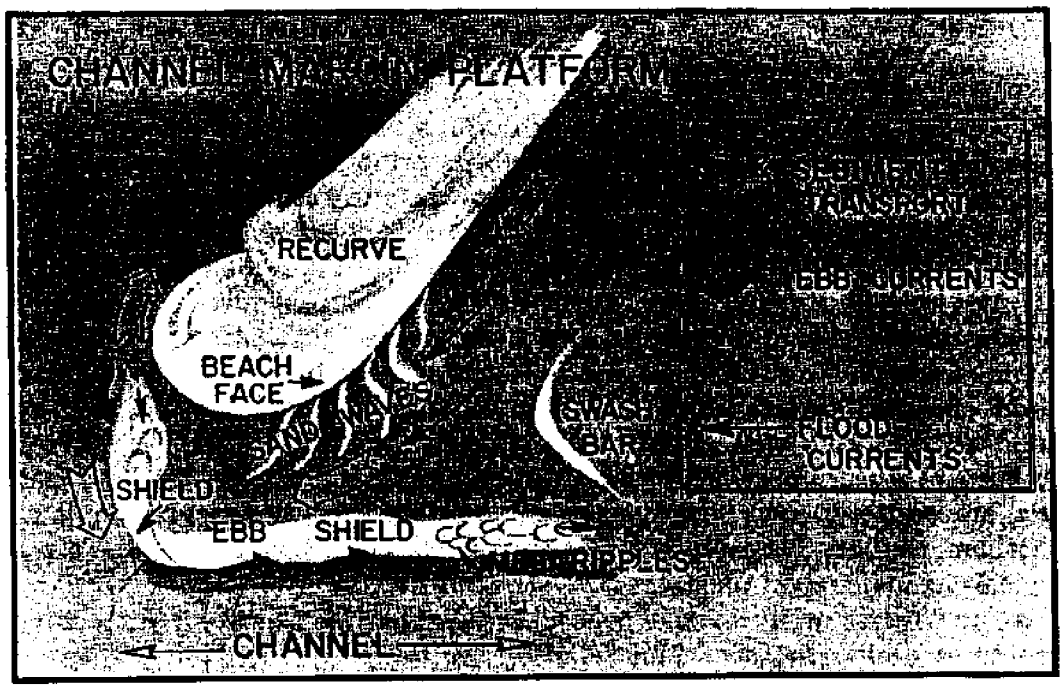


Figure 2.11 Sediment transport and morphology along recurved spits and channel margin platforms adjacent to inlets. [From Hayes 1979]

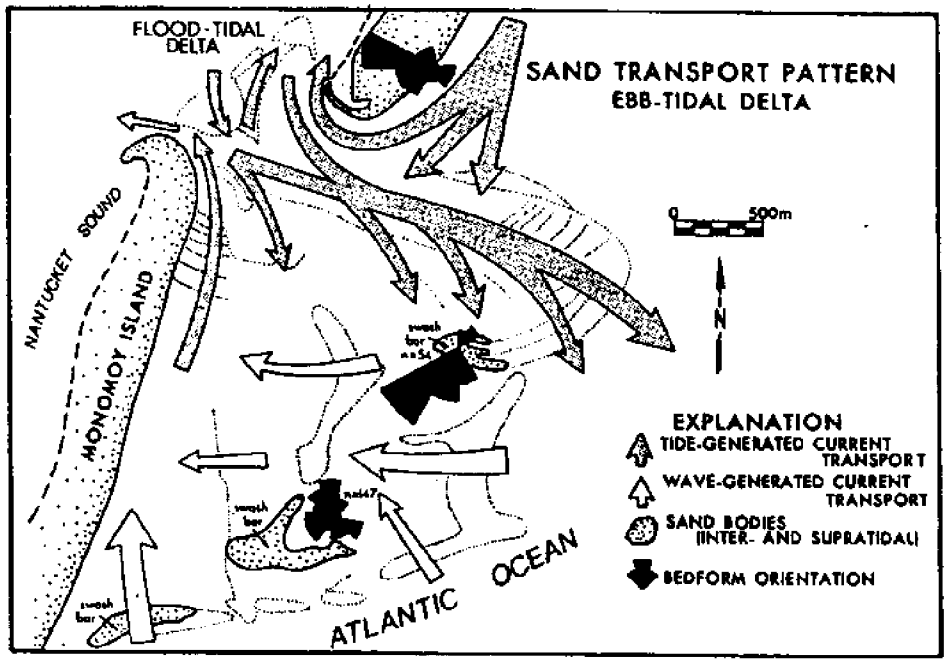


Figure 2.12 Net sand transport patterns of the Chatham Harbor (Massachusetts) inlet, based on studies of bedform orientation. [From Hine 1975]

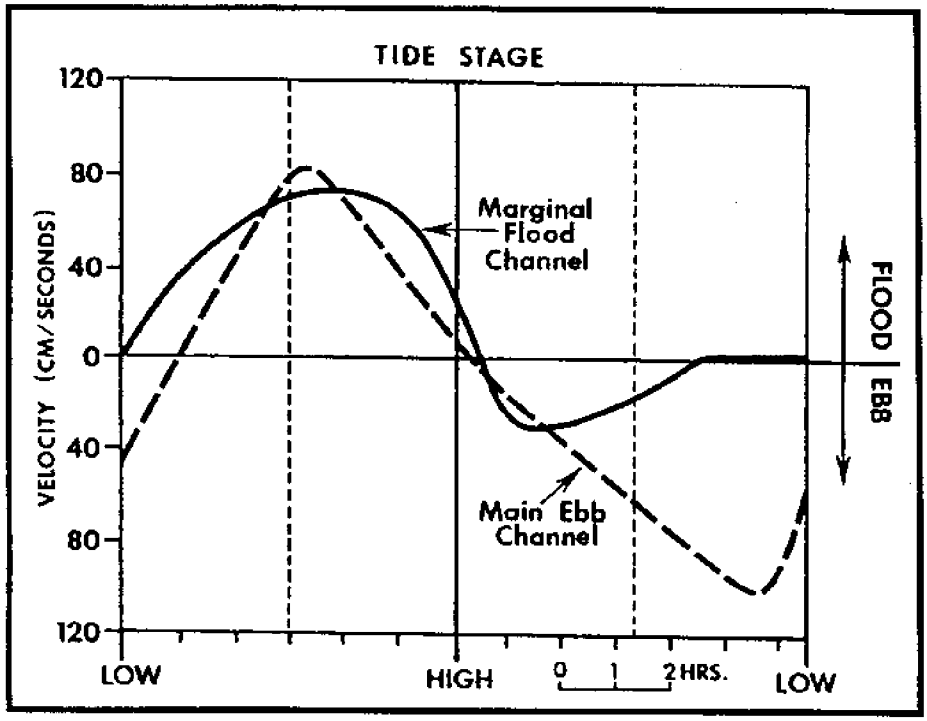


Figure 2.13 Typical tidal current, time–velocity curves for a main ebb channel (dashed line) and a marginal flood channel (solid line). Asymmetries in velocity and time with respect to the idealized tidal curve promotes a net sediment transport in each channel. [From Hayes 1976]

**Shoal Bypassing**

Since Bruun and Gerritsen's (1959) pioneering study on tidal inlets, scientists have recognized the importance of sand bypassing across inlets. In fact, maintenance of sand flow along the coast, whether by artificial or natural bypassing, has recently been incorporated into coastal zone management laws in some states (e.g., Florida). There remain questions regarding the exact nature of bypassing, how sediment actually crosses inlet channels, and how the rate of bypassing is controlled. Early researchers (e.g., Bruun and Gerritsen 1959) suggested a major pathway was the natural bridge formed by the outer shoal (terminal lobe). Longshore transport from updrift simply continued its flow around the delta terminus until it resumed transport along the downdrift beach. This may be the case for small inlets where the ebb–tidal delta is less prominent and continuous wave breaking occurs from the updrift to downdrift limits of the inlet (i.e., where the delta lobe merges with the foreshore).

However, around larger inlets, such channel crossover is considered unlikely. Deep, main ebb channels and ebb–tidal deltas extending several kilometers offshore form a natural barrier to bypassing. So for littoral transport to cross large or deep inlets, an alternate, more

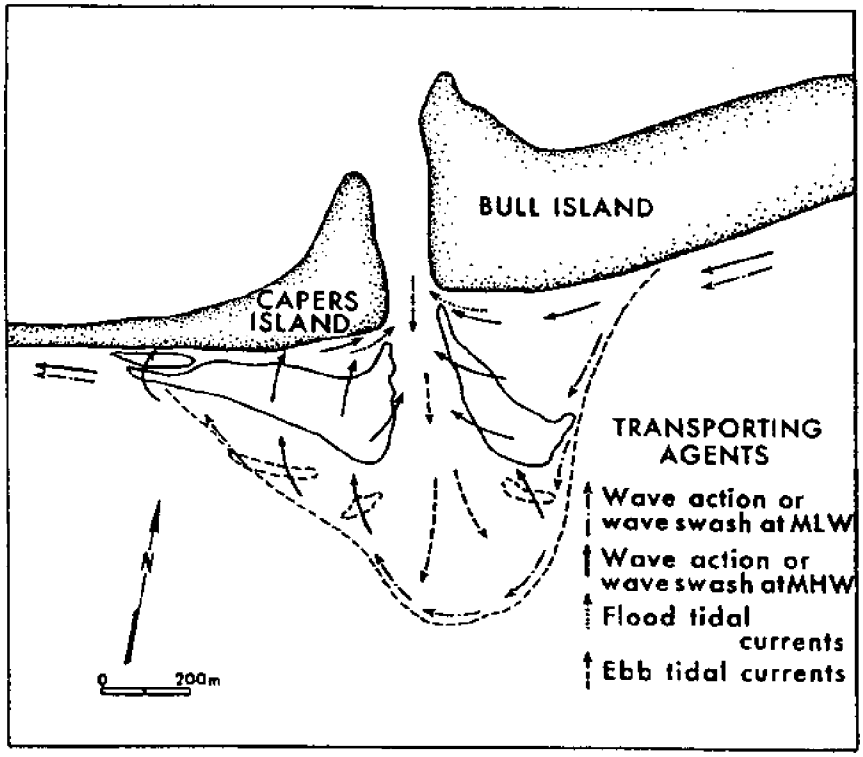


Figure 2.14 Sand–circulation pattern for Price Inlet, determined from wave refraction diagrams, littoral process measurements, bedform orientation, and inlet hydraulic data. [From FitzGerald *et al.* 1976]

circuitous route is required. The sand circulation patterns described by Hine (1975) and FitzGerald *et al.* (1976) provide evidence that sand bypassing is more commonly episodic. For sand to cross larger inlets, the ebb–tidal delta model (Hayes 1980) suggests it must first enter the main ebb channel by way of the updrift recurved spit and marginal flood channel. Once in the main ebb channel, sand will be flushed seaward and dispersed over the swash platform. If it reaches the downdrift swash platform, it can then move shoreward under breaking waves. Bypassing to the downdrift beach technically occurs when a swash platform attaches at some point along the beach downdrift of the inlet. In recognition of the episodic nature of this process, some researchers use the term shoal bypassing.

Sexton and Hayes (1983) documented shoal bypassing at Captain Sams Inlet, South Carolina, a small inlet with nearly attached terminal lobe of the ebb–tidal delta. At spring low tide, it is often possible to wade across the inlet about 0.5 km offshore over the terminal lobe. Sexton and Hayes (1983) showed that discrete, shoal–bypass events, one of which was triggered by re–channelization after a hurricane, accounted for rapid accretion of the downdrift beach. The sand volume in one bypass amounted to over 75,000 $m^3$ in this inlet, where the ebb–tidal

delta volume is of the order $10^6$ $m^3$ and the spring tidal prism is only about $3x10^6$ $m^3$ (Kana and Mason 1988).

Kana *et al.* (1985) and Williams and Kana (1987) documented two shoal bypass events downdrift of Dewees Inlet, both of which involved around $0.5x10^6$ $m^3$ of sand. In this mid–sized South Carolina inlet ($T_p \approx 10^8$ $m^3$), shoal bypassing occurred at a larger scale but over a longer period than at Captain Sams Inlet. Kana *et al.* (1983) documented a similar large–scale shoal bypass between the late 1970's and early 1980's at the east end of Kiawah Island. Figure 2.15 illustrates the shoal bypass sequence for Dewees Inlet/Isle of Palms. Kana *et al.* (1985) refer to three stages, as follows:

**Stage I** – *Offshore shoal "detaches"* from the swash platform or outer shoals of the inlet. Wave–breaking produces a characteristic crescent morphology with apex's pointing toward shore. Wave refraction around the shoal drives littoral transport into the lee of the shoal, initiating formation of a cuspate spit at the shoreline.

**Stage II** – *Shoal attaches* to the shoreline at each apex, temporarily trapping a large runnel. Waves continue to push the shoal shoreward and up the foreshore slope until it welds with the pre–attachment shoreface.

**Stage III** – *Shoal spreading* occurs as excess sediment accumulates in a bulge that becomes bounded by the shoreline. Waves break and disperse sand in either direction away from the point of attachment. The process is complete when the shoreline straightens or when there is little variation in profile changes at and adjacent to the zone of shoal bypassing. Observations of shoal bypassing by Kana *et al.* (1985) and others along South Carolina beaches suggest this process is common and exceedingly important. The volume of sand involved in some shoal bypasses is comparable to a large–scale nourishment project; therefore, the implications for nearby beaches are obvious.

The shoal bypass model (Kana *et al.* 1985) is further confirmed for South Carolina inlets by a project at Seabrook Island whereby Captain Sams Inlet was artificially relocated about 2 km updrift of its 1982 position. This February 1983 event (Kana 1989b) produced a complete bypass of the abandoned ebb–tidal delta. Four years after the cutting of a new inlet and closing of the old one, the entire ebb–tidal delta (greater than $10^6$ $m^3$) had migrated shoreward and attached to the downdrift beach.

Following inlet relocation, Kana and Mason (1988) developed a sediment budget for the new inlet. One goal was to document the rate of growth of the new ebb tidal delta. A secondary outcome of the study was the determination of the primary sediment sources

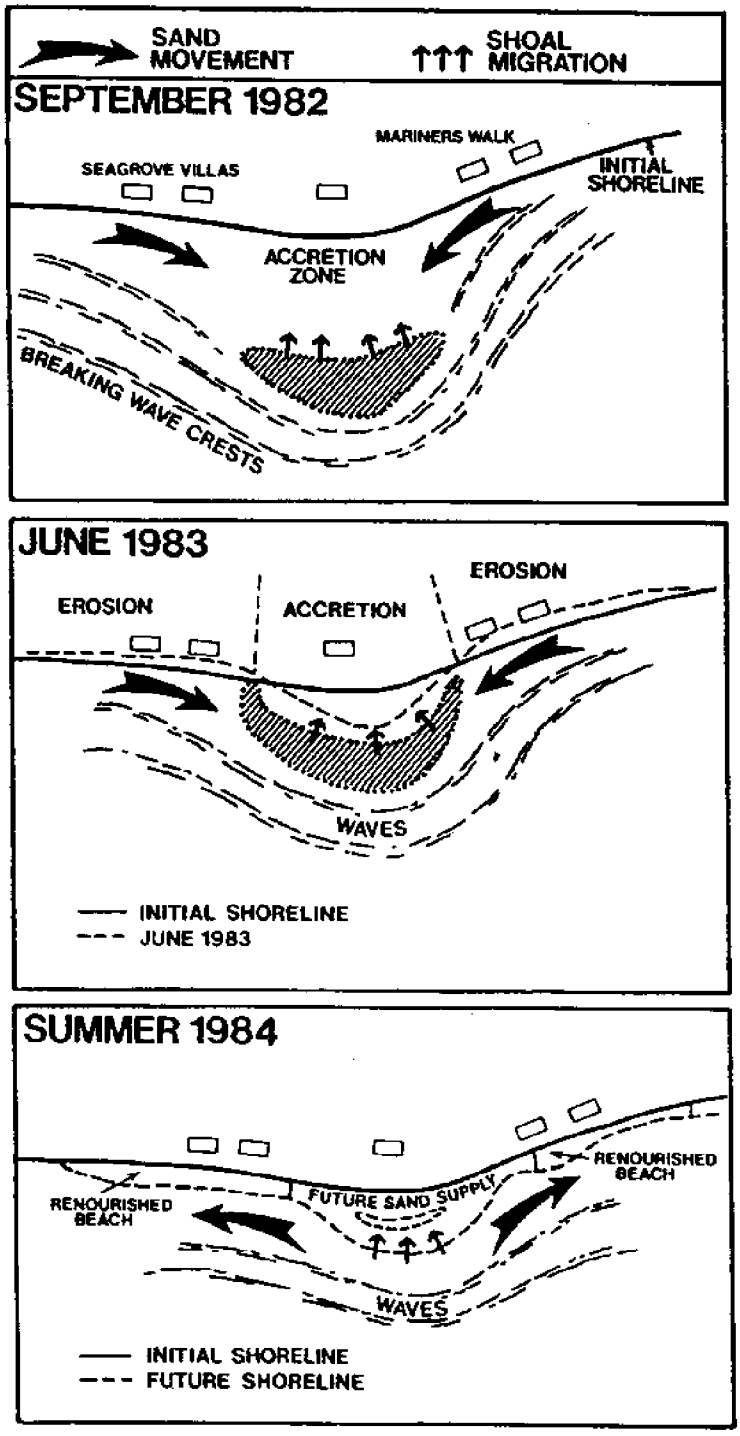


Figure 2.15 The three stages of shoal bypassing based on a case study at Dewees Inlet/Isle of Palms. [From Kana *et al.* 1985]

accounting for growth of the new delta. Figure 2.16 shows an annualized sediment budget for the first two years after inlet relocation. Despite the early stages of ebb–delta growth, sediment arriving from updrift was expended in forming the updrift recurved spit (G and A in Fig. 2.16).

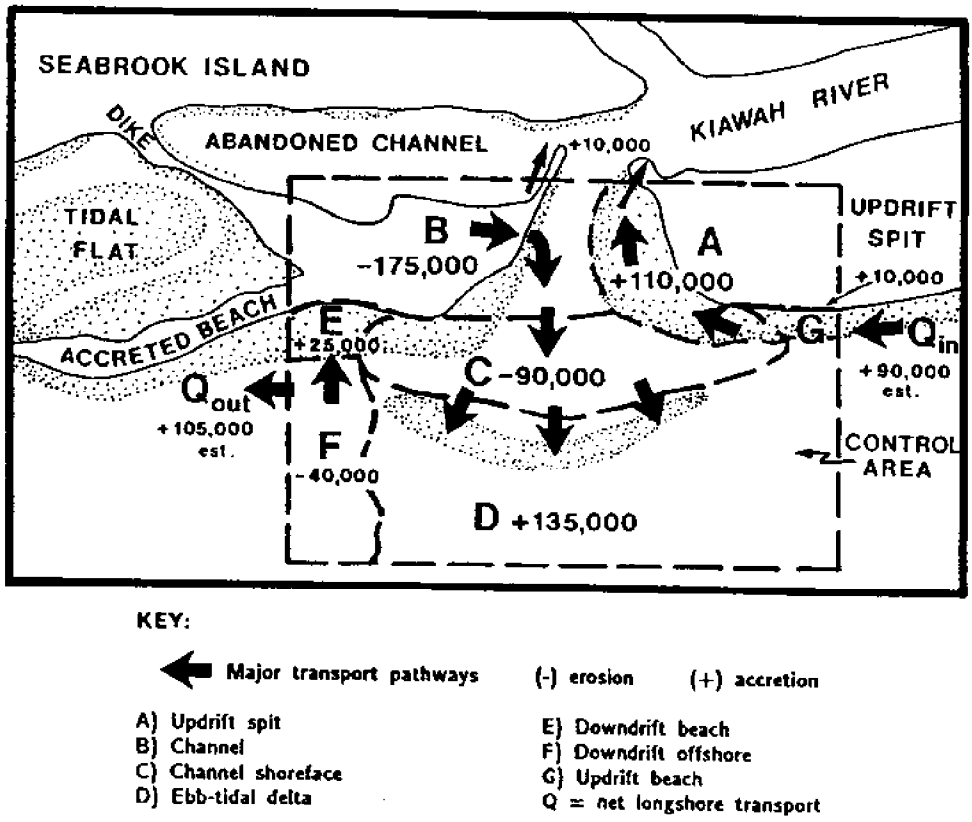


Figure 2.16 Annualized sediment budget for March 1983 to May 1985 following construction of new Captain Sams Inlet. All values are in $m^3/yr$. [From Kana and Mason 1988]

Erosion of the downdrift shoreline occurred as the updrift spit forced the main ebb channel downdrift. Volumetric growth of the ebb delta was accounted for by a combination of losses in the downdrift spit and erosion of the inner shoreface (volumes B and C). Shoal bypassing is also indicated along the downdrift shoreline between areas F and E (Fig. 2.16).

The Captain Sams Inlet 1983 – 1985 sediment budget demonstrated that sand bypassing at small inlets does not have to take the shortest route across an inlet. In fact, empirical evidence from many inlets now suggests sediment favors a more circuitous pathway, and transport becomes "partitioned" between wave–generated flows and tide–generated flows. Wave–generated sand transport predominates over shoals, along the beach face, and along recurved spits at the margins of inlets (i.e., in shallow water, high on the bathymetric profile). Tidal current generated transport predominates in the channels, is directed seaward only in the main ebb channel, and tends to occur lower on the bathymetric profile (Kana and Mason 1988).

**Simplified Conceptual Model of Inlets at Macroscale**

As a first step toward relating macroscale (conceptual) inlet models to mesoscale and microscale models, we have developed a simplified conceptual model of inlets (Fig. 2.17). This model is based on the previously referenced empirical studies and review of inlet morphology within the Georgia Bight, and provides a basis of identifying the primary driving forces and directions for sediment movement. A basic assumption is the dominance of ebb flows in the main channel which tend to flush sediments seaward. The model assumes flood tidal deltas are absent (a characteristic of most marsh–filled lagoons in South Carolina) and therefore the predominant sand bodies associated with the inlet are confined to the ocean side of the system. Four primary inlet domains are considered:

A – Main ebb channel
B – Ebb–tidal delta with broad swash platforms
C – Shoal bypassing zones
D – Recurved spits

**Domain A** in Fig. 2.17 is the main ebb channel (following Hayes' 1980 terminology), or the gorge as referenced by hydraulic engineers. Flow is controlled by tides and volumetric exchange (tidal prism, $T_p$) through the narrowest part of the inlet (the inlet throat, defined by cross–sectional area $A_c$), while the net transport is influenced by the asymmetry between the ebb and flood tides. Site–specific tidal hydrography data from North Inlet (Finley 1976; Nummedal and Humphries 1978), Price Inlet (FitzGerald *et al.* 1976), Captain Sams Inlet (Mason 1986), and others confirm a typical time–velocity asymmetry whereby the ebb flow is shorter in duration, but higher in magnitude than the flood. This velocity asymmetry produces an export of sediment on the ebb. Time asymmetry also occurs in the tidal flow (see Fig. 2.13) with peak ebb velocities occurring closer to the time of low water. This is related to increased channelization over the marsh as the tide falls (Nummedal and Humphries 1978), forcing more water into the channel toward the end of the ebb tide. Inertial effects produce a time lag between the predicted time of low water and the actual time of slack water in the inlet throat. As FitzGerald *et al.* (1976) report for Price Inlet, the sediment transport potential (a power function of current speed) is more than adequate to flush introduced sediment seaward. In this case, longshore transport reaching the inlet channel is much lower than the residual ebb transport rate. Domain A represents the beginning of the inlet sediment transport system.

**Domain B** represents the main body of the ebb–tidal delta. Others, including Finley (1976) and Walton and Adams (1976), have defined the limits of the ebb–tidal delta as the area of excess sediment seaward of the strandline above the level of the adjacent foreshore. This definition implies the delta volume can be computed from the difference between actual

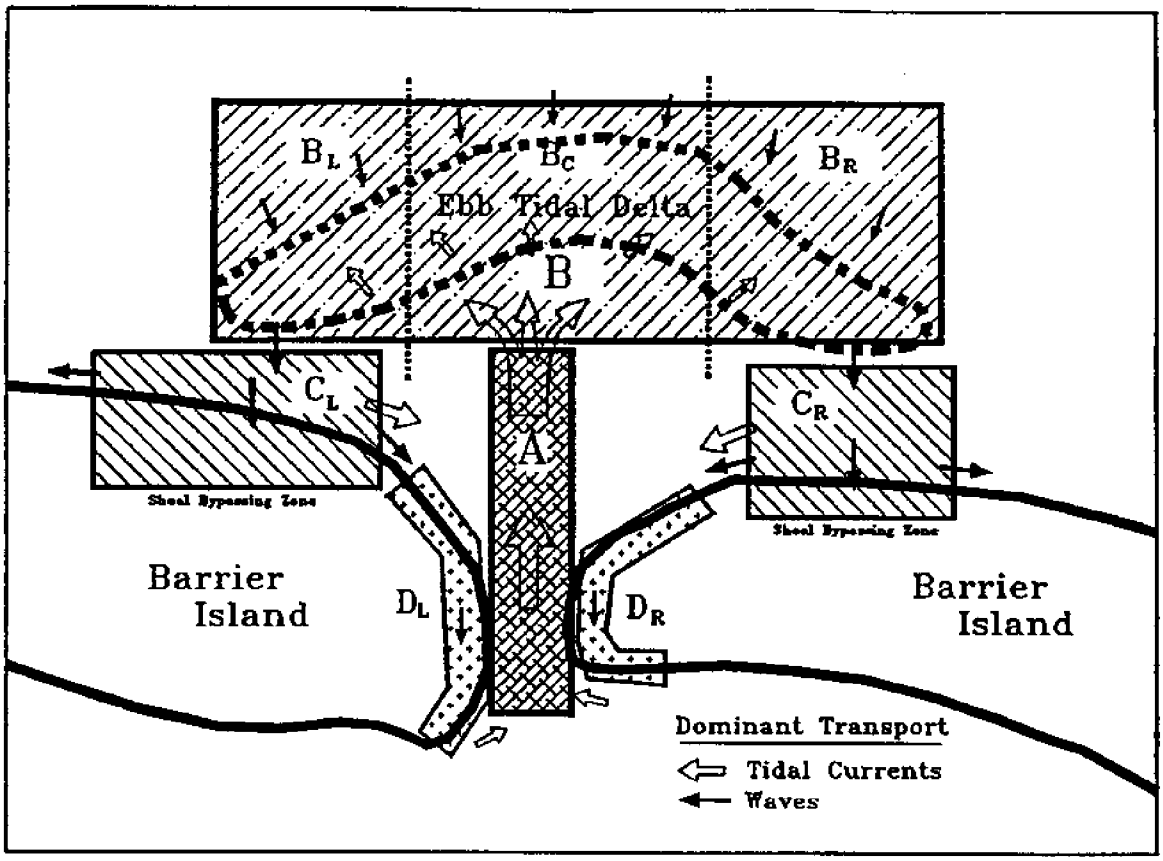


Figure 2.17 Simplified macroscale (conceptual) tidal inlet model for typical mesotidal settings showing principal model domains A–D.

bathymetry and the bathymetry that would exist if the inlet were absent and foreshore contours were straight, i.e., parallel to the coast. As sediment is flushed from Domain A to the ebb–tidal delta, tidal and wave–generated currents intersect. With the ebb discharge unconfined seaward of the throat, flow competency declines and sediment becomes dispersed in a characteristic lobate, fan–shaped deposit. A related characteristic of the deposit is its reverse slope which is counter to the hydraulic gradient and adjacent foreshore slope. The ebb–tidal delta terminates at a bathymetric high [the terminal lobe (Fig. 2.9) using Hayes' (1980) terminology].

It is generally recognized that the terminus of the delta is where tidally–generated currents on the ebb balance with wave–generated, landward flow. With a continuous supply of sediment, the delta expands and grows higher. But as this occurs, the incidence of wave–breaking increases. As Walton and Adams (1976) have shown, there tends to be some finite size limit to the ebb–tidal delta in relation to the tidal prism (Eq. 2.2). Observations at Price Inlet (FitzGerald 1984) suggest the size of the ebb–tidal delta can change in relation to yearly variations in wave energy. If more coastal storms occur in a given year, incident wave

energy increases and tends to push the terminus of the ebb–tidal delta shoreward. During years free of storms, ebb–directed tidal energy becomes more dominant, allowing seaward growth of the ebb–tidal delta. This empirical observation is confirmed by the regional increase in ebb–delta size into the Georgia Bight. Where wave energy is higher and tide range is lower, ebb–tidal delta size tends to be lower.

Within Domain B, variations in wave direction have the potential to shift sediment along–shore; therefore, the ebb–tidal delta can be subdivided into updrift, center, and downdrift areas as shown in Figure 2.17. An unstable, migrating inlet such as Captain Sams Inlet (Kana 1989b) will contain a larger part of the ebb–tidal delta in the downdrift one–third of Domain B. The extent to which the delta shoals "overextend" in the downdrift direction is related to the rate of sediment input from updrift which is driven by the longshore component of wave energy. Sediment may remain in Domain B for exceedingly long periods, particularly if the inlet is large. The principal sediment motion can be grossly described as "sloshing", whereby a particular shoal volume is maintained, but portions of the shoal shift within the domain with changes in wave direction and the ratio of tidal energy on the ebb and combined wave–tidal energy on the flood.

**Domain C** is generally situated along the flanks of the ebb–tidal delta and refers to the specific process of shoal bypassing. Landward transport dominates and the domain culminates with attachment of shoals at the shoreline. In Domain C, incident wave energy greatly exceeds ebb–directed tidal energy, allowing a portion of the ebb delta to "break off" and migrate toward shore. Empirical observations at Dewees Inlet suggest the onshore migration of shoals operating in Domain C can be rapid with migration rates exceeding 15 meters per month, once a portion of the shoal becomes emergent at low tide. Wave breaking over the shoal during a sustained portioned of the tidal cycle appears to be a prerequisite of shoal bypassing in Domain C. Presumably, the volume of sediment in a given shoal bypass is proportional to, but a fraction of the ebb tidal delta volume.

**Domain D** represents the foreshore along the adjacent beaches to either side of the inlet. Serving as a topographic boundary, the existing shoreline forces sediments arriving from Domain C to shift from onshore movement to shore–parallel movement along the beach. This transport is driven principally by obliquely breaking waves, with a secondary component due to flood currents which dominate in the marginal flood channels. Empirical data from Dewees Inlet (Kana and Dinnel 1980) confirm the completion of the inlet transport loop with sediment migrating along the recurved spit. CSE (1991) also documented longshore transport along the margin of North Edisto Inlet (Seabrook Island) in the flood (upstream) direction. Both of these cases lend support to the theory that sediment transport around inlets becomes partitioned

according to bathymetry (Kana and Mason 1988). Wave–generated transport dominates along the upper bathymetric profile, with incident waves propagating obliquely along recurved spits, driving sediment up–inlet as they break. Tidal current–generated transport dominates along the channel profile below breaker depths. Clearly, a part of Domain D represents sediment returning to the inlet for further recycling in the inlet transport loop. The remainder shifts away from the inlet and moves downcoast in the longshore transport system. For purposes of predicting impacts on the shoreline associated with bypassing, it is appropriate to assume one–half the shoal volume will shift back toward the inlet and the other half will shift away from the inlet. This sediment dispersion is likely to occur at a rate that decreases with time until the gradients in shoreline change (measured by profiles) become uniform updrift, downdrift, and at the point of shoal attachment. When this condition occurs, a new shoreline boundary is formed, one in which the foreshore is displaced seaward in proportion to the sediment volume gained from the shoal bypass. If no additional sediment is added to Domain D, this area becomes a "headland" source to the adjacent beach, at least until such time as a new cycle of shoal bypassing occurs. The frequency and magnitude of shoal bypassing in Domain C and the rate of advection in Domain D ultimately control the long–term evolution of the shoreline.

Modeling sediment transport from Domain A through Domain D is an ultimate goal of studies such as the present project. However, even this simplified conceptual model involves numerous uncertainties that must be resolved before formulating a deterministic model at mesoscales. The next section describes work in the area of microscale modeling of sediment transport and specific algorithms that are applicable to certain domains of tidal inlets.

## 2.C Microscale Models

Microscale numerical models are defined herein as simulating a spatial range of 1 to 10 km and a time range of days to months. Some such models have been developed to predict the bathymetric changes in the vicinity of tidal inlets. Most microscale models are two–dimensional, depth–averaged models. Generally, these types of models consider the effects of waves and tides on the sediment transport and consist of several sub–models such as a hydrodynamic model, a wave model, and a sediment transport model. The major limitation of the microscale model is that it is not suitable for simulations of long–term (years to decades) bathymetric changes due to its relatively small time step (seconds to minutes). The following is a description of some models used for prediction of coastal sediment transport and, in some cases, evolution of tidal inlets.

The CWSTM–H model (Veeramachaneni and Hayter 1988) was developed for prediction of cohesionless sediment transport at tidal inlets due to the combined action of waves and currents. The CWSTM–H model consists of three modules: hydrodynamics (specifically,

shallow water barotropic flow), wave transformation, and cohesionless sediment transport. The flow module, semi–coupled to the wave transformation module, is used to calculate the barotropic flow field in the vicinity of tidal inlets. The hydrodynamic module solves the depth–averaged shallow water wave equations using a finite element scheme. The wave module simulates refraction and shoaling of small amplitude gravity waves. A wave ray method is used to obtain the direction, wave length, and wave height throughout the domain. The sediment transport module calculates bed load transport induced by the flow field using an empirical procedure developed by Vincent *et al.* (1981). CWSTM–H has been used to simulate a prototype–scale hypothetical inlet system (Veeramachaneni and Hayter 1988), and is currently being used to model Murrell's Inlet, South Carolina.

Vemulakonda *et al.* (1988) developed the Coastal and Inlet Processes (CIP) modeling system to numerically simulate the sediment transport at tidal inlets. This system consists of a series of models for tides and storm surge, waves, wave–induced currents and setup, and non–cohesive sediment transport. For tidal and storm surge computation, a long wave model known as WIFM (Butler 1980) is used. This model employs an alternating direction, implicit, finite–difference scheme. The monochromatic wave transformation model of Ebersole (1985) considers combined refraction and diffraction via the "mild slope" equation. Wave climate in deep water or at the offshore boundary of the numerical grid is given. The model computes wave height, wave length and wave direction at discrete points throughout the domain. In the surf zone, the model of Dally *et al.* (1984) is used to calculate wave transformation. The sediment transport model considers noncohesive sediments. Two regions, the open coast region away from the tidal inlet and the region in the vicinity of the tidal inlet, are delineated for sediment transport computations because of different properties of sediment transport in these two regions. The open coast region is further divided into two zones, the area within the surf zone and the area beyond the surf zone. Within the surf zone, wave breaking and the resulting energy dissipation play a dominant role in sediment transport. The approach of Bagnold (1963, 1966) is used in this zone. Beyond the surf zone, the tractive force of the currents causes the sediment transport. Thus, the method of Ackers and White (1973) is followed after appropriate modification for the presence of waves. In the region near the inlet, the flow and bathymetry are highly complicated. Tidal currents are a major mechanism comparable to wave–induced currents. Here, the method of Ackers and White (1973) is also used to compute the transport. The CIP model can simulate the details of bathymetric change over time at tidal inlets. However, the CIP model is limited to the simulation of relatively short–term events due to the fact that the current model requires a relatively small time step to maintain stability in the model.

The CIP system has been applied to two inlets, St. Marys Inlet, Florida (Vemulakonda and Scheffner 1988), and Oregon Inlet, North Carolina.

Vincent (1992) developed a two–dimensional, finite–difference, depth–averaged numerical model (USF SCOUR model) for predicting sediment transport in a tidal inlet. Vincent's model consists of two sub–models, a hydrodynamic model and a sediment transport model. The hydrodynamic model computes tidal and wave–induced currents. Through scaling the transport up or down, this model considers the effects of contraction and expansion from subgrid features such as pilings or channels on the effective area of flow between adjacent grids. In the sediment transport model, the Engelund and Hansen (1967) equation for total sediment load is selected for the computation of sediment transport due to its successful uses in tidal inlet modeling (Vincent 1992; Zarillo and Park 1987) and high recommendation based on comparison to other formulas. Vincent's model accounts for the contributions to sediment transport from the actions of waves and currents, but does not include the interaction of waves and currents. The model was applied to Johns Pass, Florida, and the simulated hydrodynamics and sediment transport trends were in general agreement with documented observations. Vincent's model is limited to simulation of short–term changes at tidal inlets due to a small computational time step. For Johns Pass, the length of the simulation was 14 days and the computational time step used was 1.5 seconds.

Andersen *et al.* (1988) developed a two–dimensional, morphological model to describe the erosion/deposition pattern from man–made changes such as the introduction of structures or dredging in an area under combined wave and current action. The model simulates the morphological evolution in the area beyond the surf zone where the sediment transport is driven by the combination of waves and currents rather than breaking waves. The two sub–models, the hydrodynamic model and the wave model, are not directly coupled. The model presents the methodology which makes it feasible to predict the bathymetric changes for relatively long time durations up to 32 months. The procedure used in the model is the following: after the hydrodynamic calculations are updated, the bathymetry used in updating the hydrodynamics is re–calculated based on both the new and former hydrodynamics. The rate of change in the hydrodynamic field is then extrapolated to predict the bathymetry at a given later time. This method implies that a linear relationship between hydrodynamics and bathymetric change exists. Thus, a sensitivity analysis is needed to determine the proper time step for calculation of bathymetric changes. The model has been used to predict the morphological evolution at a cooling water intake.

A simulation system (Maruyama and Takagi 1988) has been developed to predict the nearshore sediment transport under the coupling of sea bottom topography, waves and currents.

This system consists of three sub–models: wave propagation, nearshore current induced only by waves, and bathymetric change due to currents. This system does not consider currents induced by tides. Current induced wave refraction is also neglected. In the current model, the radiation stress due to waves is considered. The bottom friction equation by Nishimura (1982) is used when waves and currents coexist. In the topography model the continuity equation with diffusion by Watanabe *et al.* (1984) is employed. The sediment transport rate formula by Tanaka and Shuto (1981) is suitable for the case of coexisting waves and currents as used in the system. To save computing time, different grids for wave and current calculations are used. The model simulation time is on the order of ten days.

The GENESIS model (Hansen and Kraus 1989) was developed to simulate shoreline change produced by longshore sediment transport gradients at the coast over a large range of space and time. The longshore extent of a typical modeled reach can be 1 to 100 km, and the time frame of a simulation can be 1 to 100 months. GENESIS is usually used to calculate the shoreline change resulting from placement of coastal structures such as groins, jetties, detached breakwaters and seawalls as well as beach fills. The fundamental assumption of this model is that the shape of the beach profile does not change. Thus, one contour can describe the change of the beach and volume. This is called an "one–line model". The basic assumptions of the GENESIS model make it flexible and simple to use in the simulation of shoreline change. However, the GENESIS model is not suitable for the simulation of tidal inlet systems because the model is developed only to describe longshore sediment transport by incident waves well away from tidal inlets.

The SBEACH model (Larson and Kraus 1989b) was developed to simulate the storm–induced changes in beach profiles. SBEACH describes the cross shore sediment transport and assumes that the gradient of the longshore sediment transport rate is negligible for the beach away from coastal structures and, as a result, is not appropriate for use near a tidal inlet. The other basic assumptions of the model are that beach profile change is mainly governed by breaking, short–period waves, and that an equilibrium beach profile will result if forcing is held constant for infinite time. The SBEACH model consists mainly of two parts, a wave model and a sediment transport model. The wave model calculates wave height and setup within the surf zone (Dally *et al.* 1985). The sediment transport rate is calculated using different relationships for different portions of the surf zone. The transport rate formulas are obtained from the results of prototype–scale laboratory experiments, i.e., large wave tank experiments, which are a reproduction of near–prototype conditions. The mass conservation equation is applied to compute the beach profile change. The finite difference approach is used in the model. The SBEACH model can give good results for the situations dominated by

cross–shore transport. However, it is not suitable for application when appreciable longshore gradients of longshore sediment transport exits, as is common near a tidal inlet.

### 2.D Mesoscale models

De Vriend *et al.* (1993), Stive and De Vriend (1995) summarize approaches to numerical modeling of long–term coastal evolution based on their research and others. These approaches classified as input reduction, model reduction and behavior oriented modeling, are discussed. They conclude that a key element in the long–term coastal behavior is reduction. Among three approaches, the input reduction technique, i.e., input filter technique, is used more often than other two. Examples are given below.

Steijn *et al.* (1989) developed a numerical model for simulation of morphological evolution in the coastal environment. The Steijn *et al.* model consists of a wave model, a current model and sediment transport model. The wave model, named HISWA, takes into account the effects of refraction due to depth and currents, and diffraction. Wave breaking is also considered. The current model, based on the WAQUA–code, is applied to compute currents induced by waves and tides. A curvilinear grid is used for a good representation of simulated geometry. The sediment transport model is called COMOR. Several transport formulae such as Bailard, CERC, Bijker or van Rijn, can be used in model. But, among these formulas, only the Bailard formula can account for both cross–shore and longshore transport. In order to reduce computational effort and allow the model to run for a longer time, a technique of schematization of input data is introduced. This results in a limited number of representative sets of input data for the model, each with its own weight factor. Thus, the computational effort is reduced greatly and it becomes feasible to simulate long–term coastal morphological changes.

Similar to the Steijn *et al.* (1989) technique of input reduction, Latteux (1987, 1992, 1995) proposes techniques for the selection of representative tides and evaluates their accuracy.

Chesher *et al.* (1995) described the HR Wallingford coastal area model, PISCES. This model contains three constituent submodules: wave propagation, current distribution and sediment transport and morphological updating. The PISCES model is restricted in its applicability to relatively short– and medium–term simulations, and does not yet handle long–term changes. To enable practical application, input filtering and process filtering are suggested. In the application of Keta Lagoon connecting the Gulf of Guinea at Keta, Ghana, the process filtering technique in the form of calculation of residual sediment transport induced by tides is applied. The implied assumption is that the processes that cause the bed changes within tidal cycle do not affect the longer–term evolution. The simulation of bathymetry over 500 tidal cycles (i.e., about 9 months) has been done. The comparison with physical model data

of an one year simulation was made. As another application example, detached breakwater case is simulated. An innovative method is developed in order to extend the applicability of the model to the long–term. Using PISCES process–based model, the trend in the bathymetric changes during the initial stage of the morphological simulation is identified. Then, time–history bed profiles over this period are fitted to an exponential function and future bed changes are extrapolated. The bathymetry results after 300 hours using the extrapolation approach are compared with the results from the PISCES model with full morphodynamic updating method. The accuracy of this approach depends on how far the bathymetry will be extrapolated. This approach exhibits promise for long–term simulations and should be tested further.

The model reduction technique primarily is used to reduce the number of calls for relatively expensive models (flow and wave) such as Broker *et al.* (1995) model. Broker *et al.* (1995) addressed a model system for modeling of coastal morphology and the method extending its applicability to long–term. The long–term approaches focus on the hydrodynamic model, a submodel of the modeling complex. The procedure is (1) "warm up" the hydrodynamic model and calculate the sediment transport field and the bed level change rates; (2) run hydrodynamic model for a period of time corresponding to a so–called "morphological time step"; (3) re–calculate sediment transport field based on updated bathymetry within the morphological time step; (4) compute wave field every k morphological time steps, where k is a arbitrary integer. In this modeling complex, there are three types of wave models: elliptic mild–slope; parabolic mild–slope; and a spectral nearshore wind–wave model. This model complex is applied to a systematic study of the morphological response to shore–parallel breakwaters.

# III. DATA REQUIREMENTS AND AVAILABILITY

The primary prototype data available to test a mesoscale model of South Carolina inlets consists of topographic and bathymetric surveys. In general, there is negligible process data, other than tide records at selected stations and daily/hourly observations of winds from which waves can be hindcast. Tidal cycle hydrographies have been completed over 13– to 15–hour periods at several inlets, including North Inlet, Price Inlet, and Captain Sams Inlet. These data yield insight on the distortion of the tide through the inlet, but do not provide extended, time–series data for driving a true deterministic model. The following is a general summary of data and field studies that offer relevant information, categorized by inlet.

**Murrell's Inlet – Primary Reference: Douglass (1987).** Studies in connection with the 1977–1980 construction of jetties at Murrell's Inlet included controlled surveys, pre– and post–construction beach surveys, inlet bathymetry, aerial photography, visual wave observations, and sporadic time–series wave data over one year from a wave–rider buoy several kilometers offshore. This study documented volumetric growth of the ebb–tidal delta after jetty completion and the onshore movement of abandoned shoals adjacent to the new inlet. Through forced channelization, portions of the natural ebb–tidal delta (Domain B) were released from the delta and driven shoreward as a discrete shoal bypass event (Domain C). Other data developed in this federal project included estimates of longshore transport from LEO (littoral environment observation) data for the period 1979–1982. Spot measurements of current speeds were taken in the inlet throat section on several occasions, but not for full tidal cycles. The Douglass (1987) study is one of the few inlet studies in South Carolina that attempts to integrate process and morphological data and develop a sediment budget. As such, it is an important and useful data set. Original survey data, synthesized in the report, should be available from the USACE–CERC.

**North Inlet – Primary References: Finley (1976), Nummedal and Humphries (1978).** North Inlet was the site of a three–year study under CERC's GITI (General Investigation of Tidal Inlets) Program. Researchers from the University of South Carolina conducted periodic field surveys that included:

- Tidal cycle hydrographies in the inlet channel.
- Beach profiles (non–reproducible).
- Bathymetric surveys.
- LEO wave data.
- Synoptic wind measurements.
- Aerial photography.

Bathymetric surveys and beach profiles are not as high quality as the Douglass (1987) Murrell's Inlet study, but the tidal cycle hydrographies offer some of the best data in South Carolina relating to inlet flow and tidal prism. These data are most relevant to Domain A and help explain the ebb dominance of mid–sized, unjettied South Carolina inlets.

**Price Inlet – Primary Reference: FitzGerald (1984).** Price Inlet was the site of a three–year USC study sponsored by the U.S. Army Research Office between 1975 and 1977. FitzGerald (1984) conducted at least 12 tidal cycle hydrographies and numerous inlet section surveys, documenting minor changes in $A_c$ as a function of tide range. Uncontrolled "pace and brunton" maps of the swash platform were made periodically to document the gross morphology of intertidal shoals in the ebb–tidal delta. These data provide qualitative evidence of ebb–tidal delta growth and erosion and onshore movement of the swash platform. Longshore transport estimates were developed for the adjacent beaches by Kana (1977).

**Dewees Inlet – Primary Reference: Kana and Dinnel (1980).** In a privately funded study, Kana and Dinnel (1980) surveyed Dewees Inlet and developed a controlled map of the shoals. The focus of the study was on erosion along the downdrift inlet margin, so the study makes specific reference to conditions within a limited reach. The study used LEO measurements to estimate longshore transport and spot hydrography measurements to monitor currents in the main ebb channel. Kana and Dinnel identified a transport loop producing landward–directed transport along the inlet margin (Domain D). The study provides a limited analysis of processes and only one set of beach and nearshore profiles.

**Breach Inlet – Primary Reference: Nelligan (1982).** This USC Master's thesis provided a detailed analysis of surficial sediments and morphological changes at Breach Inlet, a small inlet between the Isle of Palms and Sullivans Island, which is partially stabilized by a revetment along the downdrift (Sullivans Island) side. The inlet is characterized by extreme overextension of the updrift swash platform and frequent (almost yearly) shoal bypassing to the downdrift beach. Surveys lack control but the small size of the inlet and certain fixed structures such as a bridge, the revetment and several short groins provide reference for positioning Nelligan's maps and superimposing them on a more accurate map. Vibracores (28) and grab samples (100) provide one of the most detailed South Carolina data sets on ebb–tidal delta sediment textures. Uncontrolled profiles between July 1981 and February 1982 define the extent and mitigation of the swash platform during the period.

**Stono Inlet – Primary References: USACE (1977), Kana *et al.* (1981).** Limited bathymetric studies have been performed at Stono Inlet and Folly River, one of the tributaries to the inlet. The USACE (1977) study contains section data for Folly River. Some of these data may be compared with preconstruction surveys before the 1992 Folly Beach nourishment

project. Kana *et al.* (1981) completed 26 uncontrolled sections (referencing predicted tide levels at the time of the surveys) in Kiawah River and Stono River to define flow cross–sections in this multi–channel inlet system. Several random tracklines were surveyed over the ebb–tidal delta as part of the study. This reconnaissance study provides little usable data for mesoscale modeling.

**Captain Sams Inlet – Primary References: Sexton (1981), Mason (1986), Kana and Mason (1988).** Numerous surveys have been performed at Captain Sams Inlet since Sexton's (1981) study of shoal bypassing. Sequential controlled maps of the channel and ebb–tidal delta (to wading depth) are available for five dates before inlet relocation in 1983, and four dates since inlet relocation. Mason (1986) completed several tidal cycle hydrographies after construction of new Captain Sams Inlet and computed tidal prisms for several tide ranges. Kana and Mason (1988) developed a sediment budget for the first two years after inlet relocation (see Fig. 2.16). No wave data or time–series tidal measurements were made during any of these studies. Since inlet relocation, Coastal Science & Engineering, Inc. has surveyed Seabrook Island's beach to low–tide wading depth every year using controlled profile lines.

# IV. PROPOSED SEMI–EMPIRICAL MESOSCALE MODEL

## 4.A Microscale Model Tests

The CWSTM–H model was initially run to investigate the possibility of using time– and spatial–averaged quantities, and therefore larger time– and spatial–steps in a microscale model. The system simulated was a hypothetical ocean–inlet–bay system shown in Fig. 4.1. The bay (on the left side of Fig. 4.1) is 11.979 km long and has a constant bottom elevation of –4 m MLLW. The tidal inlet is 750 m wide and divides the rectangular–shaped barrier islands shown in Fig. 4.1. The bathymetry in the ocean was constructed using an equilibrium profile equation. The total width (from the landward side of the bay to the outer ocean boundary) of the simulated system is 9.733 km.

The parameters varied in the six initial CWSTM–H simulations are given in Table 4.1. The coarse and fine grids referred to in Table 4.1 are shown in Figs. 4.2 and 4.3, respectively, and represent the hypothetical ocean–inlet–bay system. The coarse grid consisted of 2613 nodes that composed 832 quadrilateral (375m by 375m) quadratic elements, whereas the fine grid consisted of 4949 nodes that composed 480 quadratic quadrilateral (375m by 375m) elements, 440 quadratic triangular elements, and 832 quadratic quadrilateral (187.5m by 187.5m) elements. The boundary conditions used in these simulations consisted of a tidal (water surface elevation) time series that was applied to the open water boundaries in the ocean. The tidal signal was constructed using the 16 major harmonic constituents determined by harmonic analysis of the NOS predicted tide at the entrance to Charleston Harbor, South Carolina. In the bay and along the shoreline of the two barrier islands, the normal velocity component was taken to be zero.

Table 4.2 shows the difference in the simulated tidal prism through the inlet as a function of time–step for spring, mean, and neap tides. As observed for all three tides, the prism decreases slightly with increasing time–steps. This difference is considered to be minimal since the largest decrease in the prism (between $\Delta t$ = 5 and 30 minutes) for a given tide is less than 4%. However, Table 4.3 shows that the predicted ebb–tidal delta volume after 30 days increases rather significantly (by more than 25%) with increasing time–step size. This increase is thought to be caused by possible numeric effects in the sediment continuity equation with increasing time–step size. This will be investigated in more detail in Year 3. Thus, the time–step size does have a significant impact on the size of the ebb–tidal delta that forms.

Figure 4.1 Hypothetical ocean-inlet-bay system modeled using the CWSTM-H microscale model.

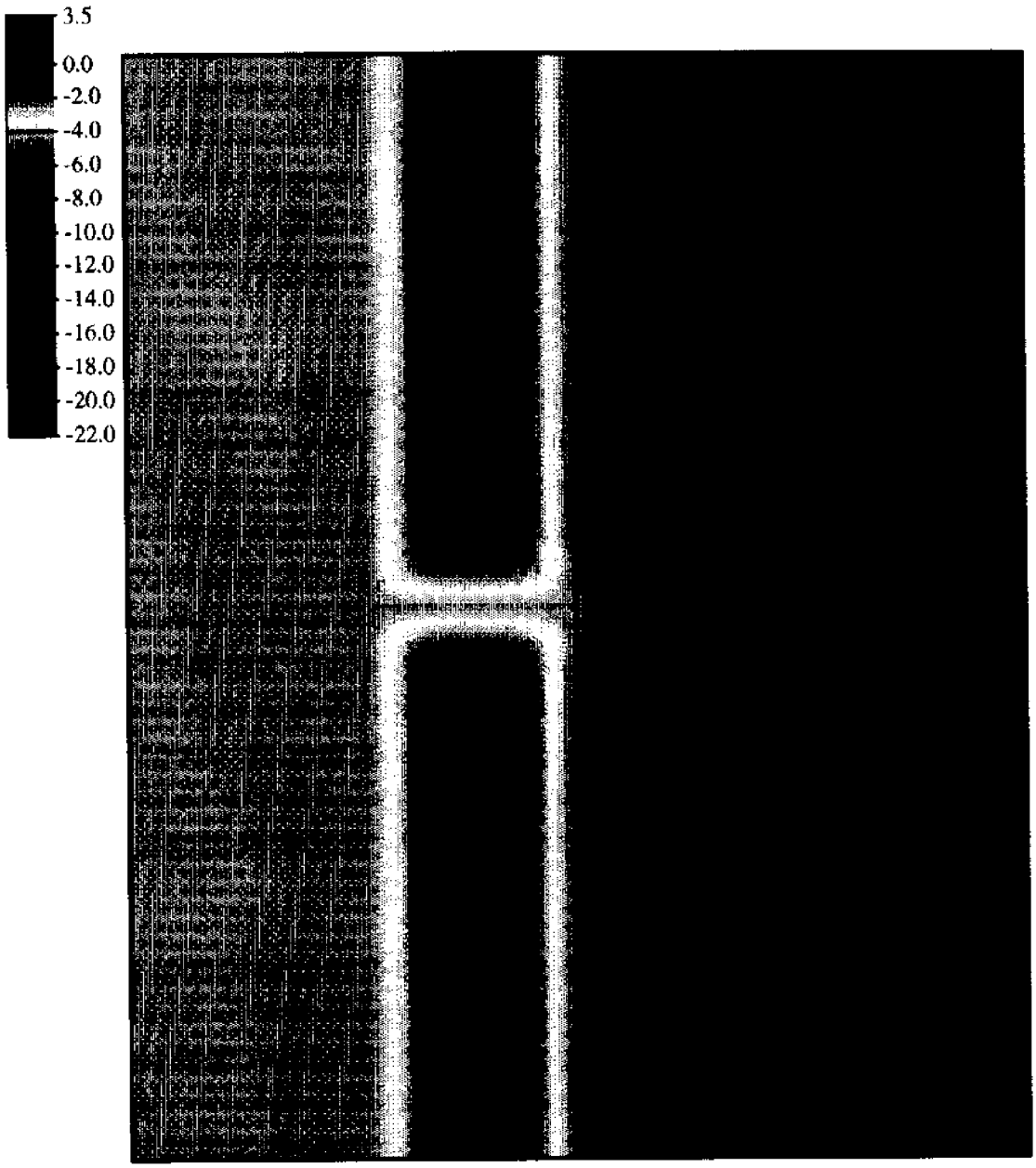

Table 4.1 Microscale model test parameters

| Case | Grid | Computational time step (min) | Time interval for saving data (min) | Location for saving data | Duration of model run (day) | Time series saved |
|---|---|---|---|---|---|---|
| 1 | Coarse | 15 | 30 | Throat of inlet | 30 | Velocity, Tidal stage, Bathymetry |
| 2 | Fine | 5 | 30 | Everywhere | 30 | Velocity, Tidal stage, Bathymetry |
| 3 | Coarse | 5 | 5 | Everywhere | 30 | Velocity, Tidal stage, Bathymetry |
| 4 | Coarse | 5 | 5 | Everywhere | 56 | Velocity, Tidal stage, Bathymetry |
| 5 | Coarse | 15 | 15 | Everywhere | 30 | Velocity, Tidal stage, Bathymetry |
| 6 | Coarse | 30 | 30 | Everywhere | 30 | Velocity, Tidal stage, Bathymetry |

Table 4.2 Effect of time–step size on tidal prism for three tidal conditions

| | $\Delta t = 5$ min | $\Delta t = 15$ min | $\Delta t = 30$ min |
|---|---|---|---|
| Spring | 7.44* | 7.37 | 7.23 |
| Mean | 6.13 | 6.11 | 6.04 |
| Neap | 4.95 | 4.87 | 4.78 |

* Tidal Prism x $10^{-7}$ $m^3$

Table 4.3 Effect of time–step size on predicted ebb–tidal delta volume after 30 days

| Time Step (min) | Delta Volume ($m^3$) |
|---|---|
| 5 | 6,500 |
| 15 | 7,780 |
| 30 | 8,290 |

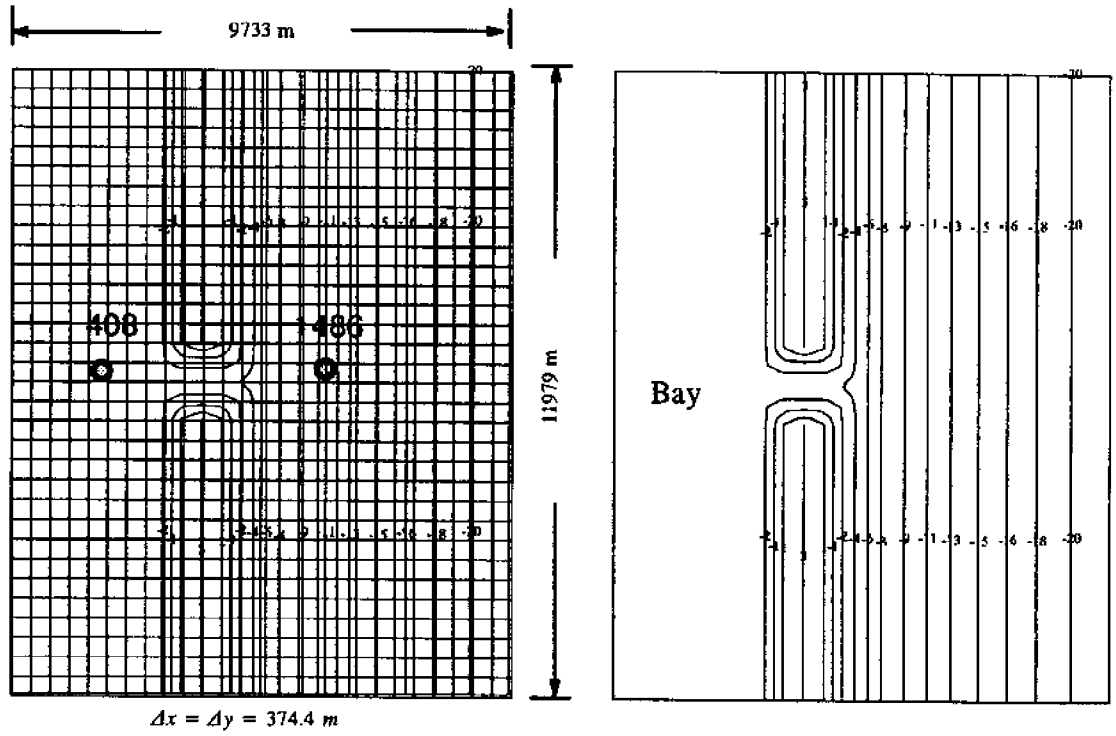


Figure 4.2 Coarse grid and bathymetry for microscale model. The contour lines seen in the right plot are the elevations (in meters) with respect to MLLW datum.

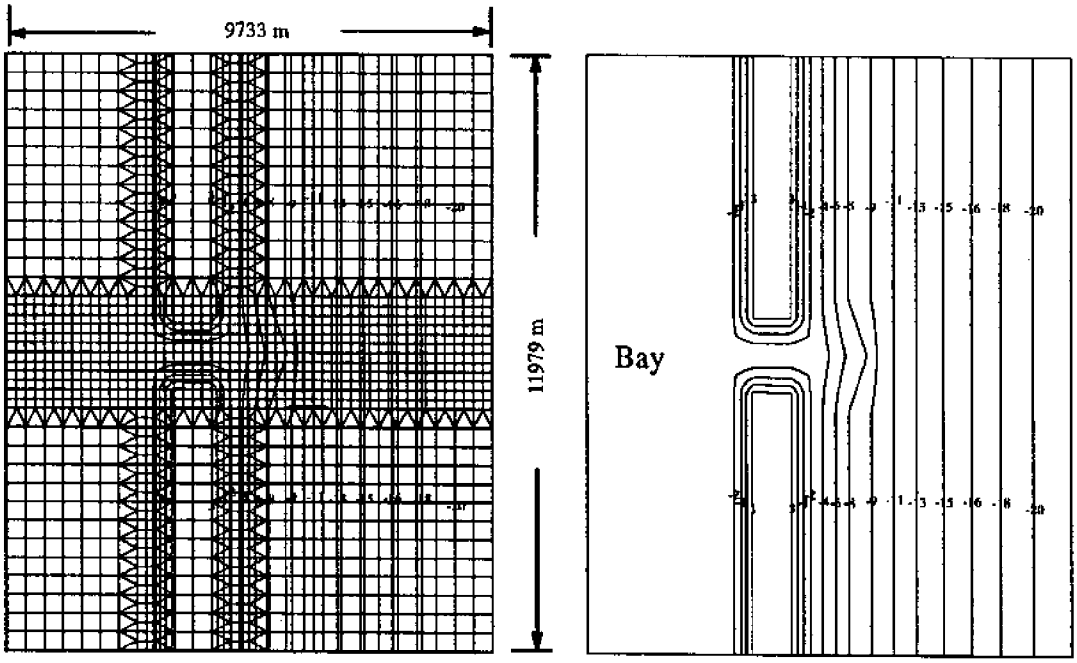


Figure 4.3 Fine grid and bathymetry for microscale model.

Using the results from the six simulations, the following specific items were also investigated to evaluate the feasibility of time–averaging the results of the microscale model.

1. Local tidal ranges

The tidal range is a measure of the magnitude of the driving force that generates tidal currents. Higher tidal ranges in general cause higher current velocities. The tidal range at a certain point inside the computed domain is related to the tidal range at the boundary and the geometry and bathymetry of the domain. While this relationship may not be linear, it is expected to be monotonic, i.e., as range at the boundary increases, the range inside the domain also increases. Figure 4.4 is an example which shows the relationship of tidal ranges between the ocean boundary and Node 408 (see Fig. 4.1) located on the bay side of the inlet. It is clearly seen for this case that the relationship of the tidal range between the ocean boundary and the internal point appears close to linear. Similar relationships were found for other internal points.

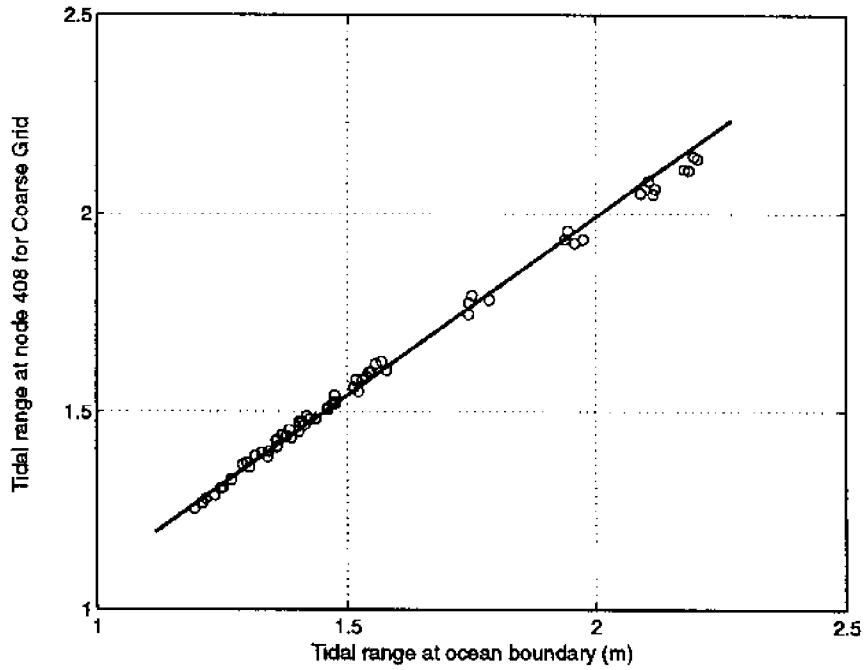


Figure 4.4 Tidal range at node 408 vs. tidal range at the ocean boundary.

2. Peak value of non–dimensional excess shear stress

Sediment transport occurs when the hydrodynamic forces acting on the particles at the bed surface exceed the forces resisting motion. Generally, the estimation of sediment transport

requires the calculation of the bed shear stress induced by currents. The following relationship is used to calculate the shear stress:

$$\vec{\tau} = \frac{1}{2}\ \varrho\ f_c\ \vec{u}\ |\vec{u}| \tag{4.1}$$

where $\vec{\tau}$ = instantaneous shear stress vector; $\vec{u}$ = velocity vector; and $\varrho$ = water density; and $f_c$ = the current friction factor, given by the following relationship (Christoffersen 1982):

$$\left(\frac{2}{f_c}\right)^{0.5} = 2.5 \ln\left(\frac{11.04h}{k_N}\right) \tag{4.2}$$

in which $k_N$ = Nikuradse's roughness, and $h$ = instantaneous water depth.

The shear stress may be expressed as a dimensionless parameter using Shield's entrainment function, $\Psi$, given by

$$\Psi = \frac{\tau}{(\gamma_s - \gamma)\ d_s} \tag{4.3}$$

in which $\gamma_s$ = sediment unit weight; $\gamma$ = water unit weight; and $d_s$ = median sediment diameter.

Sediment motion is initiated when $\Psi$ exceeds a certain value called the critical Shield's value represented by $\Psi_c$. In these tests $\Psi_c$ was taken as a constant 0.05, which corresponds to the horizontal portion of the Shield's diagram.

Using the calculated velocities from the microscale model, the excess non–dimensional shear stresses, i.e., $\Psi-\Psi_c$, were computed. Figure 4.5 shows the calculated results of $\Psi-\Psi_c$ for node 1486 (See Fig. 4.1). The peak values of $\Psi-\Psi_c$ per tidal cycle are selected from the time series of $\Psi-\Psi_c$. The relationship between the local tidal ranges and peak non–dimensional excess shear stress $\Psi-\Psi_c$ for node 1486 is shown in Fig. 4.6. It can be seen that the peak non–dimensional shear stress for this point increases with increasing tidal range, as should be expected since $\Psi \sim u^2$, and $|u|$ increases as tidal range increases.

3. Length of time during which the shear stress is greater than the critical value

The $t^+$ and $t^-$ time periods shown in Fig. 4.7 represent the lengths of time during which the sediment transport occurs in the positive and negative directions, respectively. The tides on the eastern US coast are semi–diurnal and have a period of 12.42 hours. As expected, $t^+$ and $t^-$ are always less than half of the period of tides, i.e., less than 6.21 hours. Figure 4.8 illustrates that the $t^+$ period increases as the local tidal range increases. This increase is monotonic but nonlinear. Temporal resolution of the saved data affects the results somewhat.

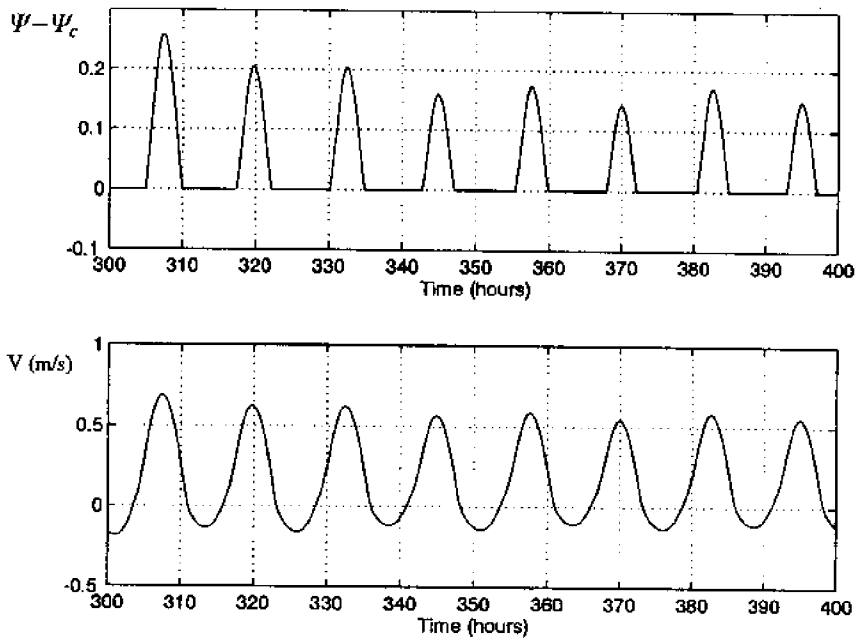


Figure 4.5 $\Psi-\Psi_c$ and velocity in x–direction vs. time for node 1486.

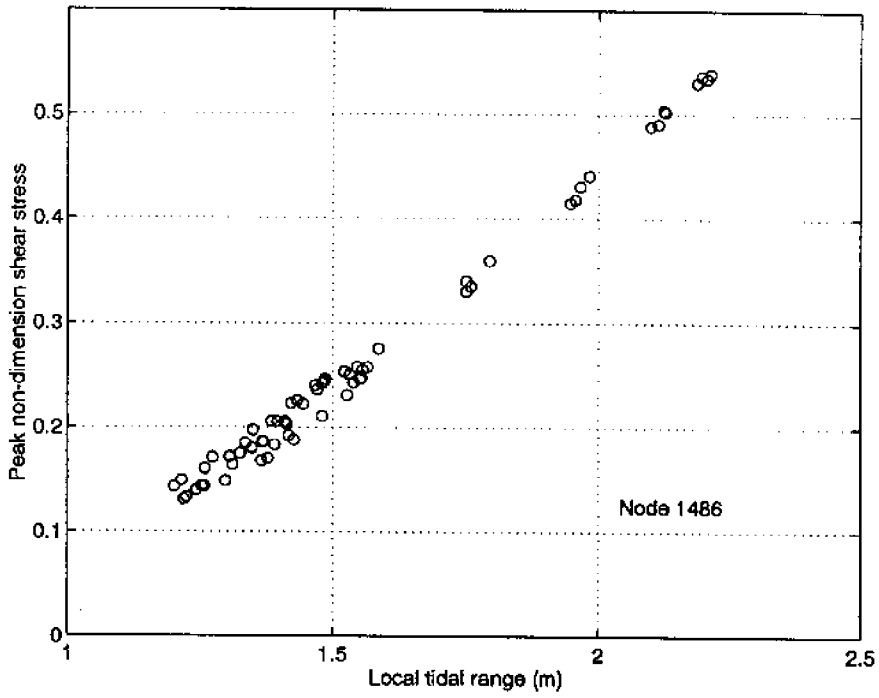


Figure 4.6 Local tidal range vs. peak value of $\Psi-\Psi_c$.

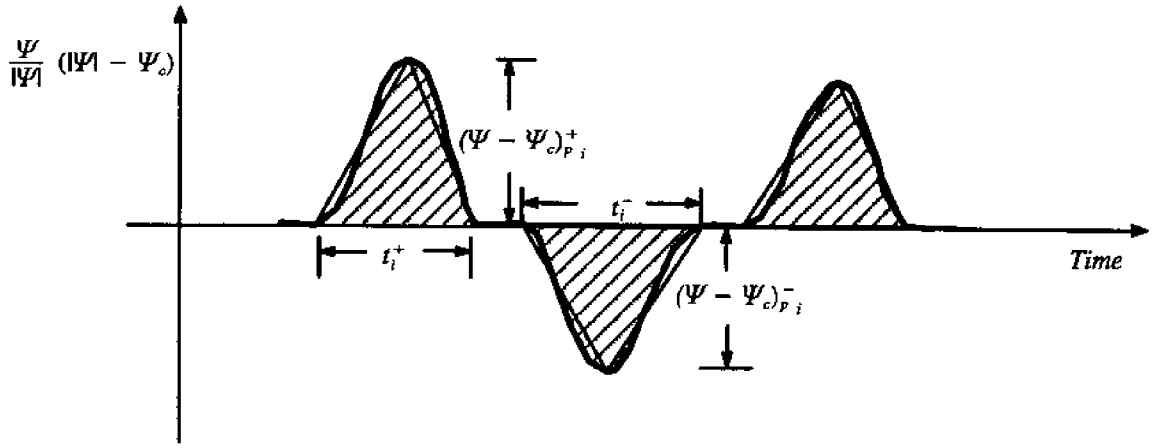


Figure 4.7 Typical time series for excess shear stress.

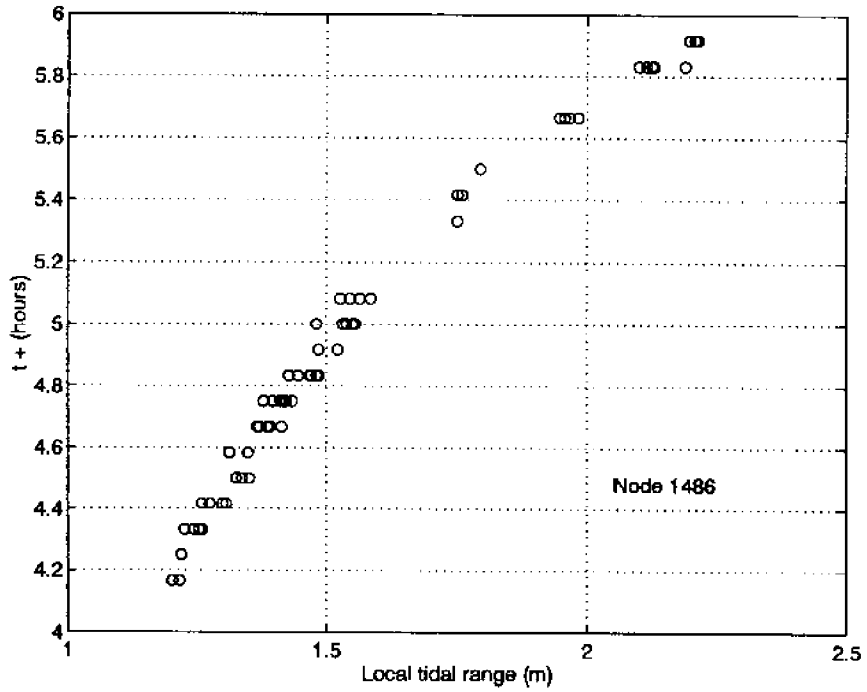


Figure 4.8 Local tidal range versus $t^+$.

4. Time integration of excess shear stress

The estimation of sediment transport requires the calculation of the time–averaged value of $\Psi - \Psi_c$, as the sediment transport rate at a point may be taken as proportional to some

power of this quantity. To simplify this calculation when a large time step (on the order of one tidal period) is used, two parameters, $\alpha$ and $\beta$, are introduced. Note in Fig. 4.7 the triangles that have been drawn to approximate $\Psi(t) - \Psi_c$. The desired integral $\int[\Psi(t) - \Psi_c]dt$ will be approximated by the sum of the areas defined by the triangles. The parameters $\alpha$ and $\beta$ are corrections to account for the deviation of the "true" curve, $\Psi(t) - \Psi_c$, away from the assumed triangular shape. These corrections are analogous to the momentum and energy correction factors commonly used in hydraulics to account for velocity variations across a pipe or channel when using the cross–sectionally averaged velocities. The parameters $\alpha$ and $\beta$ are calculated using Eqs. 4.4 and 4.5. In these equations, $t_o$ = starting time, and the terms in the parentheses with the $p_i$ subscripts in the denominators of the two integral expressions represent the peak positive and negative values of the excess shear stress (see Fig. 4.7).

$$\alpha_i = \frac{\int_{t_o}^{t_o + t_i^+} (\Psi - \Psi_c)^+ \, dt}{\frac{1}{2}\, t_i^+ \, (\Psi - \Psi_c)^+_{p_i}} \qquad \beta_i = \frac{\int_{t_o}^{t_o + t_i^-} (|\Psi| - \Psi_c)^- \, dt}{\frac{1}{2}\, t_i^- \, (|\Psi| - \Psi_c)^-_{p_i}} \tag{4.4}$$

$$\alpha = \frac{\sum_{i=1}^{n} \alpha_i}{n} \qquad \beta = \frac{\sum_{i=1}^{n} \beta_i}{n} \tag{4.5}$$

Note that $\alpha_i$ is the "true" area of one positive spike if Fig. 4.7 is divided by the area of the corresponding triangle by which the spike is approximated. The parameter $\beta_i$ is used in the same manner for the negative spikes.

If the shape of the curve of the non–dimensional excess shear stress variation with time, i.e., $\Psi - \Psi_c$ versus t, was exactly triangular, the resulting values for $\alpha$ and $\beta$ would be unity. Analysis of the microscale model results showed that $\alpha$ and $\beta$ are mainly sensitive to the location within the domain, but not to the tidal range, and that their values deviate somewhat from unity (e.g., see Fig. 4.9).

Using this representation for the excess shear stress, the following approximation for the sediment flux at a given location, $Q_s$ results:

$$Q \propto \int (\psi(t) - \psi_c)dt = \Sigma \frac{1}{2} \alpha_i t_i^+ (\psi(t) - \psi_c)^+ - \Sigma \frac{1}{2} \beta_i t_i^- (\psi(t) - \psi_c)^- \qquad (4.6)$$

5. Tidal current directions

Tidal current directions are primarily governed by the geometry of the simulated domain, relative position within the domain, and the phase of the tides. Figure 4.10 shows the changes in current directions with time and the corresponding changes of stage for node 1486. The directions of tidal currents vary with changes in tidal stages. However, it is shown from the histogram in Fig. 4.11 that dominant directions of tidal currents exist for a certain location.

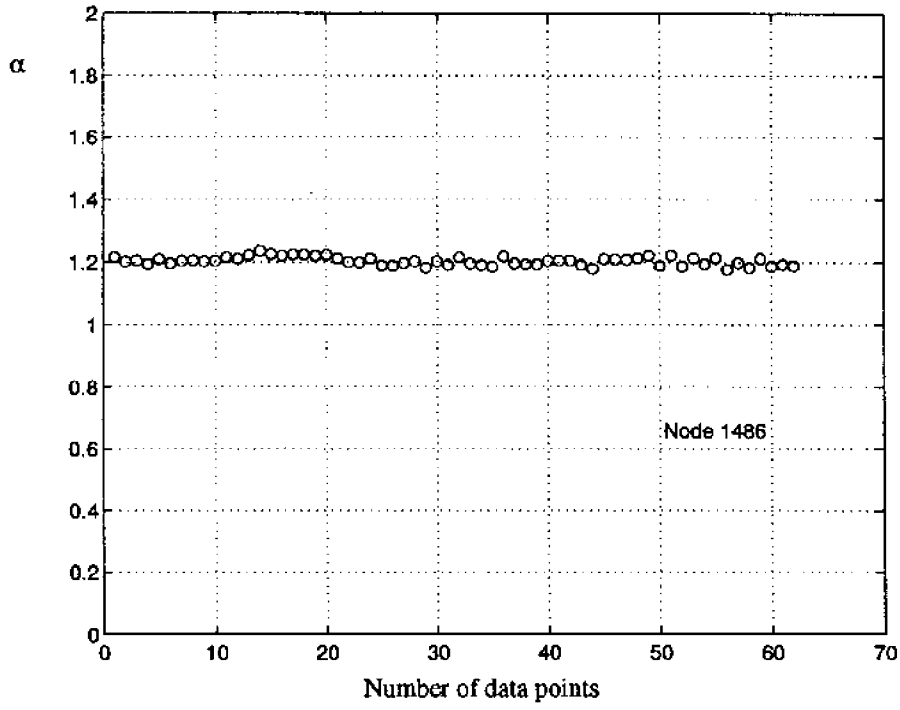


Figure 4.9 Values of α for Test 3.

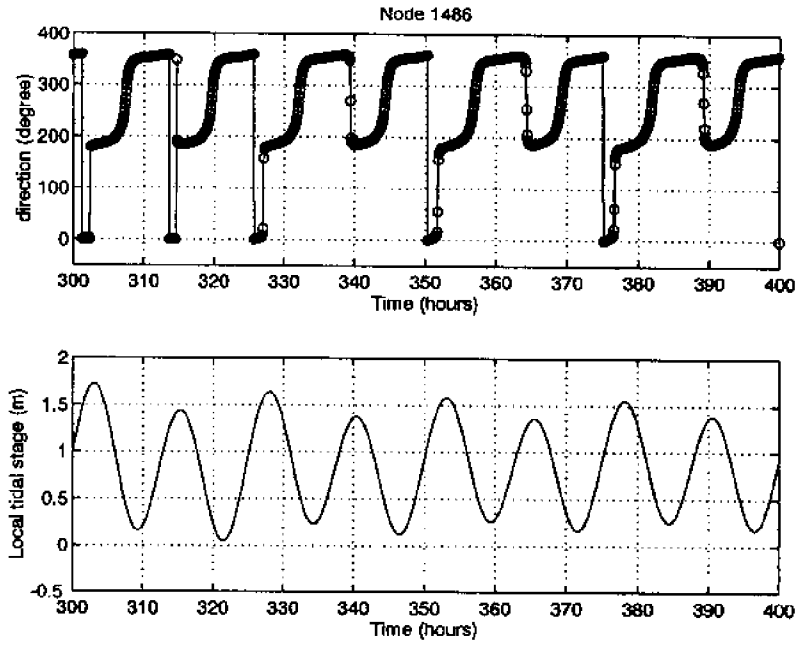


Figure 4.10 Direction of current and local tidal range vs. time for node 1486.

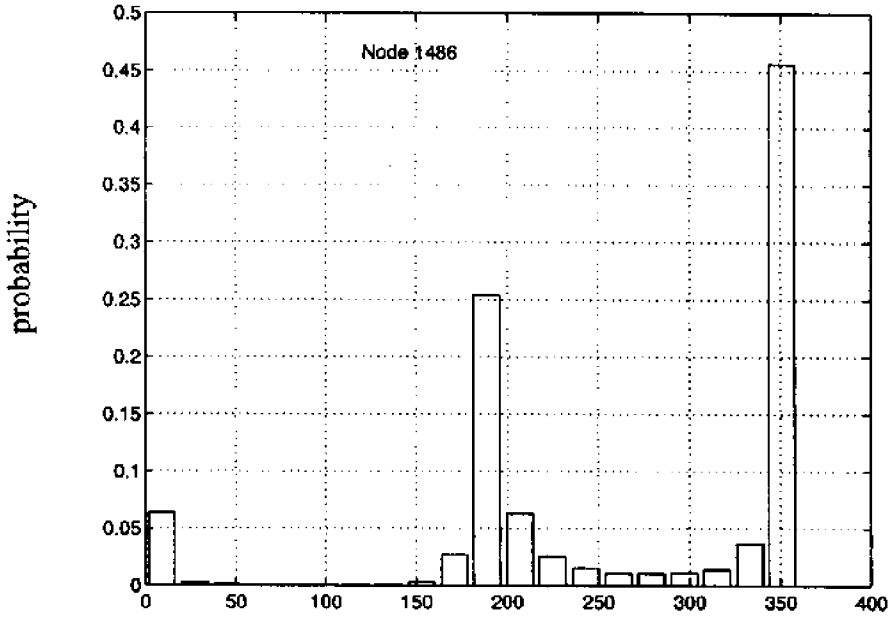


Figure 4.11 Histogram of current directions at node 1486.

## 4.B Micro→Mesoscale (or Hybrid) Model

1. Basic ideas of the hybrid model

Although microscale models are useful tools for short–term (days to months) simulations of morphological evolution of tidal inlets, they are not practical for long–term (years to decades) simulations, since computational time steps for such models are usually at most minutes to tens of minutes. Therefore, a hybrid model is proposed for this purpose. The hybrid model consists of a coupled microscale model and mesoscale model since the empirical relations needed to run the mesoscale model are based on the microscale model results.

As an initial step, the sediment transport induced solely by tidal currents is considered. The tidal effects on sediment transport are driven by periodic boundary conditions at the offshore boundary. These boundary conditions force the relevant quantities such as flow velocity and sediment transport rate into periodic behavior. It is assumed that the residual sediment transport over one tidal cycle at each point in the computational domain is closely related to the known driving forces represented by the tidal ranges at the offshore boundary. It is hypothesized that empirical relations between the residual sediment transport at internal points and the tidal ranges at the offshore boundary can be established.

In the hybrid model, the microscale and mesoscale models are dependent on each other. The microscale model provides the mesoscale model with hydrodynamic information required to establish the empirical relations. The bathymetric changes calculated by the mesoscale model dictates when the microscale model is re–run. The latter occurs when a specified maximum relative bottom change (see Eq. 4.8) is reached.

In order to reduce computation effort, the mesoscale model uses a grid which is a subset of the microscale grid. Two types of meso–grids have been used separately in the mesoscale model tests. One is called the meso–coarse grid whose size is twice that of the micro–coarse grid. The other is the meso–fine grid with the same size as that of the microscale model (see Fig. 4.12). The former grid is utilized for the entire computational domain, the latter for the region around the tidal inlet, i.e., the shadowed region in Fig. 4.12.

The mesoscale model uses a much larger time–step than the microscale model (~12 hours as opposed to 5–10 minutes). This, combined with the fact that the mesoscale model uses a finite difference scheme while the CWSTM–H microscale model uses a much more computationally intensive finite element scheme results in the mesoscale model being capable of running multi–year simulations in a few hours on a PC with a 486 CPU.

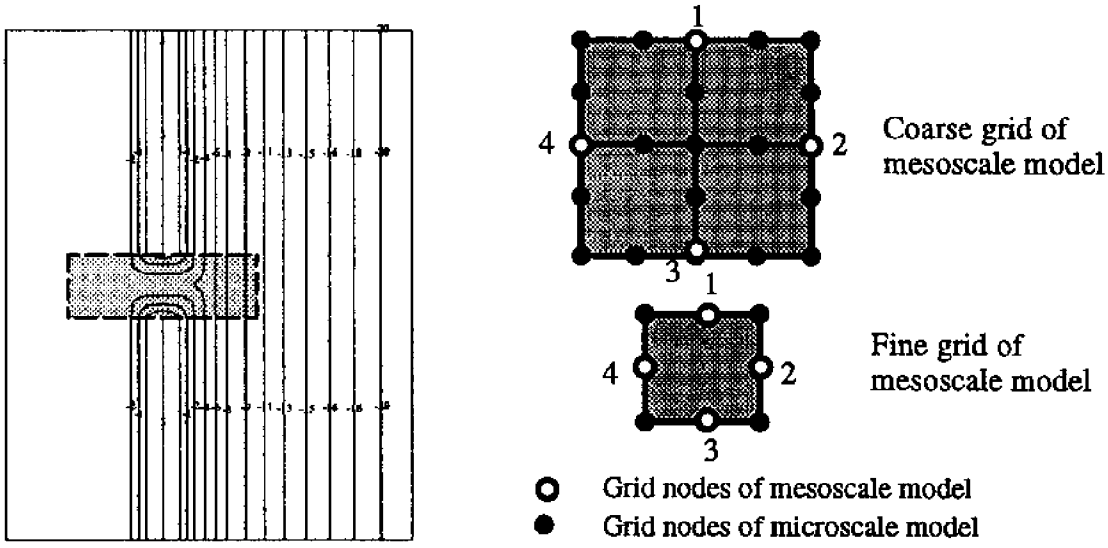


Figure 4.12 Relationships between mesoscale and microscale model grids.

## 2. Methodology

The hybrid modeling procedure is illustrated in Fig. 4.13. The following is a description of the procedure used in the hybrid model:

a. Run the microscale model for one lunar month to establish required empirical relations.

First, the microscale hydrodynamic model is run for one lunar month and the velocity and head are saved at each node of the hybrid model grid at each specific time step. Using the saved data, the sediment transport rate time series at each node is computed. Then, the residual sediment transport over each tidal cycle is obtained. The following parameters are then evaluated: maximum excess shear stresses in the positive and negative directions, time interval over which the shear stress is greater than the critical value, and the shape coefficients of excess shear stress curves within each tidal cycle. Empirical relations between the residual transport or the other reference parameters and the tidal ranges at the offshore boundary are established for each node.

It is assumed that empirical relations for all of the parameters are given by the following linear equation:

$$\Phi = a + b\,|\eta| \tag{4.7}$$

where $\Phi$ is a dependent variable representing, e.g., the residual transport or peak value of the excess shear stress, $|\eta|$ is the tidal range, $a$ and $b$ are empirical coefficients. To establish these

empirical relations, the running time of the microscale model must be of sufficient duration to span the maximum expected variation in tidal range. Thus, a run time of at least one lunar month is necessary.

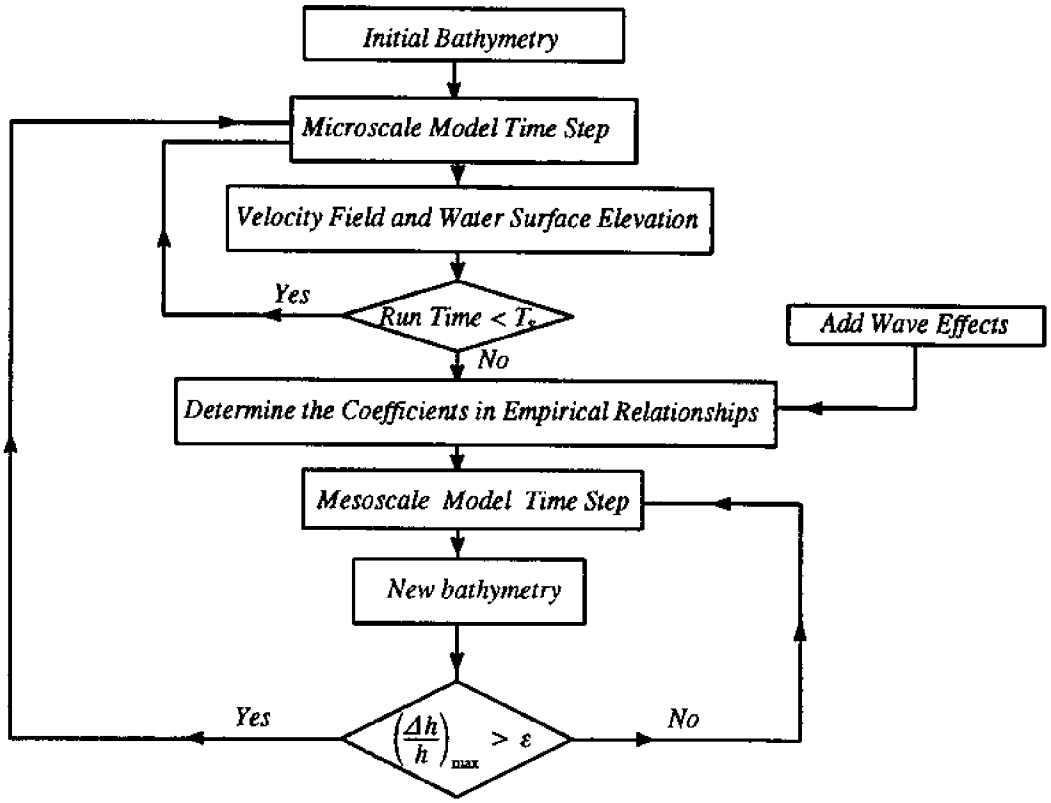


Figure 4.13 General flow chart of the hybrid model.

The linear assumption (see Eq. 4.7) for the empirical relations in the mesoscale model simplifies the computations. For most tidal ranges, it is a good approximation. Test results, however, illustrate that there are relatively large deviations from the linear approximation for very small or very large tidal ranges. A higher order assumption would be necessary to improve the accuracy of the computations.

b. Run the mesoscale model until "significant" bathymetric change occurs.

Using the established empirical relations, residual transport or reference parameters can be calculated at each node according to inputs of tidal ranges at the offshore boundary. Using a sediment conservation equation, the morphological changes are computed at each node using a much larger time step (on the order of one tidal period).

The computation of bathymetric changes is based on a sediment conservation equation. Equation (4.8) gives the finite difference form of the equation used in the mesoscale model.

$$\Delta z_b = -\left(\frac{(\bar{q}_2 - \bar{q}_4)}{\Delta x} + \frac{(\bar{q}_1 - \bar{q}_3)}{\Delta y}\right) \tag{4.8}$$

where: $\Delta z_b$ is the bottom change over one tidal cycle; $\bar{q}_i$ (i=2,4), $\bar{q}_j$ (j=1,3) are residual sediment transports per unit width over one tidal cycle in x– and y–directions, respectively; $\Delta x$, $\Delta y$ are grid sizes in the x– and y–directions, respectively.

If the bathymetry changes "significantly", the previously established empirical relations based on the microscale hydrodynamic model results become invalid since the velocity field would be modified by the bathymetric changes. At this point, the microscale hydrodynamic model must be called and re–run for another lunar month to recompute the coefficients of the empirical relations. "Significant" bathymetric change is defined to occur when the relative bottom change at any point in the domain exceeds a certain tolerance $\varepsilon$:

$$\left(\frac{\Delta h}{h}\right) > \varepsilon \tag{4.9}$$

## 3. Modeling tests

In the hybrid model an existing microscale model, the CWSTM–H model (Veeramachaneni and Hayter 1988), which uses the finite element approach described previously, is employed. The Vincent *et al.* (1981) sediment transport equation is used for computation of sediment fluxes in both the microscale and mesoscale models. To compare the bathymetric changes predicted by the mesoscale model to those predicted by the microscale model, the following microscale model runs were performed using the microscale coarse grid (see Fig. 4.2):

- 2 week run using a constant spring tidal range of 2.0 m;
- 2 week run using a constant neap tidal range of 1.1 m;
- A combination of the above two cases;
- 2 lunar month run using the harmonic tidal signal;
- 4 lunar month run using the harmonic tidal signal; and
- 6 lunar month run using the harmonic tidal signal.

Figures 4.14–4.16 show the results from the last three runs. In these three figures the computed bathymetric changes around only the tidal inlet are shown due to insignificant bathymetric changes beyond that region. From these results it is seen that there is good agreement in the erosion/accretion pattern between the two models, but that differences in magnitudes exist. The differences in computational approaches, i.e., finite element versus finite difference, used in the two models may be one reason. This matter is still being investigated.

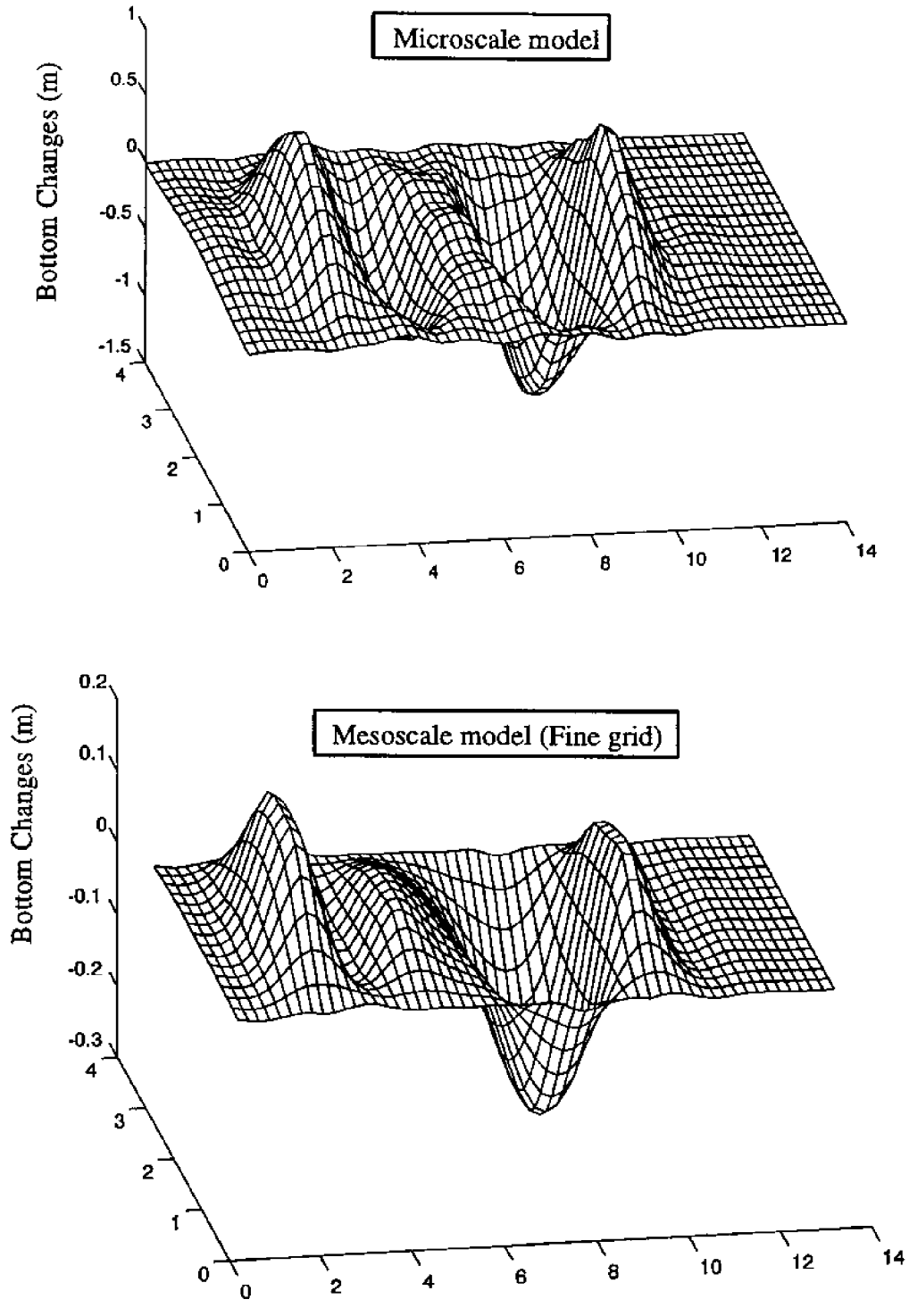


Figure 4.14 Comparison of mesoscale and microscale model results for two month run.

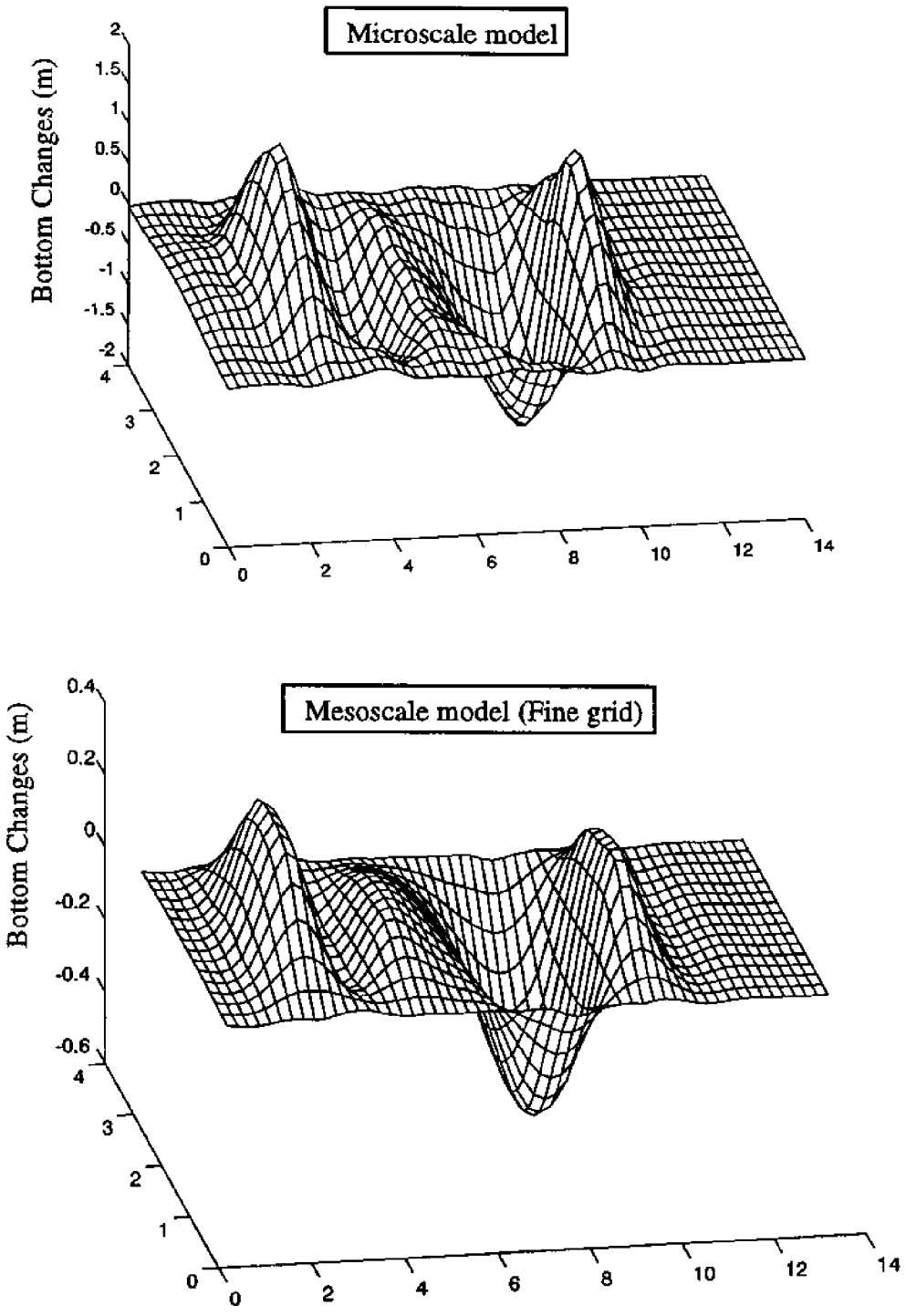


Figure 4.15 Comparison of mesoscale and microscale model results for four month run.

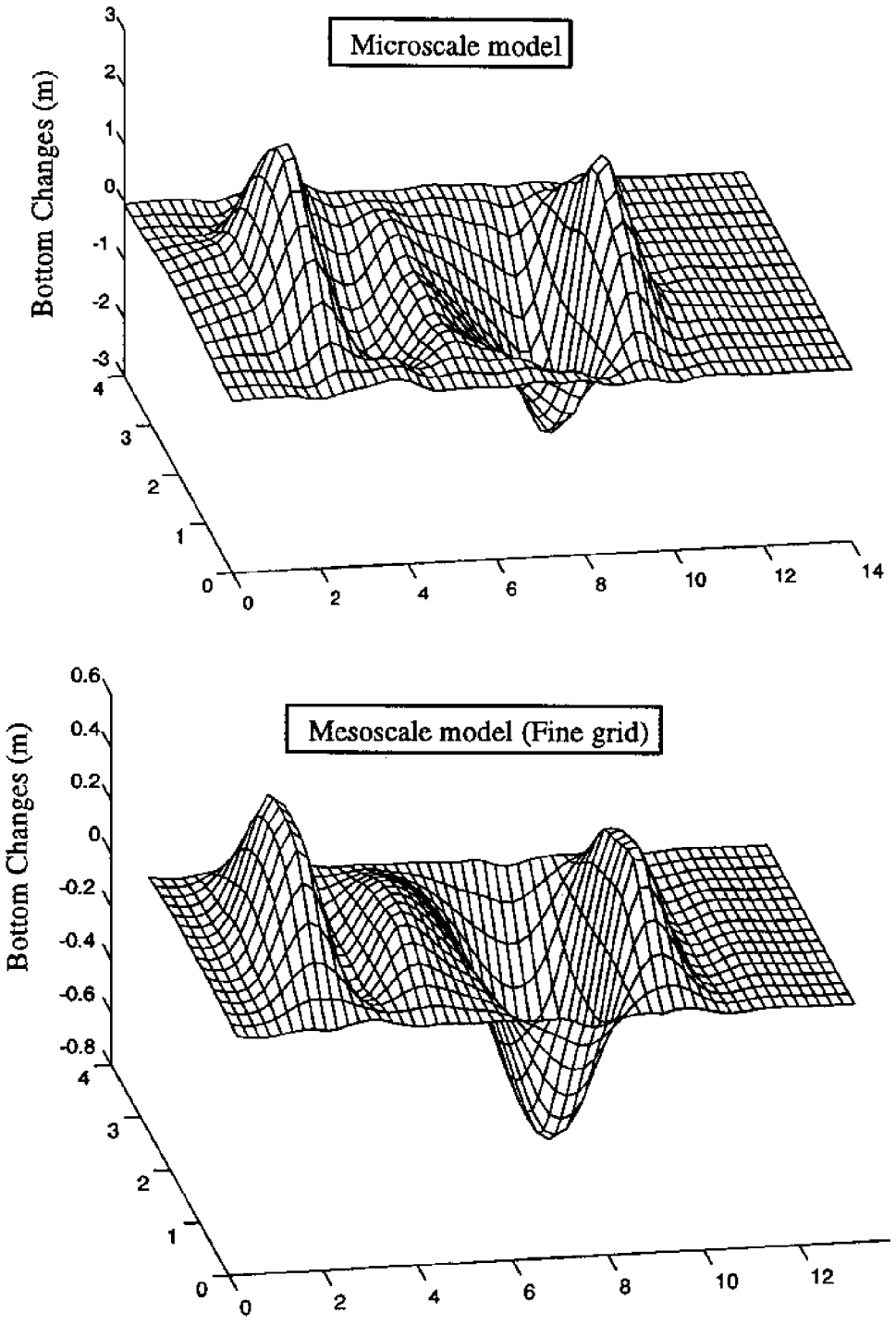


Figure 4.16 Comparison of mesoscale and microscale model results for six month run.

Test results also show that there are significant differences in the computed bathymetric changes in the vicinity of the tidal inlet using the mesoscale model with the meso–coarse grid and meso–fine grids. Therefore, the meso–coarse grid was deemed to be unacceptable for simulating relatively detailed bathymetric changes, especially in the vicinity of the tidal inlet.

To date, only sediment transport induced by tidal currents has been considered. However, wave effects on morphological evolution at tidal inlets are not negligible. A mesoscale model complex including a shoreline change model, a wave transformation model, and a combined wave– and tide–induced sediment transport model is currently being tested.

### 4.C Wave Modeling and Combined Wave–Current Effects

Although the tests described in the previous sections involved only tidal currents, it will obviously be necessary to add the effects of wind waves to be able to realistically model bathymetric changes in the vicinity of a tidal inlet. This complicates the problem significantly, because there are an infinite number of wave heights, periods, and directions possible. In addition, wave heights throughout the computational domain will change as mean water levels change due to tidal fluctuations.

Waves change in height, length, and direction as a result of a number of wave transformation processes. Unfortunately, all of these processes must be considered in the vicinity of a tidal inlet:

- Shoaling – accounts for the initial decrease and ultimate large increase in wave height as a wave "feels" the bottom. Commences when the depth decreases to one–half the wavelength.
- Refraction – accounts for the change in wave direction and wave height if different segments of a wave crest move at different speeds. This can be caused by bathymetric features, since wave speed is dependent on water depth, or by the presence of a mean current.
- Diffraction – accounts for the transfer of wave energy from regions of high energy to less energetic areas. Most important in the vicinity of surface–piercing structures or bathymetric features, or when strong wave focusing occurs due to refraction.
- Breaking – accounts for the majority of wave energy dissipation. In some situations, it is necessary to consider energy dissipation in the boundary layers of the fluid in the absence of wave breaking.
- Reflection – increases in importance as the wave period increases or if bathymetric slopes (or slopes of structures) become large.

There are a number of strategies for modeling wave transformation across a region of variable bathymetry. The first decisions to be made are: which processes from the above list must be included, whether a monochromatic or spectral representation is required, and whether a nonlinear wave theory is necessary. Analytical solutions are available for some simple cases (such as monochromatic, linear waves incident on planar bathymetry, which is governed by Snell's Law), but are generally not useful for simulation of field conditions.

Laboratory data indicate that diffraction must be considered in conjunction with refraction. Without diffraction, wave heights can be significantly overestimated in regions where wave energy is focused. Monochromatic waves also yield a distinctly different result than a directional spectrum. Spectral waves incident on a shoal yield smaller wave heights in the lee of the shoal than would be obtained using an "equivalent" monochromatic wave (Vincent and Briggs 1989).

Since simulations with time scales of years to decades are ultimately desired, it will likely be necessary to restrict wave modeling to monochromatic conditions or possibly some type of parameterized spectrum. Spectral models are available, but these are much more computationally intensive. Treatment of mean currents can also have a strong effect on required computational time. In nature, water waves can create mean currents, which in turn can influence the waves themselves, so there is some feedback. Near a tidal inlet, this motion is superimposed on the tidal currents, although linear superposition is not necessarily valid (Peregrine and Jonsson 1983). The most relevant question is how strong the wave–driven flows are with respect to the tidal currents. If the tidal currents are strong, it is common to assume that they induce wave refraction, but that the waves do not modify the currents. Under these circumstances, the mean current may be specified *a priori*. Then the wave transformation model is run to determine wave heights and directions.

If mean currents are very weak, it may be assumed that they do not modify the waves, which is the simplest case to model. If, however, the tide– and wave–induced mean currents are of comparable magnitude, then an iterative approach is required. The currents are estimated, the waves computed, the currents re–computed if necessary, etc. This computation can be very slow and is not feasible for use in a mesoscale model. The choices are listed in Table 4.4.

At a tidal inlet, regions may be identified where each of the scenarios included in Table 4.4 exist. The sizes and locations of these regions will be time–dependent because of the time–dependency of both waves and tidal currents. In the inlet throat, tidal currents will typically overwhelm wave–induced mean currents. Sufficiently far from the inlet, tidal currents will be negligible for most of the tidal cycle.

Table 4.4 Wave modeling strategies. $\overline{U}$ = tidal current, $u_w$ = wave orbital velocity.

| Relative Current Strength | Assumption |
|---|---|
| $\overline{U}/u_w >> 1$: Strong current, weak wave | Waves do not affect mean currents. Mean currents induce wave refraction. |
| $\overline{U}/u_w << 1$: Weak current, strong wave | Currents do not affect waves. Waves contribute to mean current. |
| $\overline{U}/u_w \sim 1$: Currents and waves both significant | Currents modify waves. Waves contribute to mean current. |

**Governing Equations for Wave Transformation Models**

A conservation of wave energy flux argument may be employed to develop a simple model for wave transformation which includes shoaling and refraction. Conservation of wave energy flux requires (Dean and Dalrymple 1984):

$$\vec{\nabla} \cdot E\vec{C}_g = 0 \tag{4.10}$$

where $E$ = wave energy density, and $\vec{C}_g$ = wave group velocity vector. This equation contains two dependent variables, wave height and direction, so a second equation expressing irrotationality of the wave number vector is required:

$$\vec{\nabla} \times \vec{k} = 0 \tag{4.11}$$

Equations 4.10 and 4.11, together with the linear wave dispersion relation, $\omega^2 = gk \tanh kh$, form the basis for a simple numerical model. If the waves encounter a mean current, the dispersion relation and energy flux conditions are modified. Defining $\sigma$ as the intrinsic frequency, i.e., frequency with respect to the coordinate system translating at the mean current velocity, and keeping $\omega = 2\pi/T$ = absolute frequency, i.e., frequency with respect to the fixed reference frame, the dispersion relation becomes:

$$\sigma^2 = gk \tanh kh \quad \text{where} \quad \sigma = \omega - \vec{k} \cdot \vec{u} \tag{4.12}$$

The energy flux requirement is modified such that wave *action* is conserved (Bretherton and Garrett 1968):

$$\vec{\nabla} \cdot \left[\frac{E}{\sigma}\left(\vec{u} + \vec{C}_g\right)\right] = 0 \tag{4.13}$$

where $\vec{u}$ = mean current vector.

Conservation of wave action, irrotationality of the wavenumber vector, and the dispersion relation modified by the mean current (Eqs. 4.9 – 4.12) provide the basis for the REFRACT model (Dalrymple 1988). A modified dispersion relation to account for nonlinear waves was also included as an option. A simple representation of wave breaking is also included. The largest drawback of this model is the exclusion of diffraction.

Berkhoff (1972) derived what has become known as the "mild slope equation", accounting for both diffraction and refraction:

$$\frac{\partial}{\partial x}\left[CC_g\frac{\partial \phi}{\partial x}\right] + \frac{\partial}{\partial y}\left[CC_g\frac{\partial \phi}{\partial y}\right] + \sigma^2\frac{C_g}{C}\phi = 0 \qquad (4.14)$$

where $C$ = wave celerity (phase speed), and $\phi$ = velocity potential. The elliptic nature of this governing equation leads to some difficulties because of the need to specify boundary conditions along all edges of the domain. Radder (1979) developed a parabolic model which removes the requirement for specification of wave conditions at the downwave end of the domain as a boundary condition. The parabolic approximation results in a less computationally intensive model, but breaks down if the waves propagate at large angles to the finite difference mesh. Numerous models have been developed using the parabolic approximation to the mild slope equation. The RCPWAVE model developed by the U.S. Army Corps of Engineers (Ebersole *et al.* 1986) is one example. Booij (1981) presents an approach which also accounts for the presence of a mean current.

Both time and frequency domain models have been developed for wave transformation. The results shown in the next section include examples from one model of each type. Many models have been omitted from this review. Models based on the Boussinesq equations are suitable only for shallow water, so are of limited use to the present study. Nonlinear models may warrant attention, but have not yet been addressed in detail.

**Wave Transformation Models Reviewed to Date**

A number of existing, numerical wave models have been investigated for application in this study. Some tests have been performed to investigate the suitability of some of the models. The important features of the models are summarized in Table 4.5. Note that none of the models include all of the processes thought to be important in the vicinity of a tidal inlet, so some compromises will have to be made.

Table 4.5 is not exhaustive; there are many other models that have not been included. Shallow water models are somewhat problematic for use in the situation of interest, since they are poorly–behaved as the shallow water assumption becomes weaker. The wave data available

in South Carolina to describe conditions at the offshore boundary of a wave model are limited and typically do not satisfy the shallow water requirement.

Inspection of Table 4.5 suggests that the REFDIF/S model (Kirby and Ozkan 1994) is the most suitable for application to the problem of interest. But this may not prove feasible for long–term simulations. The REFDIF/S model performs many individual simulations of different components of the offshore energy spectrum to determine energy spectra elsewhere in the domain. Computational time for this approach will likely prove to be excessive when long–term (years) simulations are desired.

Some tests have been performed to investigate the suitability of selected existing models to the problem of interest. The tests include wave propagation over idealized bathymetry or currents, as well as one real case. Tests were done using the REFRACT model (Dalrymple 1988) and the NLMSE model (Kaihatu and Kirby 1992). The latter was used in a linear mode, so the tests primarily illustrate the importance of diffraction or currents.

Figure 4.17 illustrates the coordinate system used for the tests, with the $y$–axis located at the offshore boundary and the $x$–axis pointing onshore. Figure 4.18 illustrates the bathymetry for one set of tests: a planar beach at the end of a flat wave basin. A rectangular beach nourishment project has been placed on the beach. The REFRACT model shows sharp gradients in wave height in the vicinity of the "shoulders" (i.e., ends) of the beach nourishment project. Figure 4.19 indicates that the wave direction is affected as well: the waves turn to meet the bathymetric contours. Both results have important implications for sediment transport. The commonly used energy flux method for description of longshore sediment transport rates includes dependency on breaking wave height to the 2.5 power and the sine function of twice the angle at which the wave crests meet bathymetric contours.

Figure 4.20 presents the results for the same bathymetry using the NLMSE model in the linear mode. With diffraction included, a more realistic smooth gradient in wave height is found at the ends of the beach nourishment region (compare with Figure 4.18). Wave breaking has not been included in this result, so the wave height is overestimated. But the significance of diffraction is illustrated.

Table 4.5 Wave transformation processes included in the investigated wave models

| Model | Shoaling | Bathymetric Refr. | Current Refr. | Diffraction | Breaking | Friction | Reflection | Spectral | Nonlinear |
|---|---|---|---|---|---|---|---|---|---|
| REFRACT (Dalrymple 1988) | ✔ | ✔ | ✔ | | ✔ | | | | ✔[1] |
| RCPWAVE (Ebersole *et al.* 1986) | ✔ | ✔ | | ✔ | ✔ | | | | |
| NLMSE (Kaihatu and Kirby 1992) | ✔ | ✔ | | ✔ | | | | | ✔ |
| REFDIF/S (Kirby and Ozkan 1994) | ✔ | ✔ | ✔ | ✔ | ✔ | ✔ | | ✔ | ✔[1] |
| STWAVE (Resio 1993) | ✔ | ✔ | | ✔ | ✔ | ✔ | | ✔ | ✔ |

[1] Nonlinear dispersion relation only.

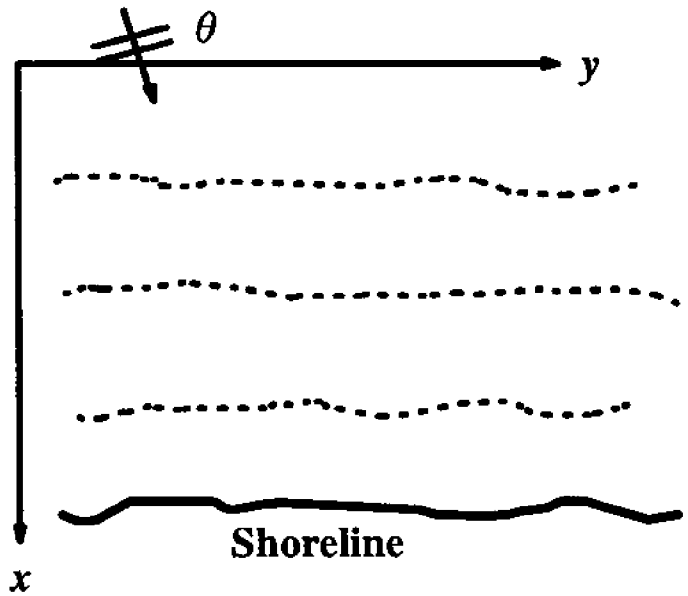


Figure 4.17 Coordinate system for wave modeling.

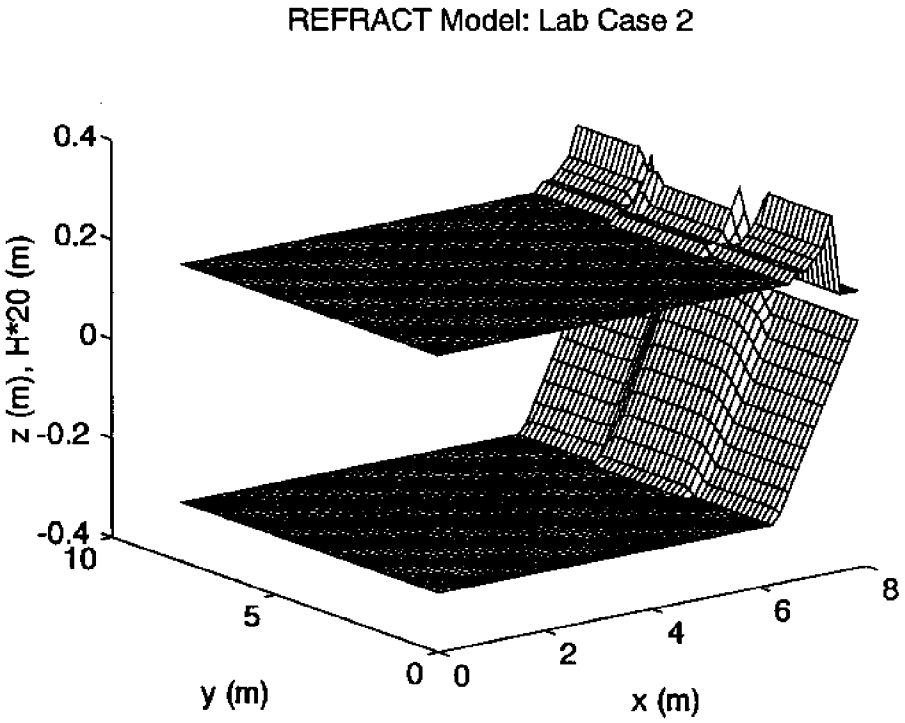


Figure 4.18 Wave heights calculated by the REFRACT model for wave propagation over idealized beach nourishment bathymetry (laboratory scale).

Digitized bathymetry data for Murrell's Inlet, SC, were used to compare results from the two models described above (Fig. 4.21). Plots indicating relative changes in wave height are shown in Figs. 4.22 and 4.23. The plots illustrate how small bathymetric features can focus (or de–focus) waves, yielding the stripes shown in the plots. Diffraction then accounts for subsequent spreading of the focused energy. Data collection for verification of a field case such as this is difficult and expensive. Field data on wave heights is the subject of the next section.

**Wave Data in Vicinity of South Carolina Tidal Inlets**

Ideally, one would have sufficient measured wave data to use as the offshore boundary condition in a numerical wave transformation model, and data from additional points closer to shore as well. The offshore data could then serve as forcing for the numerical model, and the nearshore data would allow calibration and verification of the results. To date, few studies have provided wave data of this nature. Battjes (1982) deployed two gages, one near an inlet throat and a second further offshore. Mariano and FitzGerald (1991) deployed instrumentation inside a tidal inlet channel, but did not measure offshore conditions. Kraus *et al.* (1994) describe a project at St. Mary's Entrance (at the Florida/Georgia border) which included three wave gages:

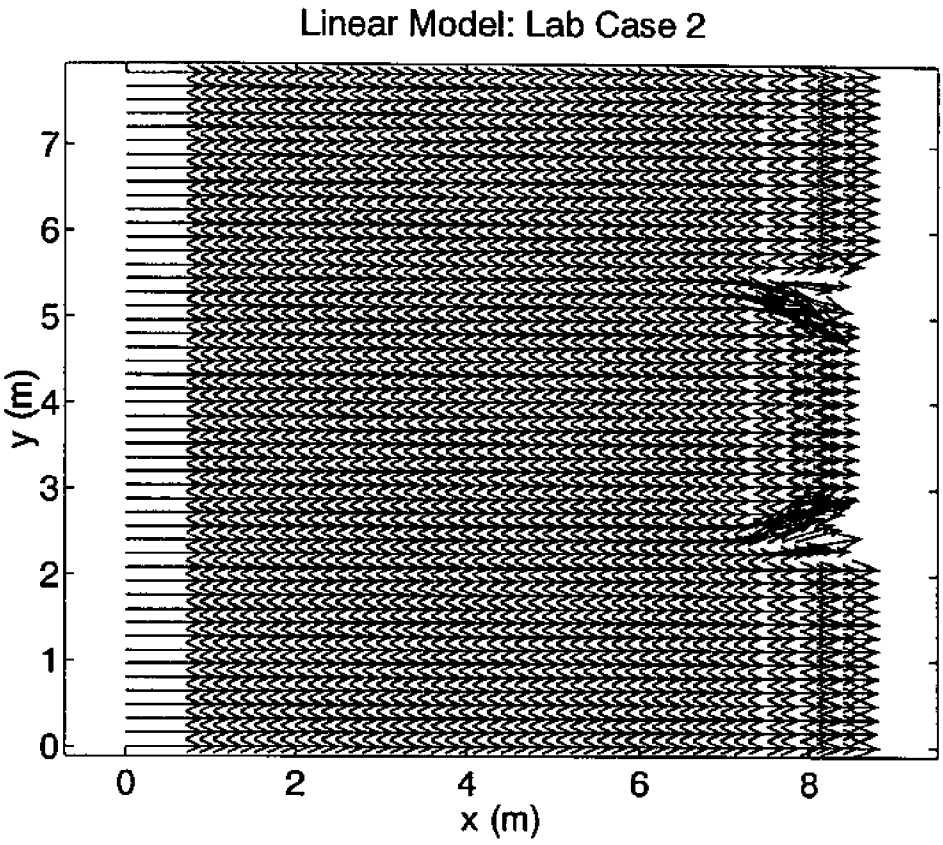


Figure 4.19 Wave height vectors for REFRACT model incident on idealized beach nourishment bathymetry (laboratory scale). Each vector indicates wave height (proportional to vector length) and direction.

two nearshore gages, one north and the other south of the inlet, near the 10 m contour, and a buoy (NDBC Station 41008) 30 km offshore of the inlet throat. The offshore gage provided a nominal five–year record, but the nearshore gage data were short–term.

In South Carolina, there are no long–term, nearshore (depths < 20 m) measurements of wave climate. The National Data Buoy Center has maintained a number of data collection packages in South Carolina waters for the past twenty years, but these stations are all in deeper waters (U.S. Department of Commerce 1993). For instance, there is presently a package (Station 41004) moored in 37 m of water offshore of Charleston Harbor. Some additional studies have included visual observations of wave climate (e.g., Kana 1977), but such data are not sufficiently accurate for verification of quantitative models of wave transformation, and record lengths are not sufficient for prediction of long–term (years to decades) morphological development.

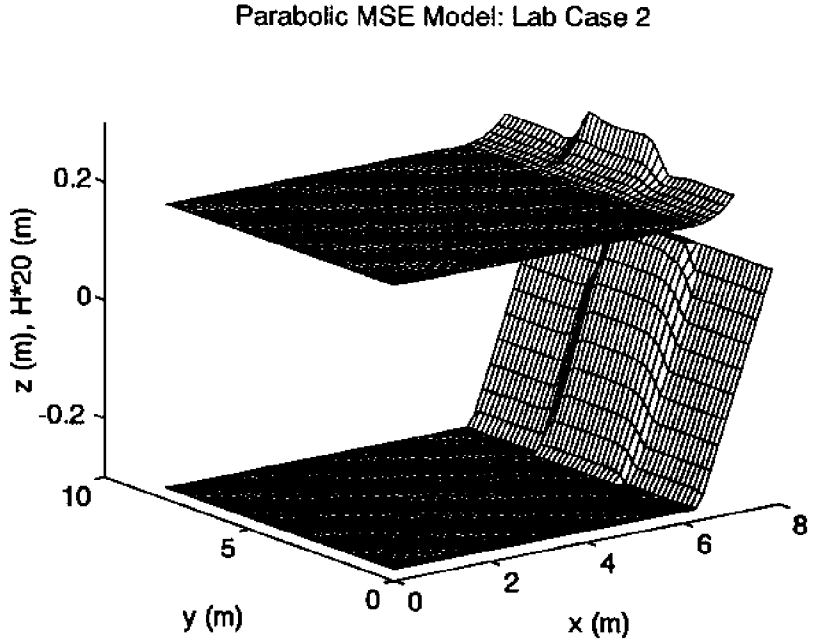


Figure 4.20 Wave heights calculated by NLMSE model for wave propagation over idealized beach nourishment bathymetry (laboratory scale).

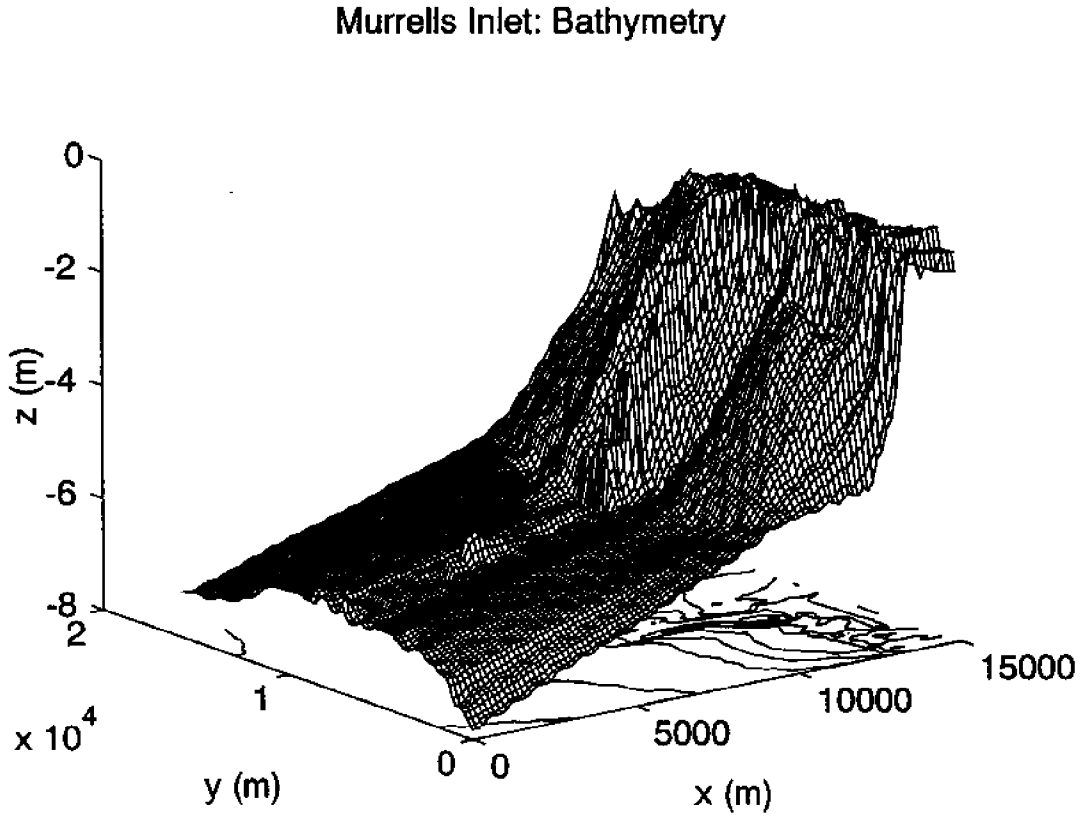


Figure 4.21 Bathymetry for Murrell's Inlet used for wave modeling tests.

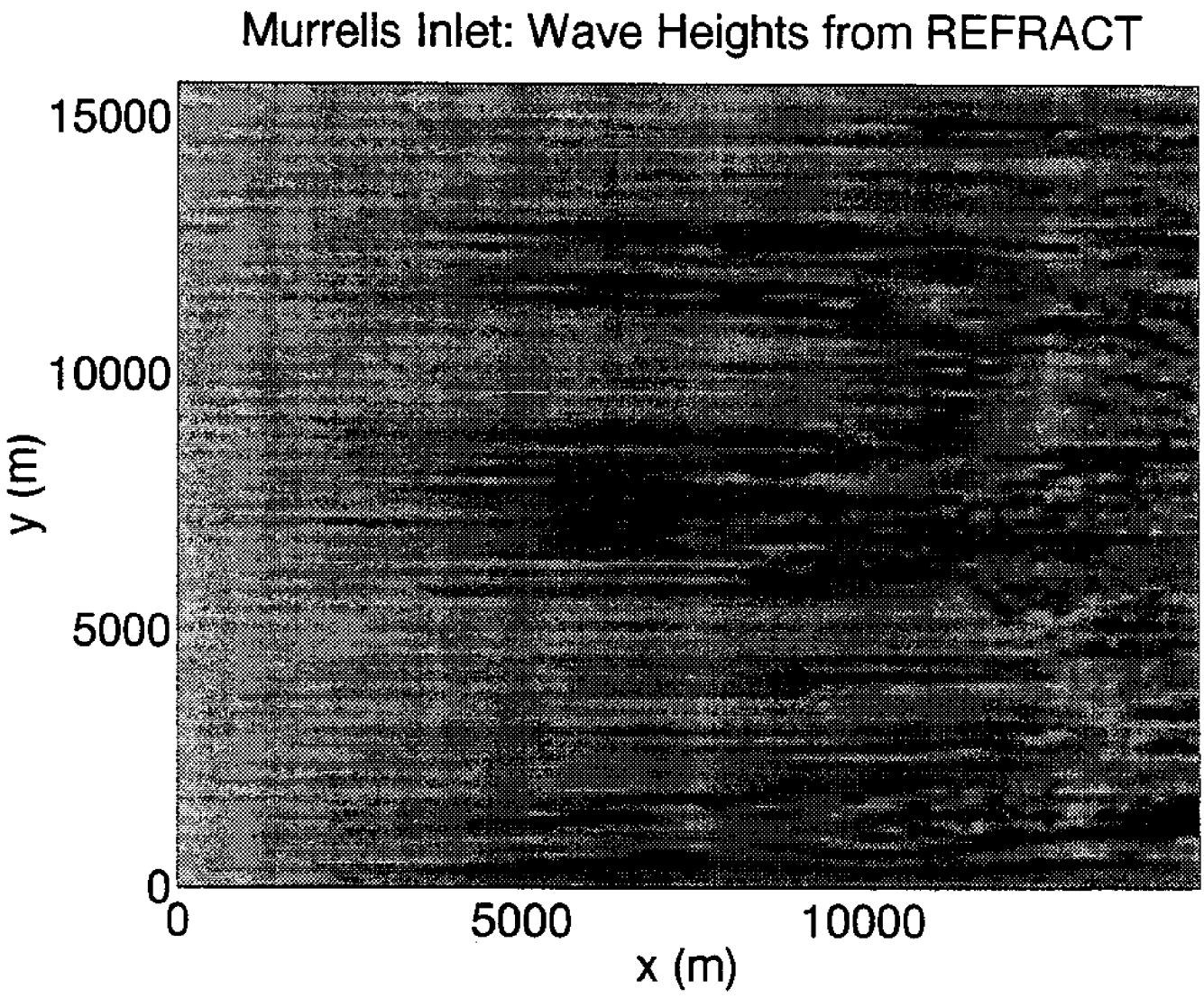


Figure 4.22 Wave heights computed by REFRACT model over Murrell's Inlet bathymetry. Model includes linear shoaling, refraction, and wave breaking.

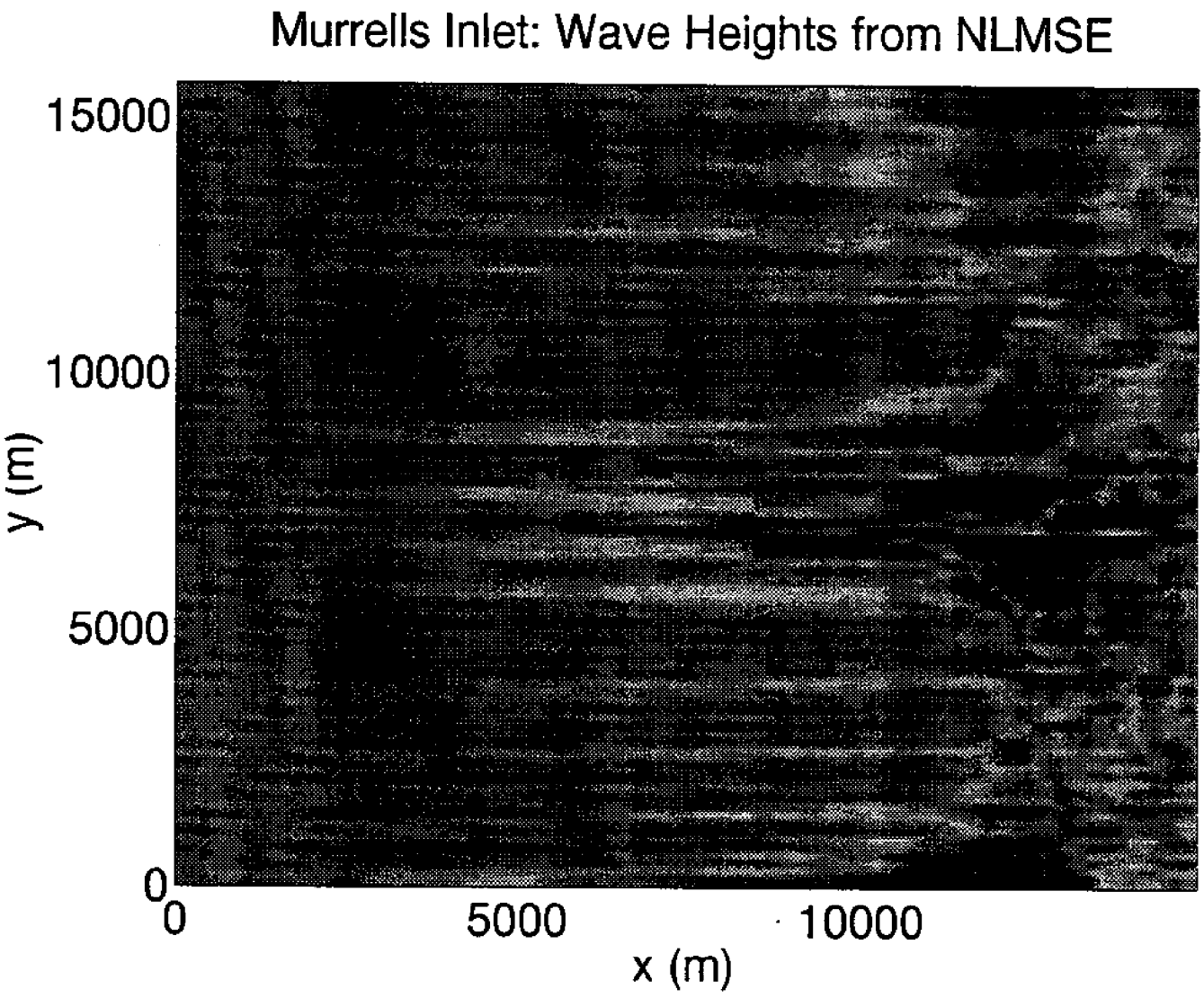


Figure 4.23 Wave heights computed by NLMSE model over Murrell's Inlet bathymetry. Model includes linear shoaling, refraction, and diffraction.

Hindcast wave data are available for the period 1956–1975 as a result of the Wave Information Study (WIS) performed by the U.S. Army Corps of Engineers (Hubertz *et al.* 1993). Statistics of the waves measured at the NOAA gage presently offshore of Charleston Harbor are compared to the WIS hindcast data from data station 35 in Figures 4.24–4.27. This comparison was done primarily to look at qualitative trends. The water depths at the two points are different and the record length for the two sites is also drastically different (20 years vs. six months). Comparison of mean and maximum monthly wave heights yields similar trends. Predicted periods at the hindcast site are significantly higher than measured. This has important implications for wave transformation, since refraction is strongly dependent on wave period. If it proves necessary to use the hindcast data, it will be necessary to determine if the hindcast methodology over–predicts wave periods.

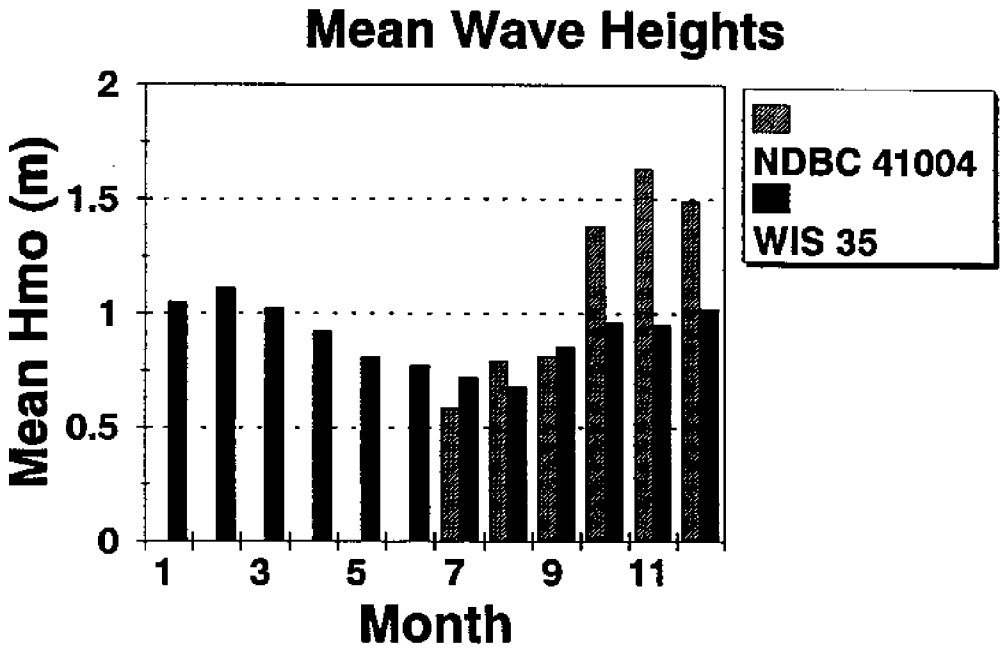


Figure 4.24 Monthly mean value of wave height ($H_{mo}$). Measured (NDBC gage, 7/93 – 12/93) vs. WIS hindcast (1956–1975).

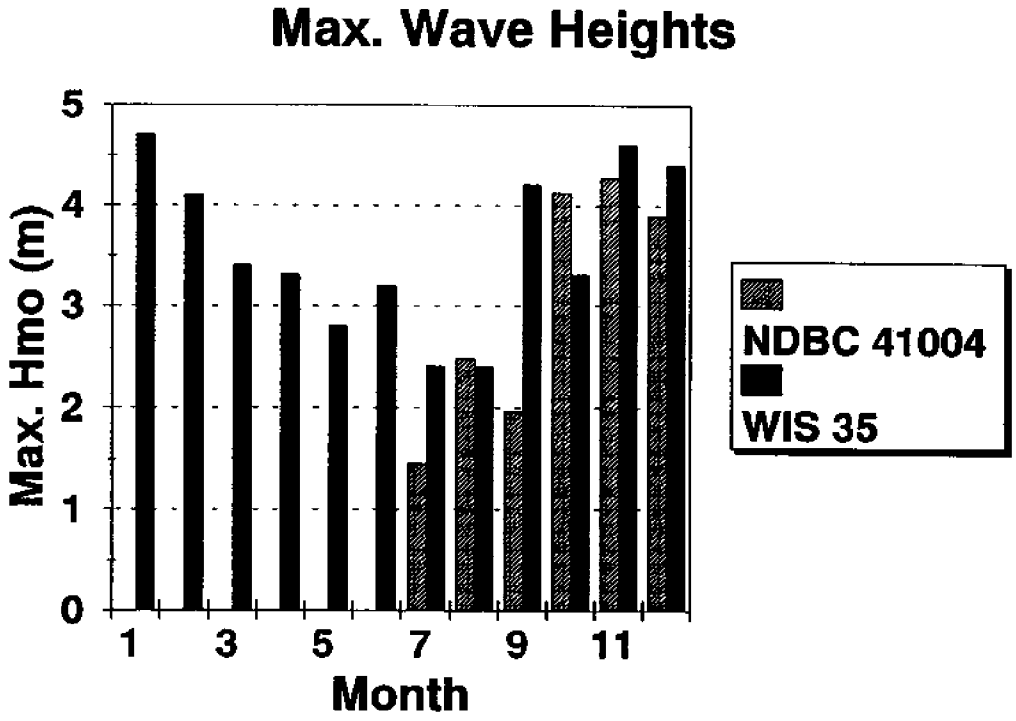


Figure 4.25 Monthly maximum value of $H_{mo}$ wave height. Measured (NDBC gage, 7/93 – 12/93) vs. WIS hindcast (1956–1975).

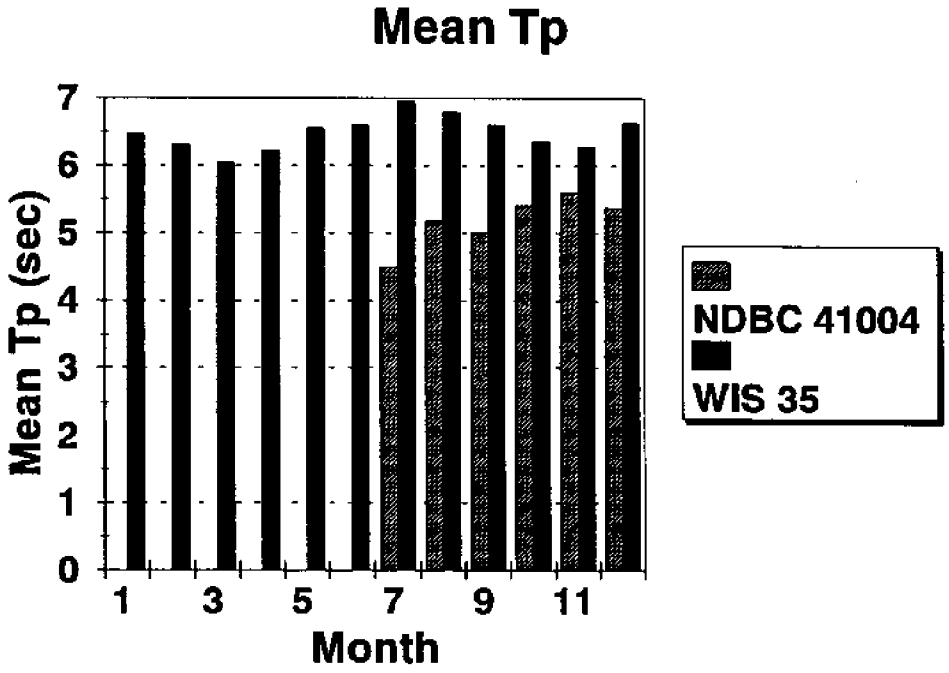


Figure 4.26 Monthly mean value of wave period ($T_p$) at peak of energy spectrum. Measured (NDBC gage, 7/93–12/93) vs. WIS hindcast (1956–1975).

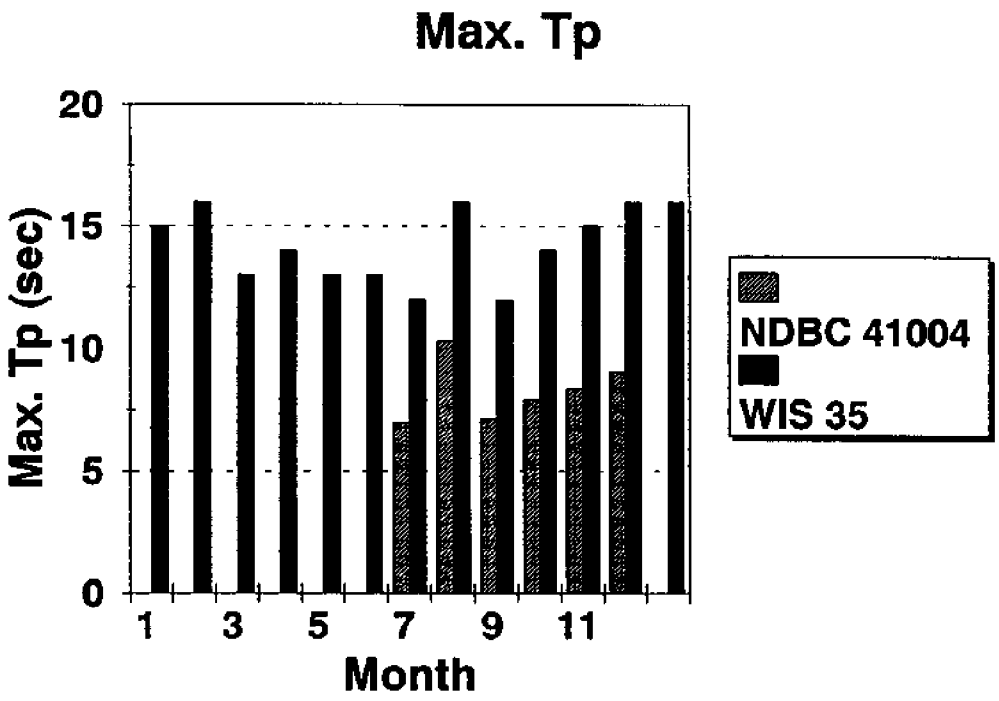


Figure 4.27 Monthly maximum value of wave period ($T_p$) at peak of energy spectrum. Measured (NDBC gage, 7/93–12/93) vs. WIS hindcast (1956–1975).

**Computation of Sediment Transport Rates in Presence of Combined Tidal and Wave–Induced Currents**

While it may later be determined that an alternate strategy is warranted, it is common to calculate sediment transport rates from a bed shear stress vector, where this shear stress is calculated using the following quadratic shear stress equation:

$$\vec{\tau} = \frac{1}{2}\rho f |\vec{u}| \vec{u} \tag{4.15}$$

where $\rho$ = fluid density, $f$ = friction factor, and $\vec{u}$ = velocity vector. In steady flow or simple oscillatory flow, this is relatively straightforward, but the problem is complicated when both slowly varying (tidal) flows and oscillatory flows (wave orbital motion) are present and that in general are not collinear. Thus the proper velocity, friction factor, and direction must be chosen. Nielsen (1992) provides a good discussion of the wave–current–bottom interaction problem.

Sediment transport is typically divided into bed load and suspended load components. Bed load is the sediment that bounces or rolls along a thin layer next to the bed while the suspended load is contained in the rest of the water column. In combined, non–collinear waves and currents it is conceivable that the net sediment transport direction may not be in the same

direction as the waves or currents. Each flow could be responsible for some transport, yielding a net direction for sediment transport that lies somewhere in between.

As the tests performed to date have involved only tidal currents without waves, the wave–current interaction problem has not yet been investigated in detail. It will be necessary to pursue this problem further for at least two reasons: a description of wave–current interaction is necessary to determine reasonable local wave conditions throughout the model domain, and then once the fluid motions are determined, their combined influence on the sediment must be calculated.

# V. OBJECTIVES OF YEARS 3 AND 4

The objectives in Year 3 are to continue the development and testing of the mesoscale modeling approach described in Section IV. Specific tasks that will be addressed include the following:

1. Uncouple the mesoscale and microscale models. This is the "backbone" of the hybrid model described in Section IV. To have a true mesoscale model, the reliance on a microscale model to periodically update the hydrodynamics when a specified bathymetric change occurs has to be eliminated. The process by which this can be accomplished is being investigated in Year 3.

2. Add a shoreline change algorithm and a simplified wave transformation algorithm to the mesoscale model. Test both algorithms using the hypothetical inlet system described in Section IV.

3. Investigate the items mentioned in Section IV; e.g., the differences in the magnitudes of erosion and deposition predicted by the microscale and mesoscale models for the multi–month simulation shown in Figs. 4.14–4.16.

The specific objective for Year 4 is to apply the mesoscale model to at least one prototype inlet in South Carolina, and then simulate specific problems including sand/shoal bypassing and rechannelization. Specific tasks that will be addressed include the following:

1. Apply the mesoscale model to Captain Sams Inlet (Seabrook Island, South Carolina) to simulate the evolution of the inlet following inlet relocation that was performed in 1983. Comparing the model results with the documented inlet/ebb tidal delta development and movement will enable an evaluation of the mesoscale model's ability to simulate shoreline, inlet and morphological changes at a small but highly dynamic tidal inlet. The mesoscale model might also be applied to a middle–sized inlet such as Dewees Inlet.

2. The mesoscale model will be used to investigate processes such as sand bypassing. Field studies have shown bypassing often occurs episodically by way of detachment and onshore migration of shoals formerly trapped in the ebb tidal delta (Sexton and Hayes 1983). But the timing and quantity of sand bypassed in these episodic events appears to vary with tidal prism. As such, applying the model to a small inlet (Captain Sams) and a middle–sized inlet (Dewees) will enable this process to be further investigated.

## REFERENCES


Ackers, P., and W.R. White, W.R. 1973. "Sediment transport: new approach and analysis." Journal of Hydraulic Engineering, ASCE, Vol. 99, No. HY11, 2041–2060.

Andersen, O.H., I.B. Hedegaard, R. Deigaard, P. de Girolamo, and P. Madsen. 1988. "Model for Morphological Changes under Waves and Currents." IAHR Symposium on Mathematical modeling of Sediment Transport in the Coastal Zone, Copenhagen, Denmark.

Augustinus, P.G.E.F. 1993. "Coastal development in Suriname at different temporal and spatial scales." In Proc. Large–Scale Coastal Behavior '93, J.H. List (ed), U.S. Geological Survey, Open File Rept. 93–381, St. Petersburg, Florida, 1–4.

Bagnold, R.A. 1963. "Mechanics of Marine Sedimentation." In The Sea, M.N. Hill (ed), Vol. 3, New York, John Wiley & Sons, 507–528.

Bagnold, R.A. 1966. "An Approach to the sediment transport problem from general physics." U.S. Geological Survey Prof. Paper 422–I, U.S. Govt. Printing Office, Washington DC, 37 pp.

Barth, M.C., and J.G. Titus (eds). 1984. Greenhouse Effect and Sea Level Rise. Van Nostrand Reinhold Company Inc., New York, NY, 325 pp.

Battjes, J.A. 1982. "A case study of wave height variations due to currents in a tidal entrance." Coastal Engineering, 6, 47–57.

Berkhoff, J.C.W. 1972. "Computation of combined refraction–diffraction." Proc. Thirteenth Coastal Engineering Conf., ASCE, New York, NY, 471–490.

Booij, N. 1981. "Gravity waves on water with non–uniform depth and current." Communications on Hydraulics, Report No. 81–1, Department of Civil Engineering, Delft University of Technology, The Netherlands.

Bretherton, F. P., and C.J.R. Garrett. 1968. "Wavetrains in inhomogeneous moving media." Proc. Royal Society of London, Series A, 302, 529–554.

Broker, I., H.K. Johnson, J.A. Zyserman, J.K. Ronberg, C. Pedersen, R. Deigaad, and J. Fredsoe. 1995. "Coastal Profile and Coastal Area Morphodynamic Modeling." MAST–G8M Final Report, 7–12.

Brown, P.J. 1977. "Variations in South Carolina coastal morphology." Southeastern Geology, 18(4), 249–264.

Bruun, P., and F. Gerritsen. 1959. "Natural bypassing of sand at coastal inlets." Jour. Waterways and Harbors Division, Vol. 85, 75–107.

Bulter, H.L. 1980. "Evolution of A Numerical Model for Simulating Long Period Wave Behavior in Ocean–estuarine Systems." In Estuarine and Wetlands Processes with Emphasis on Modeling, Marine Science Series, Vol. 11. New York, NY, Plenum.

CERC. 1984. Shore Protection Manual. U.S. Army Corps of Engineers, Coastal Engineering Research Center, Ft. Belvoir, Vir.; U.S. Government Printing Office, Washington, D.C., 2 vols.

Chesher, T.J., Price, D.M. and Southgate, H.N. 1995. "Long–term Morphodynamic Coastal Area Modeling." MAST–G8M Final Report, 7–25.

Christoffersen, J.B. 1982. "Current depth refraction of dissipative water waves." Series Paper 30, Institute of Hydrodynamics and Hydraulic Engineering, Technical University of Denmark.

CSE. 1991. Seabrook Island, South Carolina, beach nourishment project, 1990–1991. Survey Report No. 2 for Seabrook Island POA; CSE, Columbia, S.C., 37 pp. + appendices.

Dally, W. R., Dean, R. G. and Dalrymple, R. A. 1984. "Modeling Wave Transformation in the Surf Zone." Misc. paper CERC–84–8, U.S. Army Engineer Waterways Experiment Station, Vicksburg, MS. 51 pp.

Dally, W.R., R.G. Dean, R.A. Dalrymple. 1985. "A model for Breaker Decay Beaches." Proc. of the 19th Coastal Engineering Conf., ASCE, New York, NY, 82–98.

Dalrymple, R.A. 1988. "Model for refraction of water waves." J. Waterway, Port, Coastal and Ocean Engineering, Vol. 114, No. 4, ASCE, New York, NY, 423–435.

Davies, J.L. 1973. Geographical Variation in Coastal Development. Hafner Publishing Company, New York, N.Y., 204 pp.

Dean, R.G., and R.A. Dalrymple. 1984. Water Wave Mechanics for Engineers and Scientists. Prentice–Hall, Englewood Cliffs, NJ.

De Vriend, H. J. 1991. "Mathematical Modeling and Large–scale Coastal Behavior." Journal of Hydraulic Research, Vol. 29, No. 6.

De Vriend, H. J. 1987. "Analysis of Horizontally Two–Dimensional Morphological Evolutions in Shallow Water." Journal of Geophysical Research, Vol. 92, No. C4, 3877–3893.

De Vriend, H.J., M. Capobianco, T. Chesher, H. E. de Swart, B. Latteux and M. J. F. Stive. 1993. "Approaches to long–term modeling of coastal morphology: a review." Coastal Engineering, 21:225–269.

Douglass, S.L. 1987. "Coastal response to navigation structures at Murrells Inlet, S.C." CERC Report 85–8, U.S. Army Corps of Engineers, Vicksburg, Miss.

Ebersole, B.A. 1985. "Refraction–Diffraction model for linear water waves." Journal of Waterway, Port, Coastal, and Ocean Engineering, ASCE, 111(WW6), 939–953.

Ebersole, B.A., M.A. Cialone, and M.D. Prater. 1986. "Regional coastal processes numerical modeling system report 1: RCPWAVE – A linear wave propagation model for engineering use." Technical Report CERC–86–4, U.S. Army Corps of Engineers, Coastal Engineering Research Center, Vicksburg, MS.

Engelund, F., and E. Hansen. 1967. A monograph on sediment transport in alluvial streams. Teknisk Forlag, Denmark, 62 pp.

Finley, R.J. 1976. "Hydraulics and dynamics of North Inlet, South Carolina, 1975–1975." GITI Rept No. 10, CERC, U.S. Army Corps of Eng., 188 pp.

FitzGerald, D.M. 1984. "Interactions between the ebb–tidal delta and landward shoreline: Price Inlet, S.C." Jour. Sed. Petrology, Vol. 54, 1303–1318.

FitzGerald, D.M., D. Nummedal, and T.W. Kana. 1976. "Sand circulation patterns of Price Inlet, South Carolina." Proc. 15th Coastal Engineering Conf.; ASCE, New York, 1868–1880.

FitzGerald, D.M., D.K. Hubbard, and D. Nummedal. 1978. "Shoreline changes associated with tidal inlets along the South Carolina coast." Coastal Zone '78, ASCE, New York, 1973–1994.

Galvin, Jr., C.J. 1971. "Wave climate and coastal processes." Water Environments and Human Needs, A.T. Ippen (ed.), MIT Parsons Laboratory for Water Resources and Hydrodynamics, Cambridge, Mass., 48–78.

Halcrow & Partners, Ltd. 1991. The Anglian Sea defense management study: task report on sediment modeling. Final Rept. to NRA Anglian Region (in collaboration with R.B. Nairn, Imperial College, London), U.K., 43 pp. + appendices.

Hanson, H., and N.C. Kraus. 1986. "Forecast of shoreline change behind multiple coastal structures." Coastal Engineering in Japan, Vol. 29, 195–213.

Hanson, H. and N.C. Kraus. 1989. "GENESIS: Generalized Model for Simulating Shoreline Change." U.S. Army Corps of Engineers, Waterways Experiment Station, Vicksburg, MS.

Hayes, M.O. 1964. "Lognormal distribution of inner continental shelf widths and slopes." Deep–Sea Research, Vol. 11, 53–78.

Hayes, M.O. 1976. "Lecture Notes. Part 1." In Terrigenous Clastic Depositional Environments, M.O. Hayes and T.W. Kana (eds.), AAPG Field Course, Tech. Rept. No. 11–CRD, Univ. South Carolina, Columbia, 131 pp.

Hayes, M.O. 1979. "Barrier island morphology as a function of tidal and wave regime." In Barrier Islands: From the Gulf of St. Lawrence to the Gulf of Mexico, S.P. Leatherman (ed.), Academic Press, New York, 1–28.

Hayes, M.O. 1980. "General morphology and sediment patterns in tidal inlets." Sedimentary Geology, Vol. 26, 139–156.

Hayes, M.O., V. Goldsmith, and C.H. Hobbs, III. 1970. "Offset coastal inlets." Proc. 12th Coastal Eng. Conf., ASCE, New York, 1187–1200.

Hicks, S.D., H.A. DeBaugh, Jr., and L.E. Hickman, Jr. 1983. "Sea Level Variation for the United States: 1855–1980." Technical Report, Tides and Water Levels Branch, National Ocean Service, U.S. Dept. Commerce, 170 pp.

Hine, A.C. 1975. "Bedform distribution and migration patterns on tidal deltas in the Chatham Harbor estuary, Cape Cod, Massachusetts." In Estuarine Research, L.E. Cronin (ed.), Vol. 2, Academic Press, New York, 235–252.

Hubertz, J.M., R.M. Brooks, W.A. Brandon, and B.A. Tracy, B.A. 1993. "Hindcast wave information for the US Atlantic Coast." WIS Report 30, U.S. Army Corps of Engineers, Waterways Experiment Station, Vicksburg, MS.

Inman, D.L., and C.E. Nordstrom. 1971. "On the tectonic and morphologic classification of coasts." Jour. Geology, Vol. 79, 1–21.

Jarrett, J.T. 1976. "Tidal prism–inlet area relationships." GITI Rept. No. 3, U.S. Army Engineer WES, Vicksburg, Miss., 76 pp.

Johnson, J.W. 1919. Shore Processes and Shoreline Development. John Wiley and Sons, New York, 584 pp.

Kaihatu, J.M., and J.T. Kirby. 1992. "Spectral evolution of directional finite amplitude dispersive waves in shallow water." Proc. Twenty–third Coastal Engineering Conf., ASCE, New York, NY.

Kana, T.W., 1977. "Suspended sediment transport in Price Inlet, South Carolina." Proc. Coastal Sediments '77, ASCE, New York, NY, 366–382.

Kana, T.W. 1989a. "The South Carolina Coast – 1. Natural Processes and Erosion." in Barrier Islands: Processes and Management, D.K. Stauble, ed., ASCE, 265–273.

Kana, T.W. 1989b. "Erosion and beach restoration at Seabrook Island, South Carolina." Shore and Beach, Vol. 57(3), 3–18.

Kana, T.W., and S.P. Dinnel. 1980. "Bathymetry, shoreline changes, and remedial measures for shore protection on Isle of Palms adjacent to Dewees Inlet, SC." Technical Report for Beach & Racquet Club Co., Inc.; Research Planning Inst., Inc. (RPI), Columbia, SC, 63 pp.

Kana, T.W., S.P. Dinnel, and W.J. Sexton. 1981. "Bathymetry of Kiawah River, Stono River, and historical changes in Stono Inlet, SC." Tech. Rept. for Kiawah Island Company, Charleston, S.C.; Research Planning Inst., Inc., Columbia, S.C., 71 pp.

Kana, T.W., M.J. Vogel, W.J. Sexton, and M.O. Hayes. 1983. "Shoreline changes along Kiawah Island, May 1982 through May 1983." Final Report for Kiawah Island Company, Charleston, S.C., 38 pp. + appendix.

Kana, T.W., M.C. Williams, and F.D. Stevens. 1985. "Managing shoreline changes in the presence of nearshore shoal migration and attachment." Coastal Zone '85, ASCE, New York, NY, 1277–1294.

Kana, T.W., and J.E. Mason. 1988. "Evolution of an ebb–tidal delta after an inlet relocation." In Hydrodynamics and Sediment Dynamics of Tidal Inlets, D.G. Aubrey and L. Weishar (eds), Springer–Verlag, New York, NY, 382–411.

Kana, T.W., and E.J. Hayter. 1992. "Mesoscale modeling of sediment transport and morphologic changes at tidal inlets." Proposal to South Carolina Sea Grant Consortium, Charleston, SC.

Kirby, J.T., and H.T. Ozkan. 1994. "Combined refraction/diffraction model for spectral wave conditions." REF/DIF S, Version 1.1. Documentation and user's manual. CACR Report No. 94–04, Center for Applied Coastal Research, Dept. of Civil Engineering, Univ. of Delaware, Newark, DE.

Kraft, J.C. 1971. "Sedimentary facies patterns and geologic history of a Holocene marine transgression." Bulletin of the Geological Society of America, Vol. 82, 2131–2158.

Kraus, N.C. 1988. "Prediction models of shoreline change." Chapters 1–7 In Nearshore Dynamics and Coastal Processes, K. Horikawa (ed), University of Tokyo Press, 321–373.

Kraus, N.C., L.T. Gorman, and J. Pope. 1994. "Kings Bay Coastal and Estuarine Physical Monitoring and Evaluation Program: Coastal Studies." Technical Report CERC–94–9, U.S. Army Corps of Engineers, Vicksburg, Mississippi.

Latteux, B. 1987. "Transport modeling of particular matter: methodology of long term simulation of bed evolution." Lab. Nat. d'Hydr., Chatou, Rept. HE–42/87.25.

Latteux, B. 1992. "Long term morphological simulation under tidal current with non–cohesive sediment." MAST G6M Final Workshop, Paper 5.18.

Latteux, B., C. Le Normant, and E. Peltier. 1995. "Long–term morphological simulation under–tidal current with non–cohesive sediment." MAST–G8M Final Report, 7–11.

Larson, M., and N.C. Kraus. 1989a. "Prediction of beach fill response to varying waves and water level." Coastal Zone '89, ASCE, New York, NY, Vol. 1, 607–621.

Larson, M., and N.C. Kraus. 1989b. "SBEACH: Numerical model for simulating storm–induced beach change." Technical Report CERC 89–9, U.S. Army Corps of Engineers, Vicksburg, Mississippi, 256 pp.

Larson, M., and N.C. Kraus. 1993. "Prediction of cross–shore sediment transport at different spatial and temporal scales." In Proc. Large–Scale Coastal Behavior '93, J.H. List (ed), U.S. Geological Survey Open File Report 93–381, St. Petersburg, Florida., 96–99.

Mariano, C.G., and D.M. FitzGerald. 1991. "Wave–current interaction at Wells Inlet, Maine." Proc. Coastal Sediments '91, ASCE, New York, NY, 1356–1374.

Maruyama, K., and T. Takagi. 1988. "A Simulation System of Nearshore Sediment Transport for the Coupling of the Sea–bottom Topography, Waves and Currents." IAHR Symposium on Mathematical Modeling of Sediment Transport in the Coastal Zone, Copenhagen, Denmark.

Mason, J.E. 1986. "Morphologic evolution of a relocated mesotidal inlet, Captain Sams Inlet, South Carolina." Technical Report, Dept. Geol., University of South Carolina, Columbia, SC, 149 pp.

Nairn, R.B. 1990. "Prediction of cross–shore sediment transport and beach profile evolution." Ph.D. Thesis, Imperial College of Science, Tech. and Medicine, London, England, 391 pp.

Nelligan, D.F. 1982. "Ebb–tidal delta stratigraphy: Breach Inlet, South Carolina." Unpubl. Masters Thesis, University of South Carolina, Columbia, South Carolina, 221 pp.

Nielsen, P. 1992. Coastal Bottom Boundary Layers and Sediment Transport. World Scientific, Singapore.

Nishimura, H. 1982. "Numerical Simulation of Nearshore Circulation." Proc. of 29th Coastal Engineering Conf., ASCE, New York, NY, 333–337.

Nummedal, D., and S.M. Humphries. 1978. "Hydraulics and dynamics of North Inlet, South Carolina 1975–1976." GITI Report No. 16, Coastal Engineering Research Center, U.S. Army Corps of Engineers, Fort Belvoir, Virginia, 214 pp.

O'Brien, M.P. 1969. "Equilibrium flow areas of inlets on sandy coasts." Jour. Waterways and Harbors Div., ASCE, New York, NY, Vol. 95, 43–52.

Peregrine, D.H., and I.G. Jonsson. 1983. "Interaction of waves and currents." Miscellaneous Report No. 83–6, U.S. Army Corps of Engineers, Coastal Engineering Research Center, Fort Belvoir, Virginia, 88 pp.

Price, W.A. 1955. "Correlation of shoreline type with offshore bottom sediments." Project 63, A&M College of Texas, Department of Oceanography.

Radder, A.C. 1979. "On the parabolic equation method for water–wave propagation." J. Fluid Mechanics, 95, 159–176.

Resio, D.T. 1993. "Program STWAVE: Wave propagation simulation theory, testing, and application." Draft Report, U.S. Army Engineer Waterways Experiment Station, Coastal Engineering Research Center, Vicksburg, MS.

Sexton, W.J. 1981. "Natural bar bypassing of sand at Captain Sams Inlet, South Carolina." Unpublished M.S. Thesis, Department of Geology, University of South Carolina, Columbia, South Carolina, 148 pp.

Sexton, W.J., and M.O. Hayes. 1983. "Natural bar–bypassing of sand at a tidal inlet." Proc. 18th Coastal Engineering Conf., ASCE, New York, NY, 1179–1195.

Steijn, R.C., T. Louters, A.J.F. van der Spek and H.J. De Vriend. 1989. "Numerical model hindcast of the ebb–tidal delta evolution in front of the Deltaworks." In Hydraulic and Environmental Modeling of Coastal, Estuarine and River Waters, R. A. Falconer *et al.* (editors), Gower Technical, Aldershot, 255–264.

Stive, M.J.F. and H.J. De Vriend. 1995. "Advances in Modeling of Large Scale Coastal Evolution." MAST–G8M Final report, 7–6.

Tanaka, H., and N. Shuto. 1981. "Friction coefficient for a wave current coexisting system." Coastal Engineering in Japan, Vol. 24, 105–128.

U.S. Department of Commerce. 1993. "NDBC Data Availability Summary." 1801–24–02, Rev. H, National Data Buoy Center, Stennis Space Center, Mississippi.

USACE. 1977. "Folly River navigation study." Detailed Project Report, Charleston District, South Carolina, 62 pp. + appendices.

Veeramachaneni, R., and E.J. Hayter. 1988. "Mathematical modeling of sediment transport at tidal inlets." IAHR Symposium on Mathematical Modeling of Sediment Transport in the Coastal Zone, Copenhagen, Denmark, 23–32.

Vemulakonda, S.R., J.R. Houston, and A. Swain. 1988. "Development and application of a coastal and inlet process modeling system." Hydrodynamics and Sediment Dynamics of Tidal

Inlets, D.G. Aubrey and L. Weishar (eds), Springer–Verlag, New York, 54–70.

Vemulakonda, S.R., J.R. Houston, and A. Swain. 1988. "Development and Application of Coastal and Inlet Processes Modeling System." U.S. Army Corps of Engineers, Coastal Engineering Research Center, Vicksburg, Mississippi.

Vemulakonda, S.R., and N.W. Scheffner. 1987. "Application of CIP Modeling System to St. Marys Inlet, Florida". U.S. Army Corps of Engineers, Coastal Engineering Research Center, Vicksburg, Mississippi.

Vincent, C.E., R.A. Young, and D.J.P. Swift. 1981. "Bed–load transport under waves and currents." Marine Geology, 39, 71–80.

Vincent, C.L., and M.J. Briggs. 1989. "Refraction–diffraction of irregular waves over a mound." J. Waterway, Port, Coastal and Ocean Engineering, 115(2), ASCE, New York, NY, 269–284.

Vincent, M.S. 1992. "A Numerical Scour–Deposition Model for Tidal Inlets." MS Thesis, Department of Civil Engineering and Mechanics, University of South Florida.

Walton, T.L., and W.D. Adams. 1976. "Capacity of inlet outer bars to store sand." Proc. 15th Coastal Engineering Conf., ASCE, 1919–1937.

Williams, M.L., and T.W. Kana. 1987. "Inlet shoal attachment and erosion at Isle of Palms, South Carolina: a replay." Proc. Coastal Sediments '87, ASCE, New York, N.Y., 1174–1187.

Watanabe, A., K. Maruyama, T. Shimizu, T. Sakakiyama. 1984. "Numerical Simulation Model of Horizontal Topography Change Due to Artificial Structures," Proc. of 31th Coastal Engineering Conf., 406–410.

Wright, L.D., and A.D. Short. 1983. "Morphodynamics of beaches and surf zones in Australia." CRC Handbook of Coastal Processes and Erosion, P.O. Komar (ed), CRC Press, Boca Raton, Florida, 35–64.

Zarillo, G.A., and M.–J. Park. 1987 "Prediction of tidal hydraulics and sediment transport patterns in response to dredging in a tide–dominated harbor." Proc. Coastal Sediments' 87, N.C. Kraus (ed), ASCE, New York, 2030–2046.